UNIVERSITY OF NAPLES FEDERICO II

Nanoparticle in high temperature environment:

experimental techniques and aspects of synthesis properties

Mariano Sirignano

Contents

1. Abstract

The production of materials with nanoscale features is of great interest for the enhancement of the properties linked with the reduced size. Actually, the cost for the production of the commercially available nanoparticles represents the largest part of the added value of these products. This consideration has pushed the scientific community to find an economic and feasible process able to produce on large scale nanoparticles with determined characteristics. Carbon rose as suitable raw material since it is widely available. Moreover carbon is present on the earth in different form, from coal to light and heavy hydrocarbons; all these compounds have a high chemical potential that can be used during transformation process to get final products. Finally carbon based nanoparticles showed a great moiety of structural arrangements that, in principle, makes them suitable for all purposes.

In order to achieve this goal a deep knowledge of the nanoparticle formation process is mandatory to optimally set up reactor parameters. One of the most used and appealing reactor for particle production is represented by flames. Flame synthesis science has been used since the antiquity to produce engineered material. Flames can be alternatively seen as high temperature reactors and thus a set of controlling parameters can be individuated. Temperature history, residence time, mixing effect and fuel or additive structure can be changed in order to obtain the desired products. Moreover the process is autothermic, largely reducing the operative costs. Most of the knowledge about carbonaceous particle in flame is due to the decennials studies conducted in order to strongly reduce the emissions, considered noxious for health and climate. However, to produce smart nanoparticles the knowledge of particle formation has to be shifted toward a deeper level .In fact, the attention has to be paid not only to the total amount produced but also to particle features such as mean size, size distribution, chemical composition, morphological aspect, and internal structure.

In this work, lab scale reactors have been used to test the effect of single parameters on the final features of the particles mentioned above. To characterize the particles produced in hydrocarbon flame advanced experimental techniques have been set up. In particular, optical measurements have been conducted by using a conventional laser induced emission (LIE) techniques. Successively a new aspect of LIE has been developed. Time-resolved laser induced fluorescence has been set up in order to gain information on chemical composition and structural properties of the particles produced in hydrocarbon flames. Spectral evolution together with fluorescence lifetime has been correlated to the aromatization degree of the carbonaceous particles and their level of organization at atomic scale.

However large part of the work has been devoted to the development of a new numerical tool to predict and explore new fields of nanoparticle flame synthesis. The model has been developed

starting from consideration around the nature of the nanoparticles and their evolution based on experimental evidences both produced during this thesis work and from literature data. On the other hand, the model has resulted fundamental to support the results obtained with experimental techniques and thus to draw conclusions. Moreover it reliability has been used to fast explore several combustion conditions, to give indications for experimental investigations and to set up parameters of different reactor configurations. The model has moved from the precious knowledge on the kinetic scheme of gas phase compounds. In order to rigorously treat the particle evolution a sectional method has been used. This method is based on the use of lumped species which allow to numerically treat particle reactions as in the gas phase. In the version developed in this work, the model can be defined as an Advanced Multi Sectional method. It starts from a previous discrete sectional approach for particle modeling based on lumped species, which allowed to describe total amount and size distribution. The final version of the model accounts for multiple discretization, which considers for each lumped species the number of carbon atoms, i.e. the size distribution, the H/C ratio, i.e. the composition on particles and the aggregation state, i.e. the morphological organization. This model represents in the current version the most advanced numerical description of particles evolution.

Experimental techniques and modeling simulation has been applied to different reactor configurations. Premixed flames have been investigated to evidence the role of equivalence ratio and fuel structure on particle features during formation and evolution. Opposed flow diffusion flames have been investigated to understand the role of the mixing effect on the particle inception mechanisms and thus final particle characteristics. Coflow flames have been investigated to extend the consideration based on the results of the opposed flow diffusion flame and to evidence the role of oxidation and oxidation induced fragmentation as a controlling step for the determination of the final features of the particles.

Finally a non-conventional reactor has been set up, both to study and produce particles in medium temperature regime. A plug flow reactor with controlled temperature has been used. The reactors allow to have a long residence time, in the order of seconds, with temperature up to 700K. Particles produced with a conventional premixed flame have been fed to this system. The size of the particle was previously determined with a Differential Mobility Analyzer. The effect of temperature on particle coagulation efficiency has been evaluated. Looking at particle synthesis, in this reactor controlling the temperature environment it is possible to produce particles with determined size having the same composition of those produced in combustion.

2. Introduction

This brief introduction into the nano-world will be focused on the main aspects of investigation on nanoparticles properties, production processes and their possible appliances. Initially the possibility to produce nanoparticles in flame reactors will be discussed, looking at the main advantages gained from the use of this type of reactor, the disadvantages and possible ways to improve the process. Hints about metal nanoparticle flame synthesis research will be given to move further toward carbonaceous nanoparticles.

2.1. Nanotechnology: trends and challenges

Nanotechnology is a wide field of research that can be considered almost unexplored (Tenne, 2006, Service, 2004, Scheu et al., 2006, Soldano et al., 2010). Limitation of investigation in this field can be related to the difficult for the past detection systems to explore the nano-world. Moreover the effect of size at nanoscale strongly influences the main properties of the materials, making even harder their characterization (Hafner et al., 2001, Robertson et al., 1992, Sheehan and Whitman, 2005, Adams et al., 2003, Chavy et al., 1993). On the other hand these peculiar characteristics of nanomaterial are of great interest for their possible appliances to many different human fields, from drug delivery (Timothy V, 2011, Boisseau and Loubaton, 2011, Sanchez and Sobolev, 2010, Farokhzad and Langer, 2009, Uddin, 2008, Niemann et al., 2008) to ultrathin coating(Mukhopadhyay et al., 2005).

The number of scientific journals and papers in this field increases year by year, leading to wider knowledge on fundamental theoretical aspects and practical applications. In fact, since the discovery of fullerenes (Kroto et al., 1985) as a new allotrope of carbon, many scientists went back on their experiments, founding many of them suitable for smart production of these new materials (Howard et al., 1991, Pope et al., 1993). In other words, the scientific community was just not ready to see these materials but was already able to produce them. This unusual happening in scientific community can be at the base of this explosion of interest and capability in nanotechnology world.

Raw materials used for nanostructure production both as pure material and as nanocomposite range from gold (Sardar et al., 2009, Goldberger et al., 2003) to gallium (Goldberger et al., 2003), from a nonmetal as the carbon (Iijima, 1991, Novoselov et al., 2005a) to a semiconductor as the silica (Graule et al., 2005). This moiety of materials substantially reduces the problem of the sources shifting the main problem on the production costs and feasibility (Wang et al., 2002, Jiménez et al., 2009), which determine the real value of these materials.

In order to face the low-cost production problem, lot of possible reactors have been studied and implemented both on lab scale and on plant scale (Jiménez et al., 2009, Pinilla et al., 2010). Usually the possibility to have a large production is not linked with the purity of material and thus with its real feasibility. Several techniques have been tested through years such as CVD (Philippe et al., 2007), arc discharge (Shi et al., 1999), laser ablation (Amans et al., 2009), flame synthesis (Memon et al., 2011a, Wegner and Pratsinis, 2004, Strobel et al., 2006, Merchan-Merchan et al., 2010, Camenzind et al., 2010) and many others (Qiu et al., 2009).

Despite of this wide number of techniques, nowadays nanotechnologies are not influencing our life in determining way; even if part of the problem still relies into discovery of new field of appliances (Fang et al., 2008, Du et al., 2010), part of the solution will be surely found in large scale low-cost production systems (Qi et al., 2010).

2.2. Flame synthesis: a possible way

As mentioned in chapter 2.1 production of material on large scale remains an unsolved problem. From this point of view an analysis of main parameters that control the formation of nanostructure from raw material and precursors can help in the development of new reactive systems (You et al., 2011, Merchan-Merchan et al., 2010). Flame synthesis has been individuated in the very early stage of the nanomaterial discovery as a suitable method to have a high yield and productivity (Howard et al., 1991). The main problem remains the complete control of the process and the selectivity (Height et al., 2003). Hereafter main aspects of flame synthesis of nanoparticles will be presented. Starting from general reactoristic consideration the attention will move on metal based nanoparticles which are widely diffused in industrial technology.

2.2.1. Reactor benefits analysis

Producing nanoparticles from precursors generally deals with three parameters: temperature, species (not only precursors), concentration and mixing level, i.e. time-scale of the process.

The generation of a controlled high temperature environment can be artificial provided with several techniques such plasma arc (Meyyappan, 2009), laser ablation (Amans et al., 2009), chemical vapor deposition (Philippe et al., 2007). However the energy investment of these techniques can strongly affect the final cost of the process (Strobel and Pratsinis, 2007, Camenzind et al., 2010, Merchan-Merchan et al., 2010, Rosner, 2005, Roth, 2007). From this point of view a flame can produce in a direct way the necessary temperature conditions for the process sustainability. Moreover, with flame synthesis higher temperature can be reached and development of the process

can result faster. In other cases, flame synthesis can represent almost the only method to implement a synthesis process.

Large scale production is linked with continuous processes. A continuous feeding of precursors in reactor system substantially excludes the possibility to have batch operations. Flame reactors have demonstrated that the addition of fresh reactants or additive to the system in order to obtain a stable reactive process is quite simple especially compared with other processes. This key point makes flame synthesis of great interest not only on lab-scale analysis but also in real industrial processes. In general the addition of precursors can be done both as gas phase and already as nanoparticles. This latter method is often used in order to produce nanocomposite (Camenzind et al., 2010). Moreover the fuel rich condition of and hydrocarbon flame provide a continuous source of fresh reactive carbon that can be used for nanoparticle production (Merchan-Merchan et al., 2010).

In many processes the formation and growth of nanoparticles are driven by catalyst in order to have higher yield and selectivity of the process (Yuan et al., 2002, Vander Wal, 2000). This kind of process is particularly important for carbonaceous nanostructure production. Most part of this catalyst is metallic and can be fed to the system in different manner (Camenzind et al., 2010, Strobel and Pratsinis, 2007). In particular the residence time in the high temperature zone controls the growth of the nanostructure around the catalyst. This mixing effect can be controlled in flame reactor by changing the premix ratio between fuel oxidant and catalyst. A change in this ratio can lead to a different structure of the flame and thus the production of nanoparticles with different features. Also in the case in which the catalyst is not present the role of the mixing effect is quite effective (Pope et al., 1993, Merchan-Merchan et al., 2003, Goel et al., 2002, Howard et al., 1991). In fact, in a non-premixed flame the fuel rich zone has a temperature history and a concentration of precursors that can be completely different from the main oxidative part of the flame (D'Anna, 2009, D'Anna et al., 2009). The simultaneous presence of these two zones can lead to the formation of a mixture of nanoparticles with specific characteristics and the control on the premix ratio can be a key parameter in the process outlook.

2.2.2. Main challenges in flame synthesis

Most part of the effects of different parameters on the final form of the produced nanoparticles is not easy to be optimized. In fact, the high temperature environment generally enhance all the chemical process and thus also the undesired reactions. The formation of by-products is one of the main problems faced by scientific community. From this point of view the experience on the reduction of undesired species production has been fundamental in the early science of flame synthesis. On the other side most of the products which are the object of this work are of the same class of the most undesired mentioned combustion by-products. Looking at carbonaceous nanoparticles, they are generally related with soot particles, which remain one the most effective pollutant produced in normal combustion devices (Richter and Howard, 2000a, Calcote, 1981,

Kennedy, 1997, Bockhorn, 1994, Bockhorn, 2007) Flame synthesis science has always to deal with this side effect of its nature.

For inorganic nanoparticles the final dimension and form, single particles or aggregates, is of fundamental importance for the final application of the products (Pratsinis, 1998, Strobel and Pratsinis, 2007). The capability to control the process will have to set the key parameters in a narrow range of the values. Out of this range uncontrolled formation of pollutants, formation of not utilizable product or no formation at all of nanostructure will be encountered (Height et al., 2005, Height et al., 2003). This challenge will have to be faced increasing the knowledge of particles formation and growth in as many as possible combustion environment. The deeper knowledge will suggest the correct way to develop safe and productive processes.

2.3. Metal-based nanoparticles in flame

Inorganic nanoparticles are quite common in industrial processes. Production of these nanoparticles started in the 1940's with the discovery of fumed silica (SiO2) (Kloepfer, 1942) which allows to have an high production of this new material. From that moment, nanomaterials and nanocomposites received increasing attention due to their particular characteristics. In fact, some materials such as gold, which is chemical inert in the form of bulk material, can be used as an excellent catalyst if produced in form of small nanoparticles (1-5nm) (Sardar et al., 2009). Some other materials in form of nanoparticles exhibit different thermodynamic properties such as melting point (Attarian Shandiz and Safaei, 2008, Attarian Shandiz et al., 2007), magnetism (Nomura and MacDonald, 2006), conductivity (Zhang et al., 2006) and reactivity (Park et al., 2003). These different behaviors can generally be linked with the excess of surface area due to the reduced dimension respect to bulk material. Many different common metals, such as gold (Sardar et al., 2009), silver (Chen and Schluesener, 2008), platinum (Zhang et al., 2004), aluminum (George et al., 2005), copper (Yin et al., 2005), iron (Xing et al., 2003), silica (Graule et al., 2005) and titanium (Chen et al., 2007), in form of pure metal or more often as oxides, have been tested as nanoparticles or nanocomposites, giving encouraging results in terms of new properties. The exploration of new materials will lead to the use of other metals.

Flame synthesis resulted of fundamental importance since it provides in direct way the high amount of energy necessary for the nucleation of the metal forming nanoparticles. Flame synthesis of metal based nanoparticles starts from precursors of a particular material of from a mixture of them. The feeding of these materials (Strobel and Pratsinis, 2007) is operated or by vapor of material of by evaporated solution or by injection spray in flame. For all these processes one of the most important challenges in flame synthesis, especially for inorganic nanostructure, is the final morphology (Ehrman et al., 1999, Camenzind et al., 2010). Starting from the precursors, the formation of first nuclei is

immediately followed by the appearance of aggregates of nanoparticles (Roth, 2007). This form is not always desired and often completely changes the final characteristics of the product. Time scale control of the process and of the temperature history in the reactive system is fundamental for having a final material with desired characteristic. The process of sintering occurring at high temperature is the controlling step to produce single spherical nanoparticles. As this time become longer the possibility to produce aggregates and the agglomerates increase. The analysis of sintering properties at flame-reactor condition is fundamental for a correct implement of the process

Nanocomposite materials made by different metal particles are one of the most advanced sides of nanotechnology field. The final form of nanosized material depends on the initial form of precursors, their reciprocal interaction and the temperature history, which they undergo. Friedlander and co-workers (Ehrman et al., 1999) have proposed a general description for the final form of nanoparticles in depending of these parameters looking both at single nanoparticles and at aggregates.

Metal-based nanomaterials and their flame synthesis have increased their range of interest and of feasibility. However despite of great efforts spent in last 15 years many pieces of this puzzle have still to be positioned.

2.4. Carbon based nanostructures in flame

The use of carbon black goes back to thousands of years ago since men used this material to draw on the cavern walls. The technology has made great improvement from that moment in order to produce a material fit to different purposes. Even if different allotropes of carbon were already known, the discovery and isolation of fullerenes (Kroto et al., 1985) remains a milestone in the human scientific activity. The suggestive form of C_{60} fullerene has fascinated the scientists of many different fields, who took up the challenge of having the possibility of a large moiety of new materials. The carbon nanotubes (Iijima, 1991) and graphene sheets (Novoselov et al., 2005a) came just after this great discovery enlarging the possibility to manage with the carbon atoms. In the meanwhile a wide moiety of compounds prevalently made by carbon with nanometric size have been discovered and characterized (Endo and Kroto, 1992, Kroto, 1992, Sattler, 1995, Subramoney, 1998, González et al., 2001, Kroto et al., 1985). Main features of these materials result of great interest for industrial applications, pushing the scientific community for the developing of new methods of production. Flame synthesis resulted of great interest since the beginning of the story (Howard et al., 1991, Pope et al., 1993, Vander Wal et al., 2001); from that moment great efforts have been spent to increase the selectivity to these materials of combustion process. Hereafter a non-exhaustive review of the main flame synthesis process for nanosized carbonaceous material will be presented.

2.4.1. Fullerenes

Since the visionary project of Buckminster Fuller (Fuller, 1954) the form of fullerene was introduced in the human life and the discovery of Kroto (Kroto, 1992) almost 20 years later appears like a sort of revenge of the nature: that suggestive form was already inside in the nature project. Fullerenes have been extensively studied due to their particular characteristics that allow them to be applied in different fields from solar cell (Thompson and Fréchet, 2008) to medicine (Anilkumar et al., 2011). There are many forms of fullerenes (Yang et al., 1995), of which the most common is the C_{60} or buckyball (Hebard, 1993), and many possible combinations with other polymers or different species (Brabec et al., 2010). The final result is that despite of large possibility of appliances, the fullerenes are far from being a common product in our life. Main problems come from the hardness to produce them with high yield and selectivity with respect to undesired products (Kataura et al., 2001). These problems is very common in nanoparticle production and selectivity is typical of flame synthesis (Hou et al., 2009). Other methods for fullerene production have been proposed through years but flame reactors, already used just after fullerene discovery, remain of great interest for the possibility of easy scale up to industrial level. Recently scaled up flame-based reactors have been proposed an analysis of their parameters has been conducted (Takehara et al., 2005). However the process of fullerenes formation is not completely understood and the study are mainly based on empirical evidences more than previous precise calculations (Irle et al., 2006). It is generally accepted that the process of fullerene has lot of similarities with soot first nuclei formation (Chung and Violi, 2010). For a certain period fullerene were believed to be the initial step in soot formation (Homann, 1998). However, nowadays, the differences between two processes have been clearly stated and clarified. Fullerene production remains a sub-process of soot formation that can become relevant and dominant in certain conditions. Generally speaking fullerenes are a stable intermediate compound during the aromatic growth of gas phase polycyclic aromatic hydrocarbons (PAHs) in certain conditions (Richter and Howard, 2000a). Usually, in order to have the high yield in fullerenes, low pressure conditions, a rich equivalence ratio close to stoichiometric, and a highly unsaturated hydrocarbon such as acetylene and benzene (Pope et al., 1993) are used.

However, even when these conditions are achieved soot production is still ongoing and thus the final product result a mixture of fullerene and soot, which have to be chemically separated. The control of the process has to move toward an higher yield in fullerene and higher selectivity respect to soot particles (Rotello et al., 1993).

2.4.2. Nanotubes

Carbon nanotubes are belonging to the wider class of carbon nanofibers (Merchan-Merchan et al., 2010). The evidence of these classes of compounds goes back to Singer and Grumer (Singer and Grumer, 1958). After the discovery of fullerenes, the seeking of particular carbon compounds have

driven to the individuation of multiwall carbon nanotubes (MWCNs) (Iijima, 1991) and later to single wall carbon nanotubes (SWCNs) (Iijima and Ichihashi, 1993). Pulsed laser vaporization (Maser et al., 1998), arc-discharge (Gamaly and Ebbesen, 1995, Iijima, 1991) and chemical vapor deposition (CVD) (Cassell et al., 1999) rose as the first processes to produce carbon nanotubes. However due to high production costs and low feasibility at industrial scale of the process, alternative route to produce this material have been investigated. Together with the investigation on formation pathways many efforts have been devoted to discover the properties of CNTs and their possible applications. Nowadays CNT production involves metallic catalyst on which CNTs can growth in disordered way (Dupuis, 2005) or in a specific direction (Merchan-Merchan et al., 2010, Merchan-Merchan et al., 2004). Morphology, number of walls, orientation and eventual interaction with other material can strongly influence the possibility to apply this material to different fields (Merchan-Merchan et al., 2010). From this point of view the control of the process results again of fundamental importance. Flame synthesis of CNTs received lot of attention and nowadays a set of reactors have been individuated to produce a noticeable amount of CNTs. Both premixed (Howard et al., 1991) and diffusion flames (Vander Wal, 2000) have been found to be suitable for production starting from many different fuels generally with a metallic catalyst (Vander Wal, 2002). In some case it is also possible to produce CNTs without a catalyst making the process even more interesting for industrial plants (Merchan-Merchan et al., 2003). As for the fullerenes, CNTs results a particular pathway of more general high molecular mass aromatic hydrocarbon formation and growth. Soot particles are always present as by-products in the environment and can affect both the final form of the material and the costs of global process. The design of the catalyst both in terms of composition and morphology and its feeding to the combustion system are key parameters for the production on lab-scale and large scale of CNTs. Moreover different methods, such as the use of electric fields (Lou et al., 1995, Merchan-Merchan et al., 2004) and nanotemplates (Cui et al., 2005) have been tested with reliable results for the production of CNTs with certain feature in flame synthesis experiments.

2.4.3. Graphene sheets

The thinnest material on the Earth (Overbye, 2010). This is how the graphene or the graphene sheet is presented: an atomic layer of fully sp2 oriented carbon atoms (Service, 2009) . As for the related materials such fullerenes and CNTs, this material received an increasing attention from its discovery. Recently isolated by a simple experiment (Novoselov et al., 2005a, Novoselov et al., 2005b), which was worth the noble prize, graphene has been already characterized experimentally by different groups and studied by theories of modern physics for many years (Stauber et al., 2005, Radovic and Bockrath, 2005), even before Novoselov's experience (Hwang, 1995, Affoune et al., 2001, González et al., 2001, Shioyama, 2001, Duplock et al., 2004, Horiuchi et al., 2004).

The two dimensionality of this material makes it suitable for particular applications in the field of electronic (Yazyev and Louie, 2010, Bonaccorso et al., 2010, Avouris, 2010, Westervelt, 2008). The production of small amounts has been achieved with several methods ranging from mechanical

exfoliation (Novoselov et al., 2005b) or cleavage (Shioyama, 2001) to chemical exfoliation from Si-C wafer (Aristov et al., 2010). Many other pioneer techniques are in course of development, since this field results almost totally new for the scientific community (Lemme et al., 2009, Hernandez et al., 2008, Park and Ruoff, 2009). Since graphene is Younger than other related materials, graphene flame synthesis is looked with great interest for similar reasons described before for other nanomaterials (Memon et al., 2011b, You et al., 2011).

The growth mechanisms that can lead to the formation of isolated and stable graphene sheets are far from being understood (You et al., 2011, Whitesides et al., 2009, Whitesides et al., 2007). This challenge is faced both from semi-empirical point of view, trying several combustion conditions and drawing conclusions from experimental evidences (Ossler et al., 2010, Guo et al., 2011, Li et al., 2011), and with accurate calculations involving molecular dynamics (You et al., 2011) and *ab initio* method (Mattausch and Pankratov, 2007, Min et al., 2007).

2.4.4. Caron fiber, nanodiamonds and other carbon nanostructure

Many nanostructures based on the possible arrangement of carbon atoms were produced and used even before the discovery of fullerenes. Mayor part of these compounds has not a unique characteristic but they exhibit a range of characteristics in dependence on the way they are formed and after treated. Most part of these materials can also be found in nature in different form. The engineering effect on this material is particularly noticeable in the production of nanostructures of tailored sizes. Even if purity of material can be not that high as in fullerene CNTs and graphene these can still be used in many different fields.

Carbon arrangement at nanoscale can assume different form from those exposed before. In particular carbon nanofibers, CNFs, as filamentous carbonaceous material were already observed in the past. In the beginning they were substantially a pollutant dangerous for the surviving of catalyst (Rostrup-Nielsen, 1984). CNTs were discovered also due to the increased knowledge in controlling nanofiber formation (Terry et al., 1994). CNFs can be found in form of nanocoils (Varadan and Xie, 2002) or nanoribbons (Campos-Delgado et al., 2008) . The production by flame synthesis of these materials has many similarities with carbon nanotubes. In a certain way these materials can be seen as imperfect products, which still exhibit interesting properties. Despite of lower quality CNFs coils or ribbons results easier to be prepared with lower costs.

Nanodiamonds are nanostructures organized as diamonds lattice generally found in detonation event (Dolmatov and Kostrova, 2000). Recently they have been found also in common candle and have showed possibility to be applied to drug delivery science (Li et al., 2010, Lam and Ho, 2009, Moreau et al., 2009, Donnet et al., 1998).

Onion-like nanoparticles (Maksimenko et al., 2010, Donnet et al., 1998, Kroto, 1992) are probably the nanostructured material most similar to annealed soot particles. The onion-like structure has been also individuated in soot particles, although with high number of defects. The constitution of these multicage system offer lot of implementations; for example, they exhibit solvent affinity very different in dependence on their features.

Coating with multilayer of carbonaceous material organized at nanoscale can be easily applied to the coating field. The possibility to have a super hydrophobic thin layer for ultrathin coating has been already explored by Puri's group giving an example of possible application of these materials (Mazumder et al., 2011).

The main reason for researching these materials is due to the fact they are more easily to be produced in large quantity and with higher selectivity. This allows to have an easy scale up from lab-scale to plant scale (Jiménez et al., 2009). In particular flame synthesis is one of the most common ways to produce them. The possibility to use large number of fuel and a wide range of combustion condition in terms of reactants ratio and temperature history make this process very appreciable.

3. Aim of thesis

This work has been focused on carbonaceous nanoparticles. The thesis proposes experimental and numerical tools to investigate and control the combustion processes and the by-products emitted from lab-scale and real actual operating combustion systems. A deepen knowledge of processes can be fundamental step in order to produce carbonaceous nanomaterial with tailored properties such as size, chemical composition and internal structure.

4. Carbon particle formation in flames: state of the art

In this chapter a description of the main opinion of the scientific community about carbonaceous particle formation and evolution in combustion environment will be furnished. Experimental techniques and numerical studies that led to these conclusions were described further

on. Hints of particle features will be furnished whether these would be useful to better understand process description, leaving to chapter 5 a more detailed description.

Carbon particle formation has been faced through years and some round-table discussions (Bockhorn, 1994, Bockhorn, 2007) have represented milestones for upgrading and sharing the knowledge in this field. However, a deep and complete knowledge of all mechanisms involved in particle formation is not achieved yet (D'Anna, 2009, Wang, 2011).

Probably inception mechanism, i.e. the step which leads to the formation of three dimensional structures starting from gas phase molecules, remains the less understood topic. To face this problem, combustion community has extended its field of interest toward an interdisciplinary route, which largely involves physicists and chemists beside of engineers. This melting pot of knowledge has opened new frontiers in this research field. Molecular dynamic (Schuetz and Frenklach, 2002, Herdman and Miller, 2008), ab initio calculations (Kubicki, 2005, Kubicki, 2006), mass spectrometry (Apicella et al., 2007, Grotheer et al., 2004, Grotheer et al., 2011) and use of synchrotron light (Yang et al., 2007, Li et al., 2008, Taatjes et al., 2008) represent innovative techniques not only for combustion community and are becoming fundamental in the study of combustion formed particles.

The main pathway for formation process starts with gas phase pyrolysis and oxidation of fuel, moving in some conditions toward the formation of large gas phase PAHs (see 4.1). This part result fundamental for a critical analysis and prediction of particle formation in flames. The stiffness of the problem strictly links gas phase products with particles, making the analysis even more complicated.

After the formation of large PAHs the process of growth continues leading these molecules to form larger structure. At certain point, these structures assume a three dimensional shape (see 4.2), stop to behave like gas phase species and start to exhibit properties typical of condensed phases (density, viscosity plasticity etc.) (see also 5.2).

The formation of these incipient three dimensional structures open the route to the loading of particulate matter, mainly operated by gas phase species such as acetylene and PAHs (see 4.3). This process is generally chemically and thermally driven and has been largely studied by combustion scientific community.

Another phenomenon found in flame is the coagulation (see 4.4). The formation of new entity through coalescence coagulation, or aggregated particles through aggregating coagulation, has been found and extensively studied for metallic combustion formed nanoparticles. The sintering process, which is at the base of the two phenomena and their discerning, has been recently evaluated also for carbonaceous particles. Primary particles are now better distinguished from aggregates with respect to the past.

A side work about combustion formed particles can generally be found in the study of the oxidation mechanisms of these latters (see 4.5). Catalytic and homogenous oxidation of soot particles have been studied in the past by aeronautical and engine research groups in order to find a better way to minimize the final emissions of real combustion devices. On the other hand people who were looking at the formation process of the soot, paid attention to the oxidation for its role in diffusion flames. Both these study routes are now focused more on the features of the particles coming from combustion devices, such as reactivity and, thus, possibility to be oxidized. In fact, a different production process can influence not only the natural emission of a combustion device but also the efficiency and the effectiveness of the after treatment stages.

Most of the processes mentioned above are generally accepted, even if specific discussions about the exact mechanisms are still ongoing. On the other, lately new data on some soot samples have started the debate on the remarkable presence of aliphatic compounds on the surface of particles. This different evolution has been not completely clarified and widely accepted by combustion community.

4.1. Gas phase reaction mechanisms

Gas phase analysis is of fundamental importance to characterize the combustion process of different fuels and in different conditions. In particular, the analysis of the main gas phase products, such as H2O, CO2, H2 and CO for a hydrocarbon combustion, can give and immediate response regarding the final combustion efficiency. Moreover a deeper analysis of other intermediate products of fundamental relevance, such C2H2, CH4 and some radical species such as OH, can give even more information on the evolution of combustion.

A complete analysis of mechanisms involved in primary fuel oxidation/decomposition it is beyond the aim of this thesis and it is remanded to some review articles present in literature (Ranzi et al., 2001, Simmie, 2003, Zádor et al., 2011). However, the formation of large molecular weight compounds, in particular PAHs, has to be given, at least as hints, since it is strongly related to the formation of incipient particles and soot growth.

Nowadays PAHs are universally recognized as the precursor of soot particles (D'Anna, 2009, Wang, 2011) and their kinetics have been extensively studied and reviewed (Richter and Howard, 2000b, Frenklach, 2002b).

This chapter will move from the description of the main formation pathways of benzene, the first aromatic compound. This step is of fundamental importance for the understanding of the multi-ring structure formation, that, in some way, can be seen as an extension of the same mechanism (Frenklach, 2002b). Two main reaction routes have been individuated for the formation of first

aromatic ring: the first one involves C2H2, whereas the other involves radical species. In both cases the formation of benzene comes from a sequential addition of small molecules.

The acetylene pathway for benzene formation goes back to 1980's (Frenklach et al., 1985, Bittner and Howard, 1981) and it has been studied for more than 10 years in order to catch correct values for thermodynamic properties and rate constants (Frenklach, 2002b). After all, this pathway has been found to be determinant at medium-low temperature regime (Frenklach et al., 1988, Miller and Melius, 1992b), which is not typical of a premixed rich flame of aliphatic.

On the other hand, to fill this gap another route has been proposed by Miller and Melius (Miller and Melius, 1992b). The self-recombination of propargyl radicals has been proposed as key step in first aromatic ring formation. Successive studies have recognized this reaction and some similar (Colket and Seery, 1994, Marinov et al., 1998b) to be predominant in high temperature environment.

Multi-ring formation has been almost immediately seen as the limiting step in particulate formation due to its low rate. As for the first aromatic ring, many pathways have been proposed through the years (Frenklach and Wang, 1991, Melius et al., 1996, Marinov et al., 1998a, D'Anna et al., 2000) and some of them have been found to be more reliable for the prediction of these high molecular mass compounds. Moreover, a general expression for the molecular growth has been found out with possible application to larger compounds (Frenklach, 2002b).

Mechanisms can be again divided on the base of the molecules involved. Acetylene is again one of the fundamental reactants for the formation of PAHs. The idea of using a sequential addition of acetylene goes back to Frenklach and Wang paper, presented at the Twenty-third International Symposium on Combustion (Frenklach and Wang, 1991). They used for the first time the acronym HACA (H-abstraction-C2H2-addition). Even if the term was only due to the word limit of the conference paper, its appeal made it a worldly known term to define this process. As suggested by the extended name, this reaction pathways starts with an abstraction of a hydrogen atom to form a radical activated species. Successively the addition of an acetylene molecule increases the molecular weight of the species. These two steps have been widely studied. A brief discussion of these mechanisms will be useful for the successive description of the larger aromatic compounds growth. The formation of radical through the loss of a hydrogen atom can be addressed in different ways: the abstraction can be driven by another radical such as H or OH, largely abundant in flame conditions, or by other gaseous species or via unimolecular reaction. In dependence on the temperature and species concentration, these pathways can have a different relevance. However, the abstraction driven by H and OH atoms has been found to be dominant for a large number of flame conditions (Wang and Frenklach, 1997). Of course, the reversibility of the process is of fundamental importance since it balances the formation of radical species (Mauss et al., 1994). It has been found that the reverse reaction step is important when the recovery of energy is not addressed. Otherwise the reaction can

be considered almost irreversible; this is the case of the formation of a series of PAHs ,which minimize the energy, called stabilomer series (Stein and Fahr, 1985). Another important aspect of the growth through acetylene is the edge migration. This phenomenon has been deeply investigated by Frenklach, Moriarty and coworkers in several papers (Frenklach et al., 1998, Moriarty et al., 1999). The final finding has suggested the possibility to have a formation of a closed ring after the formation of a 5-ring structure. The reverse reaction has been taken into account finally sketching a continuous change in the edge of a large aromatic structure. Indeed, the larger is the aromatic multi-ring structure, the higher is the migration rate (Frenklach, 2002b).

The other route to form multi-rings species involves resonantly stabilized free radicals (RSFR) (Castaldi et al., 1996, Marinov et al., 1996, Marinov et al., 1998b). Resonantly stabilization is typical of aromatic species due to their high capability to delocalize the unpaired electron through all the electronic clouds. Radical recombination is favored by the low activation energy; at same time they can reach considerable high concentration in flame environment. From the radical recombination many different PAHs can be formed. Naphthalene, whose formation has been firstly explained with HACA mechanism, has been found to be formed through the cyclopentadienyl recombination or through benzyl and propargyl radicals (Marinov et al., 1998b, D'Anna et al., 2000). These routes are fast enough to provide large amount of naphthalene in flame environment. Phenanthrene and biphenyl are formed in similar way involving cyclopentadienyl-propargyl and cyclopentadienyl-indenyl recombination respectively (Marinov et al., 1996, Marinov et al., 1998b).

Past and more recent literature is still debating on the relative importance of the HACA and RFSR mechanism for the formation of PAHs in combustion environment (Richter and Howard, 2000a, Frenklach, 2002b). Since the combustion conditions can be quite different in terms of gas phase species concentration and temperature history, very often some extreme conditions have been analyzed drawing generally valid conclusions. As for other steps in particle formation, it is very likely that these mechanisms march together and just in some case one is completely prevalent with respect to the other. The final picture of gas phase PAHs in combustion results a complex dance with more than one leading role

4.2. Inception

Inception is the fundamental step that, moving from two dimensional structures, leads to the formation of three dimensional ones. This definition tries to be as wide as possible, since any restriction could affect the general validity of some considerations around this process. In fact, the individuation of the first particle, which belongs to the class of particulate matter, can be far enough from the gas phase products and some important species and processes could be missed (D'Anna, 2009, Wang, 2011). Moreover, the hardness of defining this “first particle”, in terms of size,

morphology, thermodynamic and physical properties, makes the task of finding the missing link between particles and gas phase even harder. Indeed, a clear distinction between these two classes of compounds has been somewhat ruled out by recent findings in this field. Hereafter, the description of the inception process will be presented as a growth process which involves species with molecular weight between 128-202amu (naphthalene-pyrene) and 2000amu. These latters have an equivalent spherical diameter around 1.5nm. These high molecular mass compounds exhibit intermediate characteristics between gas phase and solid state carbon compounds, which will be described further on (see chapter 5). The process of growth will be treated separately for chemical and physical pathways. The first one is quite similar to the steps described above for multi ring formation, whereas the physical one is somewhat different in terms of interaction forces involved.

4.2.1. Chemical path for particle inception

Aromatic nature of high molecular mass compounds found in flame has been universally recognized. Small gas phase PAHs have been individuated as main precursors of these compounds (D'Anna, 2009, Richter and Howard, 2000a, Bockhorn, 1994, Bockhorn, 2007). However the growth process of PAHs can lead in principle to very different compounds. The acetylene growth described for gas phase is thought to form always a closed ring, enlarging the wideness of aromatic island and leading towards larger graphene-like sheet with a high degree of aromatization. In fact, after pyrene formation, this growth mechanism would lead very fast to the formation of larger pericondensed structures (Frenklach, 2002b). The first aromatic in this series is coronene followed by larger molecules such as circumcoronene. These very large structures would remain in the two dimensional world, until some other process occurs. The detection of similar species in flame has helped in drawing the conclusion that these species could explain the gas-to-particle transition. Homman proposed a bending of the structure on the base of morphological similarity between soot particles and fullerenes to justify the three dimensional structure formation (Homann, 1998). The presence of five member ring necessary to bend the structure, present also in fullerenes, was linked to the relevant amount of this kind of compounds in flame. This hypothesis appears now overcome. This kind of so large molecules can be hardly found in flame environment, probably just as trace species and in particular conditions (Wang, 2011). Moreover recent thermochemical calculation almost ruled it out (Wang, 2011). However, acetylene addition and the pericondensed pathway are still reliable up to certain molecular weight. It means that certain species, such as pyrene-to-coronene PAHs can play a dominant role in inception process (Schuetz and Frenklach, 2002, Herdman and Miller, 2008).

Another important chemical pathway, that has to be considered within inception process, involves the PAHs radical recombination. Based on the similarity for the formation of the first and the second aromatic ring, this process has been described for the first time by D'Anna and coworkers (D'Anna et al., 2001b). The main idea is that the formation of aromatic aliphatic linked hydrocarbons

(AALH) overtakes the large pericondensed ones. AALH can be formed through the combination of an aromatic radical with another radical or its stable form. The formation of an aliphatic bond, or sigma-bond, within the structure introduces a non-rigidity point. The structure can rotate around this bond according with the laws of free energy and quantum mechanics. This biphenyl-like structure can go from very simple interconnection between PAHs, such as the formation of bi-pyrene, up to very complex geometry which involves tens of PAHs.

These structures can grow by chemical addition of PAHs or acetylene. The final compound would have memory of the different species added since it was formed. In fact, since the first aliphatic bond is introduced within the structure, the planarity is lost due the free rotation around the axis of this bond. However, topologically speaking, these structures are more like a large irregular surface which is bent into itself, rather than a real three dimensional structure. In fact, in the above description no growth mechanism out of plane occurs. However, the original hypothesis takes these structures as the only responsible for the formation of first compounds which can be considered a particle.

In several conditions this pathway has been demonstrated to be dominant and several experimental and numerical investigations have found that small particles can effectively look like a hank of relatively small PAHs (D'Anna, 2009, D'Anna et al., 2000, D'Anna et al., 2001b). However, these findings are not matching the final form of soot particles, suggesting that some other process induces higher degree of aromatization in the structure during the evolution in flame. This process is mainly linked not only with the final form of the structures but also with their inception mechanism. Hence, aromatization, or graphitization process (Dobbins et al., 1996) can form a stronger linked and more stable structures able to survive for a long enough time in flame conditions (see also paragraph 4.3).

In conclusion, chemical pathways are not completely explaining the inception process. Large efforts in small particle characterization have furnished lot of clues for the understanding the first moments in particles formation. These features have revealed that large macromolecules can be formed and grow. Due to chemical nature of the process high temperature and concentration of precursors (small gas phase PAHs) can strongly favor this pathway. A significant large presence of acetylene can influence this route moving toward a more aromatized structure.

4.2.2. Physical path for particle inception

Physical path involves different forces with respect to chemical reactions and the final product is not a chemically bonded structure. The base of this process is linked with the van der Waal intermolecular forces. These forces are responsible for the attraction of instantaneous and/or permanent dipoles present in the molecules. Moreover they are not anisotropic and thus depend on

molecule orientation beside of the chemical nature of the molecules involved (Schuetz and Frenklach, 2002, Herdman and Miller, 2008, Chung and Violi, 2011). In the PAH molecules, the pi-electron cloud extends over the aromatic island formed by the condensed aromatic rings. This large electronic structure can behave as a part of the dipole attraction involving van der Waal forces. Indeed, the attraction between two PAHs is strongly linked to the interaction of the pi-electron planes and thus to the orientation these planes. Once the two planes are parallel oriented, the attraction between two planes can be enough strong to hold together the molecules. In graphite the out of plane interaction is due only to these forces and the strength is around 5kJ/mol per carbon atom (Donchev, 2006). The extension of the plane of interaction up to hundreds of atoms might make this interaction as strong as a chemical bond.

Out of plane interactions of gas phase PAHs and their stacking have been supposed to be the key step for the formation of three dimensional structures (Miller, 1991, Frenklach and Wang, 1994, Frenklach and Wang, 1991). Through years the PAHs considered for this process ranged from very large molecule with more than 7 rings to very small PAHs like naphthalene (Schuetz and Frenklach, 2002, Herdman and Miller, 2008). Great attention has been paid to pyrene stacking (Sabbah et al., 2010), considered the first of aromatic with a high sticking efficiency. Lot of studies has been conducted to experimentally evaluate the concentration of PAHs in flame and to numerically test the influence of the stacking on the final concentration of small and large particles. For many PAHs, which can be found in flame environment, the calculated strength of interaction is smaller than kinetic energy of the molecules. This mismatching is the weak point of the theory of stacking. However the calculation of the interaction results not easy. Many side effects have to be considered to correctly represent the real situation. Presence of other molecules, residual charge on the molecules involved (ions), correct method of calculation of potential involved in the process with Density Function Theory (DFT) and ab initio calculation, dispersion of energy due to intramolecular forces and re-arrangement, additional vibrational level due to the presence of side chain in the colliding molecules are the main issue that still remain unsolved in this investigation field. On the other hand, experimental evidences of the presence of interacting planes within the first particles have been recognized and are pushing the scientific community toward filling this gap (Grotheer et al., 2004, Grotheer et al., 2011).

Despite of this lack of knowledge, lots of semiempirical methods for the evaluation of this process have been carried out and implemented in numerical models. Most of reaction rate expressions come from some evaluation on the sticking efficiency of similar species with some assumption on the potential of interaction. Further discussion on numerical models and way of threat this delicate issue will be given further on (see Chapter 7).

In conclusion, most part of the scientists believes that stacking is fundamental in the inception process but the exact mechanism is still under debate.

4.3. Surface growth

Once formed the first particle, or, more correctly, the first species which no longer behaves like a gas phase compound, its evolution is driven by some specific processes. One of these processes is the molecular or surface growth. The term surface growth immediately refers to the fact that the addition of molecules from gas phase to existing condensed compounds can occur preferentially on the surface. Although particles exhibit some nanoporosity, the addition rate is generally fast compared to diffusion inside the particle.

The most important species involved in molecular growth is acetylene (Frenklach and Wang, 1994). Molecular growth is responsible for the soot loading, i.e. the formation of large amount of particulate in terms of volume fraction. In particular, the addition of acetylene follows a reaction pathway similar to the HACA mechanism found and described for the gas phase (Frenklach and Wang, 1991). As for large PAHs, one of reasons of this easy addition relies in the fast migration edge that allows acetylene to form a closed ring each time is added. This phenomenon has been theorized and modeled by Frenklach group after his development of HACA mechanism. However the link between acetylene and soot was already investigated and some empirical correlations had been founded (Frenklach et al., 1985).

Together with acetylene other gas phase species can contribute to the growth of particles. In particular aromatic compounds have been individuated as alternative route to acetylene pathway. These compounds can be chemically linked to particles forming aliphatic linked structure similar to those found in the very first particles (D'Anna et al., 2000, D'Anna et al., 2001a, D'Anna et al., 2001b). Similarly aromatic growth can lead to the formation of larger particles independently from acetylene addition. If this process takes place the character of these large particles would be very similar to small particle one, in contrast with experimental evidences. As stated in 4.2.1 aromatization process can form larger aromatic islands and thus a more packed structure (Dobbins et al., 1996). Moreover, as for the inception, probably for most part of the combustion conditions particles come from both pathways: surface growth by acetylene and by aromatics contribute together for the final form and amount of particles (D'Anna, 2009, D'Anna et al., 2009).

However, in both cases reactions are depending on the active sites on particle surface. In fact, the reactions involve molecular species and particles with active sites (Woods and Haynes, 1994). These active sites have been discussed in literature with different hypothesis on their nature. However since the surface growth shows lots of similarity with gas phase HACA and aromatic growth also these active sites have been associated with the correspondent in PAHs chemistry (Frenklach and Wang, 1994). It means that radical formation on soot surface is the limiting step for the surface growth. In fact during the study of the evolution of the particles in flames, it came out that aromatization process changes the physical properties, as stated before, together with reactivity of particles and, indeed, the number of active sites on the surface. On the other hand a correct

characterization of the number of active sites is mandatory for the correct prediction of molecular growth. From this point of view molecular growth is depending on aging process occurring on surface (Blanquart and Pitsch, 2009, Sirignano et al., 2010).

These studies are not conclusive for the understanding of the aromatization process since it is not possible to isolate this process. However actual knowledge suggests that the aromatization can be driven by very high temperature environment and, more important by some radical species, able to extract hydrogen from particles. This extraction makes the particles more aromatic and reduces the number of active sites on the surface.

As mentioned in the first part of this chapter, recent experimental studies evidenced the aliphatic content in soot particles (Cain et al., 2010, Cain et al., 2011). The role of aliphatic seems to be predominant on the surface of the final form of soot particles. However, great uncertainty is still present for the results. Since most part of the studies has been conducted on sampled material, artifacts due to sampling system are still possible and can significantly affect the conclusions. Moreover this process does not dramatically affect the general picture of particles formation and growth here presented, even if leaves some open question in particle evolution.

4.4. Coagulation of particles

Coagulation process controls the numerical concentration, the size and the final morphology of soot particles (Smoluchowski, 1916). Coagulation of particles belongs to the aerosol science and, in fact, early works can be addressed to this field (Friedlander and Wang, 1966, Lai et al., 1972, Pich et al., 1970). However most of the studies regarded large aggregates and agglomerates whose size range from hundreds of nanometers to some microns. These particles belong to the continuum regime according to the classic theory. However as the size decreases the free molecular regime is approached and the influence of nonlinear factor, e.g. the Cunningham correction for the diffusivity, becomes not negligible. This is the case of combustion formed particles. Soot is emitted generally in form of large aggregates of a hundred nanometers. Despite of these relatively large compounds, particles formed in combustion range from tens of nanometers for primary soot particles down to few nanometers for the very small particles.

Moreover flame conditions are quite extreme regards number concentration. Studies on size distribution function of particles below 10nm showed that in a rich premixed flame particle number concentration can arise up to 10^{14}#/cm^3 (Sgro et al., 2003), whereas larger ones are just of few orders of magnitude less. This numerical concentration is fundamental not only for the evaluation of the emissions of a combustion system but also for the evaluation of the evolution of particles in flame. In fact, different coagulation rates lead to the formation of different particles in terms of size and number concentration (D'Alessio et al., 2005). These changes reflect into different reaction rates for

other reactions, such as surface growth. It means that the control of the process, both to prevent emission and for producing *smart* nanoparticles, passes through a correct understanding of particle coagulation.

Particle coagulation in flame has been studied for many different types of elements. Metal particles have received great attention in this sense (see Chapter 2.3). However the knowledge achieved for this kind of particles can be in a certain way extended to carbonaceous particles. Lot of studies moved from this consideration and tries to threat the coagulation in a general way. Unfortunately some parameters that control this process strongly depend on physical characteristics of particles. Indeed, the combustion conditions, which are responsible for the nature of the particles and control the inception process, indirectly affect also the coagulation rate and, thus, the surface growth (D'Alessio et al., 2005).

Soot particles were studied firstly in the form of chain-like structures, which is also their final form. Starting from this point, the studies went deeper in the analysis of the primary constituents, i.e. primary particles. Further on the new advances in technology allowed to investigate inside primary particles with high precision and determine their internal structure with enough reliability.

4.4.1. Coalescent coagulation

Properties of particles and their coagulation efficiency have been correlated on the base of experimental evidence and numerical calculations. In particular the internal structure of particles has been found to evolve with residence time in the flame (Calcote and Manos, 1983, Ciajolo et al., 1996, Megaridis et al., 1996, Alfè et al., 2010). This evolution usually moves particles toward a more rigid structure through an aromatization process. A solid state character can be reached and at certain point some of the viscoelasticity typical of very small particles get lost (Minutolo et al., 1998, Barone et al., 2003).

At same time the coagulation process takes place with different final products. Very small particles or, more properly, condensed species, due to their viscoelasticity during coagulation act like small droplets and tend to form a single larger particle. This process can be associated with coalescence and after that the identity of the colliding particles is lost (Dobbins and Megaridis, 1987). This process is quite similar to what happens during physical inception process. Also in this case van der Walls forces are responsible for the attraction of the species and the formation of intra- and intermolecular bonds. Comparing this process to those studied in metal nanoparticles formation, it is possible to see lots of similarities. In metal nanoparticles usually sintering process is used to explain the phenomenon that leads to the formation of a new larger particle from the collision of two smaller ones (Camenzind et al., 2010). Sintering time scale is short compared with contact time when this

process is effective. Changing the properties of the particles sintering time scale can change moving toward conditions unfavorable for coalescence.

Looking at the results on the dimension of primary particles and very small nanoparticles, it is almost universally accepted that size dependent coagulation is driving toward a bimodal distribution in particle formation during combustion (Zhao et al., 2003, Sgro et al., 2007). The small mode is due to particles as small as 2-4nm whereas large primary particles with sizes of 15-30nm can be found in the larger mode. Sticking coefficient measured for small nanoparticles is temperature dependent and in flame conditions can be up to three orders of magnitude smaller than at room temperature. This very low sticking efficiency makes these nanoparticles a not negligible intermediate state from gas phase to large particles. They survive along the flame reactor and can be emitted (Minutolo et al., 2008). The exact value of coagulation efficiency depends on the internal structure of these nanoparticles, as stated before. However, for a large number of flame conditions, efficiency relies in a narrow range of values. Coalescence efficiency increase reaching almost the unity for particles around 7-10nm, which can be seen as primary soot particles (D'Alessio et al., 2005).

Coalescence efficiency of large primary particles decreases rapidly with increasing size. In flame environment it is not easy to find isolated primary particles with size larger than 40nm. On the other hand, particles as small as 10nm can still coalesce forming larger ones. This means that primary particles can relies just in a narrow range of values as found in flame. These particles are hard to be found as isolated ones because, even if the coalescence efficiency is low, the total coagulation efficiency is high. Indeed, large aggregates are immediately formed and the final form of soot is reached (Mitchell and Frenklach, 1998).

4.4.2. Aggregating coagulation

The particle size distribution functions of soot can be measured in lab scale or real combustion devices or numerically calculated in flame predictions (Puri et al., 1993). In both cases it has to be considered that large aggregates are the main constituent of soot. Hence, the mean dimension of an aggregate is only one of the parameters that can define its nature. Many experimental and numerical works have given some hints about the correction necessary to take into account the nonsphericity of these aggregates (Mitchell and Frenklach, 1998, Puri et al., 1993, Farias et al., 1995, Koylu and Faeth, 1992, Charalampopoulos and Chang, 1991, Köylü et al., 1995). These aggregates usually are in fractal form. Hence, one of the most important parameters is the fractal dimension. This parameter has been evaluated for a large number of carbonaceous aggregates and it ended up that it relies in a narrow range, between 1.8 and 2 (Patterson and Kraft, 2007, Balthasar and Frenklach, 2005a). Into these aggregates there is a large variety of particles in terms of structure and size due to the fact the final form is usually the result of a continuum process occurring along the flame. The mean dimension of aggregates and their molecular weight is thus dependent on the flame history which these aggregates

undergo. However, despite of this large number of variable some studies have showed that particle size distribution function is self-preserving, approaching a limit curve that in the case of Brownian motion can be assimilated as a lognormal distribution (Balthasar and Frenklach, 2005b, Friedlander and Wang, 1966).

Aggregates are formed from coagulation of two primary particles, or smaller aggregates, which have no longer the capability to give coalescent coagulation. For these large particles the coagulation efficiency is unitary. However the definition of the starting point of aggregating coagulation, after coalescence stops, is harder. Probably there is not a break point in this process but, more likely, there is a large moiety of intermediate situations. It means that some particles have a partial capability of giving coalescence coagulation or, more correctly, they partially coalesce. The result is a compound in which traces of the identity of colliding particles can be still observed but a new species is formed at same time.

4.5. Oxidation

Oxidation process of large soot particles and small nanoparticles has been studied in past years (Neoh et al., 1985, Echavarria et al., 2011). A first great distinction can be done between gas phase oxidation and catalytic oxidation. The latter is widely diffused in after treatment system, e.g. in engine particulate filter stages, due to the possibility to maintain low emissions (Messerer et al., 2006, Choi and Foster, 2006, Seipenbusch et al., 2005, Seipenbusch and Friedlander, 2004, Retailleau et al., 2004). These systems are becoming one of the most expensive technologies in the car design. On the other hand, combustion technology demonstrated to be able to produce much less amount of soot reducing this problem at source stage. Moreover, the mean size of particle produced in combustion is decreasing and their number concentration is increasing. Oxidation of these new particles can represent a new border line problem for the after treatments systems (Vander Wal and Tomasek, 2003).

Gas phase non-catalytic oxidation has been on the contrary studied as a limiting stage during soot formation (Villasenor and Kennedy, 1992, Stanmore et al., 2001, Prado et al., 1981, Neoh et al., 1985). The influence on total amount of soot produced depends on the oxidation resistance of soot itself and on the capability of the combustion environment to give place to oxidation process. The first problem is linked with the characteristic of the particles produced and in particular with the possible points of attack by oxidant species (Vander Wal and Tomasek, 2003). Molecular oxygen, O_2, and hydroxyl radical, OH, are the main oxidant species in combustion environment. Other species such as CO2 (Kapteijn et al., 1994) and water (Stanmore et al., 2001) have been selected as oxidant species in some specific and not ordinary conditions. Molecular oxygen is not easy to be found in rich environment and thus is generally more effective in lean conditions. OH radical instead is always

effective due to his presence in almost all combustion conditions, becoming the most important and almost the only one present in rich conditions (Neoh et al., 1985).

Oxidation process is always active and thus intimately linked with growth process. This makes the correct evaluation of growth process even harder. An underestimation in oxidation process can easily lead to an overestimation in total soot amount.

In order to better study oxidation process a sort of decoupling has been tried in the past. In particular Sarofim group used a combustion generated soot aerosol as feed for a secondary combustion process (Neoh et al., 1985, Echavarria et al., 2011). The secondary process was conducted in an environment where particle formation does not occur, i.e. lean, stoichiometric or slightly rich conditions. In these conditions, the oxidation of the fed particles could be systematically studied. However, even this smart attempt suffers of some problems linked to sampling process and evaluation of the particle size. This latter is quite hard to be correctly evaluated with conventional and commercial systems when sizes approach molecular regime.

A global evaluation of reaction rate based on this and other experiments, together with numerical prediction for kinetic expressions, represents the actual knowledge of oxidation process (Kazakov et al., 1995, Harris and Maricq, 2002). However since the first studies on the oxidation process two kind of oxidation steps were individuated: surface oxidation and oxidation-induced fragmentation (Neoh et al., 1985, Garo et al., 1990). The first process is always active and is due to all oxidant species. The latter regards both aggregates and primary particles and has been found to be active in some conditions and mainly driven by molecular oxygen. Surface oxidation limits the total amount of particles and reduces their size. Oxidation-induced fragmentation mainly affects the number concentration of particles and their size. This aspect indirectly affects soot reactivity: an increase in number concentration and surface area enhances all the processes, included surface oxidation. This phenomenon can strongly affect evaluation of global oxidation rate in lab-scale and real combustion systems. Moreover the smaller particles produced by oxidation-induced fragmentation can be emitted. These will have dimensions down to those of small nanoparticles produced in combustion after inception process. On the contrary, their characteristics can be similar to those of mature soot particles, from which they come from.

4.5.1. Surface oxidation

Oxidant species can attack the particles wherever some weak or activated points are present. The nature of these points can be different in dependence on the oxidant species (Vander Wal and Tomasek, 2003). Molecular species, such as oxygen, need to have an activated site in order to effectively react. These active sites are totally similar to those needed for molecular growth. This means that growth and oxidation by molecular species compete for the same active sites. These sites,

as stated before, are more likely present on the surface and thus the oxidation occurs prevalently there. Radical oxidant species, such as OH, do not need an active site to give reaction. However, the presence of weak points in the structure, such as aliphatic bonds, can favor this process. Chemically linked aromatic structures represent possible sites of oxidation for these species. On the contrary a complete aromatized structure is harder to be oxidized. Due to its radical nature the oxidation driven by OH results fast and thus mainly occurring on the surface of the particles.

4.5.2. Oxidation induced fragmentation

Fragmentation has been recognized in several condition and results fundamental for the correct prediction of the particle size distribution .(Neoh et al., 1985, Garo et al., 1990, Harris and Maricq, 2002) Reducing the mean dimension, fragmentation increases number concentration of particles. Experimental equipment has been set up to isolate or at least enhance this phenomenon. Overall it is widely accepted that this occurs prevalently in presence of large quantity of molecular oxygen, i.e. lean conditions, whereas it appears less evident or determinant in rich conditions. Moreover recent studies have evidenced that this phenomenon concerns both aggregates and primary particles (Echavarria et al., 2011). Fragmentation of aggregates, here named primary fragmentation, i.e. the breakup of a chain-like structure, has been recognized first. Primary fragmentation is supposed to occur after the attack of oxygen in a certain zone of the structure, more likely the contact points between particles into the aggregates. If the bond, which holds together the aggregate, is weaken enough by oxygen, a breakup occurs. From primary fragmentation the products can be aggregates or primary particles in dependence of the size, the number of particles into the aggregate and the point of attack of oxidant species. This phenomenon takes place from a reaction which occurs onto a particular point of the structure.

However, another type of fragmentation can occur. Oxygen, due to the fact that its oxidation reaction rate is considerably smaller than OH radical, can diffuse through the nanoporosity present in the particles. This leads toward an internal burning that can weaken the structure from the inside. The effect can be an explosion of the particle and thus the production of fragments as small as few nanometers (Secondary Fragmentation). Secondary fragmentation has been observed and introduced in the general discussion about oxidation after the evidence of a huge raise in lean conditions of particles with size much smaller of primary particles. This has suggested that the primary fragmentation model could not be the only one considered.

These small new nanoparticles may be similar in structure and composition to the mature soot particles from which they are generated and indeed different from nanoparticles that come from the inception process. This may influence their properties such as light absorbance, water affinity, effective risk for human health and finally capability to be oxidized in after treatment stages.

5. Main features of flame generated particles

Soot and *nanoparticles* are just definitions. In principle it is not possible to associate to these terms to some specific compounds. Due the wide moiety of compounds present in flame, underneath soot and nanoparticles definitions it is possible to find a very different species in terms of chemical composition, morphology and internal structure. Probably the most correct way to understand what is soot and what are nanoparticles is referring to experimental evidences and findings of last years.

Historically soot has been detected first and characterized. As the level of knowledge increased scientific community has individuated a class of compounds with features considerable different from particles studied so far. Nanoparticle idea was growing up. After 20 year of investigation the distinction now is almost universally recognized. However, properties of these compounds have not been completely understood and investigated.

Here a brief overview of the actual knowledge about main properties of soot and nanoparticles are presented. Most of the characteristics described below were discovered using several techniques. Some of them will be described in details in the next chapter.

5.1. What is soot

Soot particles at high temperature environment become incandescent and start emitting. In fact, soot is responsible for the large emission and, due to this important property, soot is desired when high heat transmission radiation coefficient is needed. Hence, laser induced incandescence has been used as system to detect particles in combustion environment (Shaddix and Smyth, 1996, Shaddix et al., 1994). However in the beginning soot was studied taking sample from deposited material or, similarly, directly from the flame, eventually extracting it in solvents (Haynes and Wagner Gg, 1981). Measurements were conducted by using microscopy techniques or mass spectrometry on sampled material and by measuring absorption and scattering properties by in situ measurement (Richter and Howard, 2000a). These techniques have been used since the first 1960's, whereas scanning electron microscopy (SEM), transmission electron microscopy (TEM), atomic force microscopy (AFM), differential mobility analysis (DMA), size exclusion chromatography (SEC) have recently given more information on mean size, size distribution, morphology and internal structure of

soot particles. Moreover gravimetric and elemental analysis give quantitative information about total production and composition of soot in flame (D'Anna, 2009, Bockhorn, 2007).

Looking at the results obtained with these techniques in a wide range of combustion conditions, it is possible to better define soot characteristics.

Soot can be defined as a mix of large single particles and aggregates of particles composed prevalently by large aromatic carbon compounds. Structure of soot was originally compared to structure of graphite due to the turbostratic disposition of the aromatic plane within the particles. Other principal constituents are hydrogen and oxygen; occasionally soot may contain sulfur or nitrogen, especially if these were present within the fuel composition. Hydrogen atoms are generally found to be up to 30% of the carbon ones. They can be responsible for the incomplete aromatization of aromatic compounds and the introduction of defects within the structure with respect to graphitic one. Primary, or single particles, can go from 20nm to 40nm whereas aggregates can reach size as large as 200nm. Equivalent mass measured range from 10^6 to 10^{10}u. Internal arrangement of the structure depends from fuel nature and temperature history. Interdistance between planes in the turbostratic structure and medium size of these planes have been investigated and vales have found to rely within a narrow range. Mature soot particles can exhibit a plane interdistance of 0.35nm with an average size of length of the aromatic islands around 1nm. These values can reach 0.5nm for the interdistance and below 1nm for the aromatic island. Due to chemical composition and morphological arrangement, soot is not soluble in water and in main organic solvents. One of the possible definitions of soot is based on this property. However some stable suspensions used to analyze soot with ex-situ techniques have been made using N- methylpyrrolidone. Recently an analysis of soot surface has evidenced the presence of aliphatic more than in the core of the particles. However, these studies are still ongoing and conclusions are still under debate.

5.2. What are nanoparticles

Nanoparticles can be defined as a class of compounds within carbonaceous material produced in combustion. However this and other definitions normally try to fit these new compounds in some previous categories, giving place to misunderstandings and incomprehension. Perhaps there is no need to strictly define these nanoparticles; a definition based on more than one physical characteristic would be more reliable (Bockhorn, 2007, D'Anna, 2009). Large part of the information presented here can be found in the proceeding of the last round table on combustion formed particles (Bockhorn, 2007)

The upper limit in terms of size for nanoparticles is given by soot definition. The lower limit is less obvious and some misunderstanding could be encountered. In fact, as stated in other sections, large aromatic compounds, which come from incomplete combustion of hydrocarbons, can keep

growing, forming macromolecules. These macromolecules, which can further grow becoming soot particles, have ideally intermediate properties respect soot and gas phase compounds. Extraction in organic solvent from deposited carbonaceous material led to the identification of some compounds, which were not similar to large soot aggregates but, at same time, were significantly larger than small gas phase PAHs. However, the condensed phase nature, typical of nanoparticles, was still far to be demonstrated. First detection of these particles was probably due to optical techniques. Successively laser induce emission, differential mobility analysis and atomic force microscopy have given proof of existence of nanoparticles. Gravimetric and elemental analyses conducted on soluble material have given other important information on nanoparticle formation and features.

Nanoparticles are UV absorbent species which exhibit small scattering signal. Nanoparticles generally emit giving a fluorescence signal, if excited with a laser source. Wavelength peaks in fluorescence signal can be correlated to the extension of the aromatic islands within the particles. A signal typical also of gas phase PAHs , which are the constituent of nanoparticles has been detected. Moreover nanoparticles exhibit an H/C molar ratio typical of small gas phase PAHs.

Despite of these similarities with gas phase compounds some differences have been individuated. Analysis of quantum yield has evidenced the condensed phase nature of nanoparticles. Nanoparticles do not exhibit a solid state character typical of soot particles. However, recent studies have confirmed that particles as small as 1.5nm has a condensed phase feature with some viscoelastic properties. This behavior has induced the scientific community to define these particles as liquid-like compounds. Their size goes from near-molecular range (below 1nm) up to 4nm. Coagulation efficiency for nanoparticles has been also evaluated. Coagulation efficiency has been found to be size-dependent and temperature dependent, driven by potential attraction based on van der Waal interaction. Isolated nanoparticles with larger diameters are quite hard to be found, due to their rapid coagulation toward soot particles. Structural organization of nanoparticles looks like a large polymer or macromolecule with internal interactions, which hold together the constituents compounds. In dependence on combustion conditions and temperature history nanoparticles can reach relatively extreme features some high level of organization or low H/C molar ratio making them more similar to very small soot particles rather than completely different compounds.

6. Experimental characterization of particles in flames

6.1. In situ characterization: Optical techniques

In situ measurements are in principle a non-intrusive technique. This allows to better analyze the feature and the production process of particles in flames. These techniques are based on the interaction of the light with particles, which give difference signals. Correlation of detected signals with particle characteristics results quite hard, especially due to the presence of wide moiety of emitting species in flame environment. Moreover in some cases also these techniques can introduce perturbation in the system, making conclusions harder to be drawn. However, nowadays optical techniques are largely used for detection of large molecular weight species and particles in flame, although new aspects and fields of appliance are still under investigation.

Hereafter some of the most used optical techniques will be described. Further description can be found in literature. Innovative aspects of some of these techniques developed during this research period will be also presented in this chapter.

6.1.1. Optical techniques: a brief introduction

Laser Induced Emission (LIE) is a particular case of the general phenomenon of stimulated emission. In this case the emission comes after an incident light generated by a laser source (Light Amplification by Stimulated Emission of Radiation). The high coherence and purity of laser light makes easier the identification of the signals and the correlation between signals and structure.

Light absorption

The ability of a mean of absorbing a radiation depends on many factors; firstly it depends on nuclear and electronic constitution of atoms and molecules of the mean, on the wavelength of the incident radiation, on the absorbing substance thickness and on the intensive variables which set the aggregation state of the mean (temperature and concentration particularly).

If a homogeneous mean is considered and it is defined the intensity of an incident monochromatic radiation with $I_0(\lambda)$ - intensity of the sample ray, the emerging radiation intensity $I(\lambda)$ - intensity of the referring ray is given by the Lambert-Beer law:

$$ln\frac{I}{I_0} = -K_{ext}(\lambda) \cdot L \qquad (6.1)$$

where K_{ext} is the extinction coefficient, which counts both absorption and elastic light scattering of light, and L is the optic path of the light. The extinction coefficient is the result of an absorption coefficient and a diffusion coefficient sum:

$$K_{ext} = K_{abs} + K_{diff} \qquad (6.2)$$

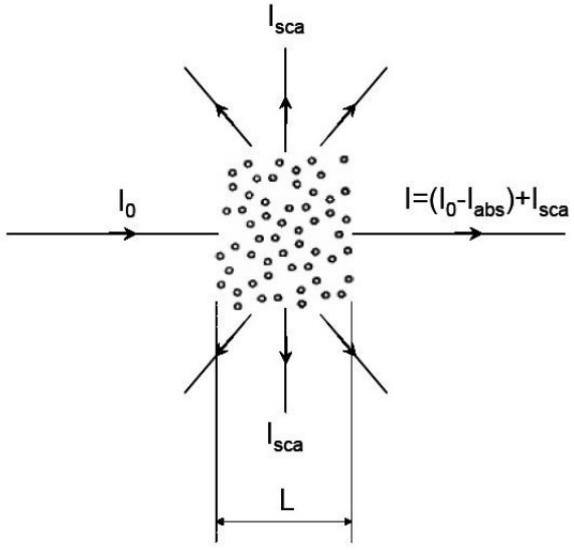

Figure 6.1 Schematization of scattering and absorbing phenomena of a particle cloud.

Generally, with the wavelength of maximum absorption λ_{max}, another variable is reported, the molar absorptivity ε (defined also as molar extinction coefficient). Molar absorptivity is the proportional constant between K_{abs} and the molar concentration of the sample ray, which is:

$$K_{abs} = \varepsilon(\lambda) \cdot c \qquad (6.3)$$

In this way the concentration contribution and the incident wavelength contribution are separated. Equation 6.3 is subjected to a great number of exceptions because the linearity between molar extinction coefficient and molar concentration does not take count the interaction phenomena. These occur both in very concentrated solutions (solute-solute interaction, dimerization, etc.) and in very diluted solutions (solvent-solute interactions). On the contrary, the Lambert-Beer law in its differential form set a linear dependence between the incident light intensity and the absorbed light intensity.

Nevertheless is useful to remember that in the absorption an important rule of organic chemistry takes place: the higher is the number of multiple conjugated bonds present in a compound, the higher is the wavelength of radiations absorbed by the compound.

Scattering

The first of the possible emissions due to the presence of compounds in a volume of gas excited by a laser light is the scattering signal. This phenomenon is due to the reflection of the light mostly generated in casual direction. When a particle is struck by a beam of light, the quantity and the angular distribution of the particle scattered light, like the absorbed light rate, depend on the polarization state, frequency and wavelength of the incident light ray and on the nature of the particle, i.e. on its shape, dimension, space position and on substances which constitute the particle (Charalampopoulos, 1992, Sorensen, 2001).

The particle light scattering phenomenon can be explained by supposing the particle divided in a lot of small zones, in which the incident electromagnetic field will induce a dipole momentum. In elastic scattering case these dipoles oscillate all at the same frequency of the applied field, but with different directions. The result is the quenching of the primary electromagnetic field and an electromagnetic radiation generation which has the same wavelength of the primary radiation, scattered in all directions. The exact solution of Maxwell equations is possible only for a spherical particle and the deriving theory is called Lorentz-Mie theory. A rounded solution, due to Rayleigh, for anisotropic small particles is available but their dimensions should be small compared with the radiation wavelength.

If in the process the total kinetic energy and momentum are preserved, it will talk about elastic scattering; on the other hand, it will have anelastic scattering if only the momentum is preserved.

When light is scattered from an atom or molecule, most photons are elastically scattered (Rayleigh or elastic scattering), such that the scattered photons have the same energy (frequency) and wavelength as the incident photons. However, a small fraction of the scattered light is scattered by an excitation having a frequency different from, and usually lower, than the frequency of the

incident photons (anelastic scattering). In a gas, Raman scattering can occur with a change in vibrational, rotational or electronic energy of a molecule.

The polarization of the emitted light is generally casually oriented. However, it is possible to collect just the signal of emitting light with a certain polarization. This procedure, in particular the choice to have vertical polarization for both incident and collected light, has been developed to avoid the effect of angle of incident light on scattering signal and, thus, better analyze the information gained. In fact, in this case the signal is not depending from the angle but jus on the properties of the particles and the sixth power of the diameter. This means that the signal results quite dependent by the size. As example, a hypothetic mixture of large and small particles would scatter the light in very similar way to a volume which contains only large ones.

LIF

In the phenomenon of the fluorescence a molecular electron is collided with an electromagnetic wave of the ultraviolet radiation. In absorbing the energy of the radiation, it moves upon an outer orbital, but the excessive vibrational energy suddenly acquired by the molecule is scattered in a very short time (about 10^{-10} – 10^{-7} seconds) in the environment, leaving the electron in a particular unstable state from which it will return in the previous position, by emitting a photon. In figure 6.2 the two curves represent the energy of the electron as function of the distance from the nucleus, while the horizontal line into the curves are the vibrational energetic levels of the orbital. An electron situated in the first vibrational level of the ground state orbital has been struck by an electromagnetic radiation and it absorbs the energy of the latter thanks to which it is pushed on an outer orbital, on a higher vibrational level; then it lose energy until it reaches the lower vibrational level.

This is, however, an unstable state, so the electron falls back to the starting orbital, the ground state one, emitting an electromagnetic wave belonging to the ultraviolet if the energetic transition is high, or belonging to the blue-green in the visible if the energetic transition is held down (the wavelength of the radiation is lower as the energetic transition is higher). Generally, the emitted radiation has a lower energy, that is a lower frequency, than the incident radiation since the fluorescence phenomenon has origin in the falling of the electron from the lower vibrational level of the first excited electronic state to one of the vibrational levels of the ground state, so the fluorescence spectrum is, generally, similar to the absorbing spectrum but shifted to higher wavelengths.

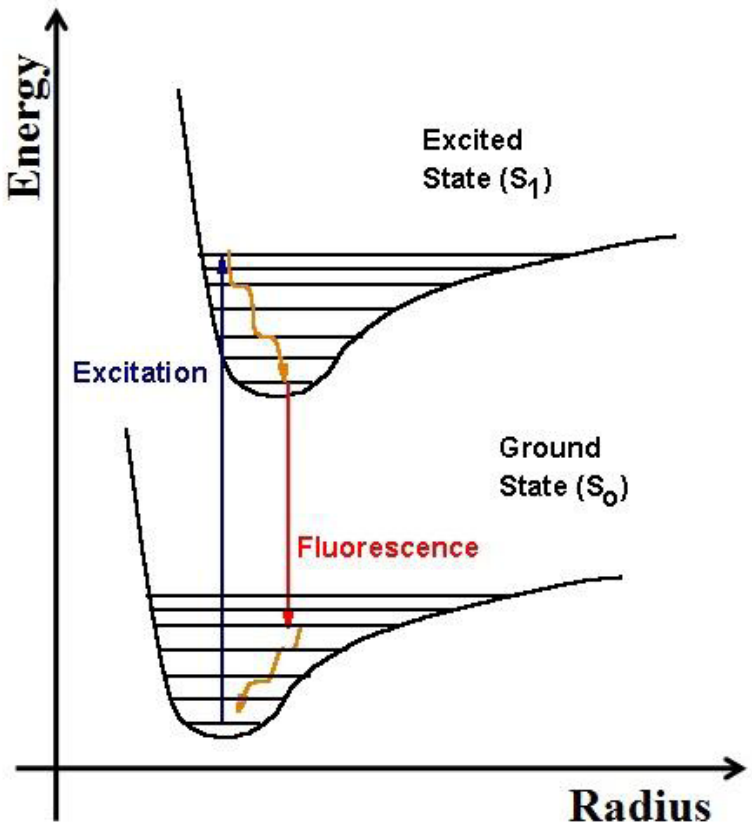

Figure 6.2 Fluorescence phenomenon

LII

Laser induced incandescence consists in bringing particles, presents in the measurement volume, to very high temperature by the absorption of a pulsed laser beam, and in detecting the emitted thermal radiation. The difference between incandescence, fluorescence and phosphorescence is that the last two are radiations emitted by the molecules due to electronic states variations of the electrons, while the incandescence is due to a kinetic and vibrational energies variation of the molecule itself. Thanks to the absorbed laser energy, the particles in the flame vaporize (at a temperature of about 4000 K), and they emit a blackbody radiation greater than the natural brightness of the flame (Schulz et al., 2006).

In the reality any material body behaves as a blackbody exactly (since a blackbody can absorb every electromagnetic radiation that strikes it), even if some bodies, like the black carbon (BC), can absorb some spectrum zones radiations at all. The name blackbody is due to Kirchhoff which began, during his researches on the thermal emission, a study about its properties. Lummer and Kurlbaum realized a device which can behave like a blackbody: it is a hollow body, of any shape, with the wall being dull to radiations and internal covered with black carbon; a small hole is made on it and

radiations that pass through the hole penetrate in the body and are completely absorbed by inner walls after a series of reflections.

As the laser pulse ends, the particle temperature quickly decreases and, whit it, the vaporization rate exponentially. An excess heat emission in the form of convective, conductive and radiative fluxes is observed. The heat radiative flux is represented by the very well-known Stefan-Boltzmann law:

$$q_b = \sigma \cdot T^4 \tag{6.4}$$

which represents the heat amount emitted per time and surface units from a blackbody, where σ is $1{,}355 \bullet 10^{-12}$ $cal \bullet sec^{-1} \bullet cm^{-2} \bullet K^{-4}$.

The Stefan-Boltzmann law can be obtained by integration from Planck distribution law, which says that a blackbody brought to a temperature T emits an energy radiative flux $q_{b\,\lambda}\ d\lambda$ (blackbody radiation) in the range [λ, λ+d λ] which is a function of the only temperature:

$$q_{b\lambda} = \frac{2\pi c^2 h}{\lambda^5} \cdot \frac{1}{e^{hc/\lambda KT} - 1} \tag{6.5}$$

where c is the light velocity in vacuum, h is the Planck constant and K is the Boltzmann constant.

The Planck distribution law calculates the energy emission value in function of the wavelength, with the maximum that shifts to higher frequencies (lower wavelengths) as the temperature increases, following the Wien shifting law:

$$\lambda_{max} \cdot T = \frac{c \cdot h}{4{,}9651 \cdot K} = 0{,}2884\ cm \cdot K \tag{6.6}$$

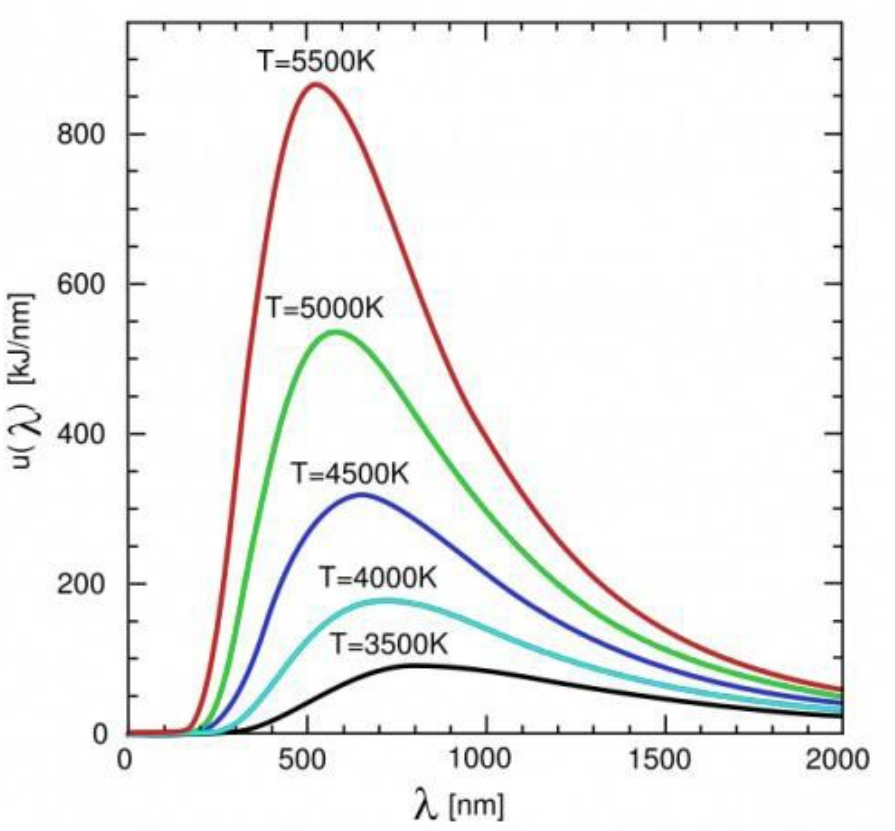

Figure 6.3 Planck's blackbody emission curves, evaluated at different temperatures

6.1.2. Spectral analysis

Spectral analysis is one the first techniques applied to combustion formed pollutant detection. The technique is widely tested and many of the conclusions presented in the first part have been drawn from results obtained with these. Hereafter a brief overview of the main results of the spectral analysis in flames is reported.

Correlation between wavelength and structure

As explained before, both light absorption and emission are strictly connected to the structure of investigated species. However, in the case of combustion generated species the high number of compounds, present at same time and giving similar light response, makes quite hard to distinguish the single contribute to the collected signals. Instead, it is possible to analyze the material present in flame as classes of compounds. The differences would not be recognized looking at the single peaks in the collected spectra but at the macro-differences between two signals.

As example, it is possible to compare the LIF signal collected for a single PAH in solution and the LIF signal collected in a zone of the flame with high concentration of PAHs and nanoparticles. In

the case of pure compounds, the spectrum is generally localized in the UV region and many structured bands are quite visible, whereas a broadband non structured fluorescence is collected in the flame case.

Starting from the analysis of single PAHs usually present in flame conditions some general considerations can be drawn. Very small PAHs, such as Naphthalene and Acenaphtene, exhibit a LIF and absorption signal concentrated in the UV region. As the molecular weight increases signals undergo to the so-called redshift, i.e. the emissions and absorption signals are localized generally at longer wavelength (Vander Wal, 1996b). Similarly a broadband of fluorescence peaked in the UV can be associated to a structure constituted by very small PAHs. When larger wavelength signals are collected one of the possible explanations is that the mean size of aromatic islands is increased (Minutolo et al., 1996, D'Alessio et al., 1992, D'Anna et al., 1994, Ciajolo et al., 2001c, Ciajolo et al., 2001b, Ciajolo et al., 2001a). However enlargement of aromatic island is not the only responsible for the redshift within the structure; also a change on the morphology and internal structure can induce this phenomenon (D'Anna et al., 2009). In fact, signals detected with a mean wavelength larger than 450nm are hardly to be assigned to very large PAHs, since the correspondent mean size of PAHs would be larger than coronene and thus assigned to species not widely present in flame. Signals detected at wavelength even larger, i.e. 500nm and more, are generally associated to incandescence signal and thus to very large particles. Absorption signal results quite similar to emission described above. In fact, nanoparticles, generally formed by small UV-emitting PAHs, results also visible transparent compounds. On the other hand, large particles or more graphitized structures undergo the redshift becoming absorbent in the visible region (Minutolo et al., 1996, D'Alessio et al., 1992).

These tools resulted fundamental in the first understanding of the nanoparticle nature and their different features with respect to soot particles. Nowadays they represent a valid and easy technique possible to be applied also to real combustion systems.

However, scientific community is now more interested to gain information about the internal organization at atomic scale of nanoparticles. Optical techniques need to develop new instruments to be able to give this information. Time resolved laser induced emissions raised as a possible way to fill this gap.

6.1.3. Time resolved Laser induced emission

Time-resolved analysis of light emission can be a useful technique to gain information about particles features in flame conditions. TRFPA (time resolved fluorescence polarization anisotropy) and time-resolved laser induced fluorescence are the most promising fields of development of these techniques. Hereafter TRLIF is larger descripted due to its use in particle detection during this thesis work, whereas details on the use of TRFPA are described in literature (Bruno et al., 2008).

TRLIF

Differently from TRFPA, TRLIF refers to a single fluorescence signal collected in flames despite of the depolarization ratio (Bruno et al., 2007). Laser induced fluorescence after the excitation due to the laser beam raises up to a maximum value decaying in intensity within a certain time. TRLIF links this decay time to the structure of the fluorescing species. This is quite new technique and, thus, it is probably not possible to give exact absolute values, valid for all the structures present in flames. However it can give remarkable results if used in comparison between two zones of the flame or two compounds in similar environment conditions. The definition of laser induced fluorescence phenomenon is based on the assumption that radiative phenomena are in competition with other non radiative ones. These non radiative phenomena can be due to presence of other compounds that dissipate through collisions the energy absorbed, quenching the emission signal. Similarly these non radiative phenomena are linked with an internal dissipation of energy. This latter appears more interesting due to intimate link between possible internal energy dissipation and structure. In fact, roto-vibrational degrees of freedom of the structures are the main responsible for this conversion. In other words, the excited species dissipate the excess of energy vibrating and not reemitting the light through fluorescence phenomenon. This mechanism is well described and known in literature. In order to measure the natural fluorescence lifetime of pure species, very often samples are prepared in absence of external quenching molecules and cooled down to tens of Kelvin degrees, to avoid non radiative effects. In flame, the presence of oxygen, which is one of the most effective quenching molecules, the high temperature environment, which increases the vibrational pathways, and the possible aliphatic links present within nanoparticle structures, which introduce degrees of freedom, strongly favor the non-radiative pathways, reducing the fluorescence lifetime to few nanoseconds. However, in some conditions, where oxygen is not present, temperature is significant lower and inception pathways form more packed structures, the radiative pathway is enhanced and fluorescence lifetime results as long as tens of nanoseconds, comparable with natural lifetime of fluorescing species.

These simple considerations have been applied to study level of organization of incipient nanoparticles formed in different conditions within a diffusion flame. Results are supporting the validity of conclusions and are confirmed also by other experimental techniques and modeling results, making this new tool reliable and promising for future studies.

6.2. Optical measurements – experimental apparatus

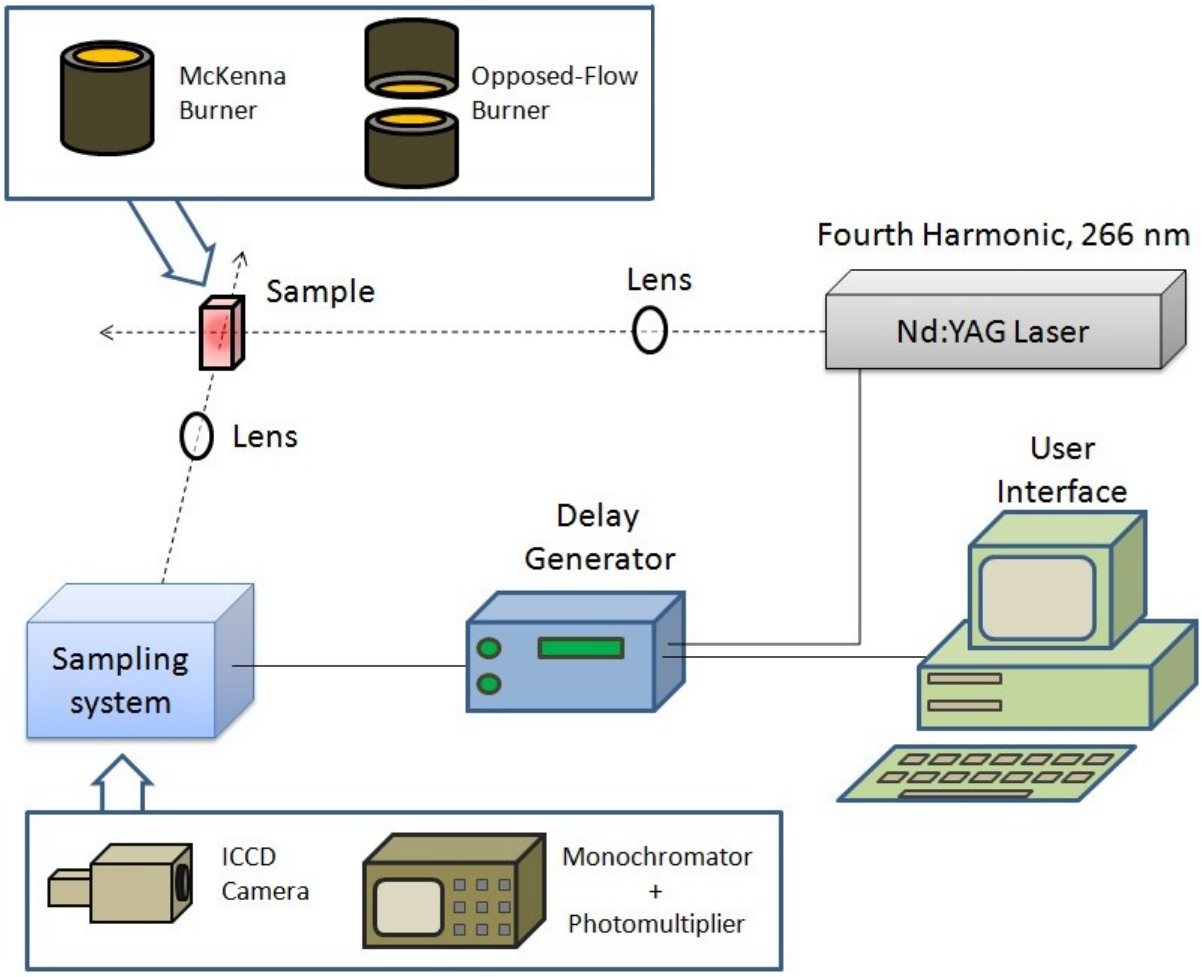

Figure 6.4 Laser induced emission experimental apparatus

Figure 6.4 reports a sketch of the experimental apparatus used for optical measurements during this thesis work. The apparatus was mainly constituted by a source of light with specific characteristic, which in this case was the fourth harmonic of a ND-YAG pulsed laser (266nm); the sampling system was an ICCD camera for the spectral measurements or, alternatively, a Monochromator coupled with PhotoMultiplier Tube (PMT) and an oscilloscope for time resolved emissions; a delay generator, which was used to trigger the detection system with the laser pulse; the investigated reactor, indicated as the sample in the figure, which was a premixed or a diffusion flame.

Generally, in order to detect particles which cannot be defined as soot, Laser Induced Fluorescence is more suitable. Figure 6.5 (top panel) reports a typical spectral profile of the LIE signal as measured in an opposed-flow diffusion flame (D'Anna et al., 2009), which can be taken as example of spectra collected in flames. The spectrum shows the scattering signal at 266nm, a broad fluorescence emission in the region between 290nm and 500nm with two distinct maxima in the spectral regions 300-350nm and 400-500nm, and a continuum due to the incandescence emission of

solid particles which maximizes at longer wavelengths. A more detailed analysis evidences that fluorescence emission can be considered as combination of four main contributions. In fact, the spectrum acquired after 100nm from the laser pulse reported in the lower panel of Fig. 6.5, clearly shows two distinct delayed fluorescence maxima at 340nm and 390nm.

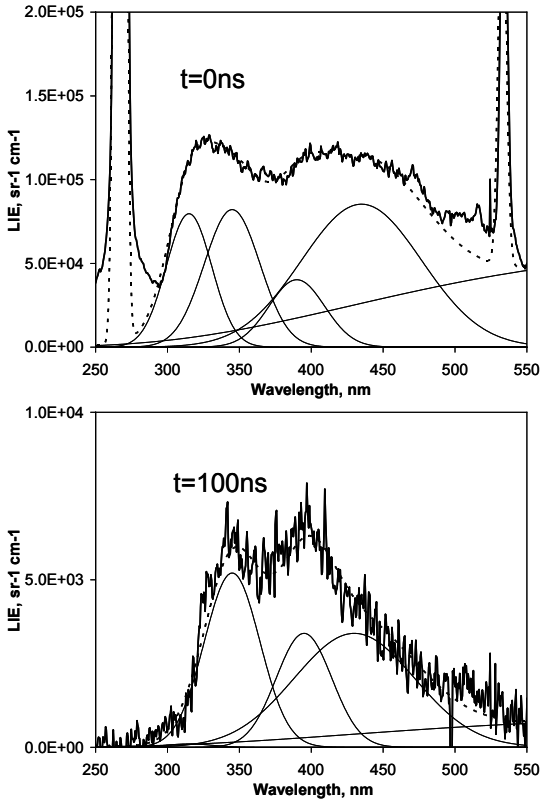

Figure 6.5 Laser induced emission spectra collected at 3.5 mm from fuel jet nozzle, synchronized signal (t=0ns, top) and delayed signal (t=100ns, down). The four Gaussian-shaped and black body radiation utilized for the spectral deconvolution are reported as thin solid lines. Their sum is reported as dashed line (D'Anna et al., 2009).

In order to isolate contributes of each fluorescence emission band, a deconvolution procedure of the fluorescence signals was operated. A combination of four Gaussian-shaped curves was used; more specifically, two curves fit the UV spectral region with maximum located at 310nm and 340nm, respectively, and other two curves, with maximum at 390nm and 440nm, fit the visible region of the spectrum. Maximum positions and widths at half maximum of these bands were maintained constant to fit the emission signals detected along the flame. Changing the type of the curve used for the fitting procedure, in particular using log-normal shaped curves, the data fitting does not substantially change.

The scattering signal at 266nm, together with the second order at 532nm, was also fitted by two Gaussian-shaped curves. Finally, the continuum in the visible was fitted by black-body radiation at 4000K, according to literature data (Schraml et al., 2000), matching the measured emission intensity values at 550nm. Although particle temperature is not known, below 500nm the black-body spectrum slightly changes with particle temperature, little affecting only the 440nm fluorescence signal. Therefore, the uncertainty on the 440nm band is of about 5% whether 4000K or 3500K is used.

For the time resolved LIE measurements the signals were collected by the ICCD camera, which had a fast shuttering system, delaying the opening time of the gate from the beginning of the laser pulse up to 10ns. The ICCD exposure time was fixed at 200ns. The intensity of the signals with the opening time of the gate fixed at t*, is the integral from t* to t* + 200ns. Figure 6.6 schematizes the signal acquisition procedure. It is worth noting that the signal after 200ns is practically negligible.

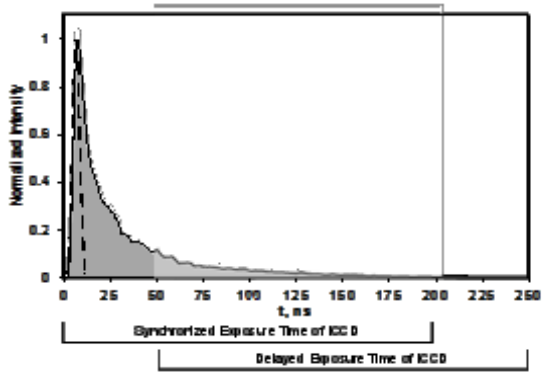

Figure 6.6 Typical emission signal collected by monochromator with oscilloscope (solid line) and by ICCD (shaded areas). Laser pulse measured at 266nm is reported as dashed line.

Signals were acquired up to a delay time of 100ns; steps of 1ns were used up to 10ns of delay time and steps of 5ns up to 100ns of delay time. Since the laser pulse is relatively long (8ns), the total acquired signal IT results to be the convolution of the laser pulse IL and the emission signal IE:

$$I_T = I_L \otimes I_E \qquad (6.7)$$

Figure 6.6 shows the contribute of laser pulse to the total signal as a dashed line. A deconvolution of the temporally resolved signal was operated with the aim of obtaining the actual emission signal.

A fluorescence decay time, $\tau_F^{'}$, defined as:

$$\frac{\int_{\tau_F'}^{+\infty} I_T dt}{\int_0^{+\infty} I_T dt} = 1/e \qquad (6.8)$$

was calculated from the signal collected with the ICCD camera.

In order to have a better temporal resolution, and to confirm the results obtained with the spectral resolved procedure, selected measurements were performed with a monochromator coupled with a photomultiplier tube. Such optical set-up allowed to detect a narrow range of wavelengths with fast response and high sensitivity. A Tektronix TDS 500C Digitizing Oscilloscope, with temporal resolution down to picoseconds, was used to acquire signals. The acquisition set-up is similar to that used in the literature to study time-resolved laser induced emissions (Bruno et al., 2005). After the deconvolution procedure (eq.2) to take into account for the laser pulse interference, fluorescence decay was approximated with an exponential law:

$$I_E = e^{\left(-\frac{t}{\tau_F}\right)} \qquad (6.9)$$

Although the literature suggests a multi-exponential behavior for fluorescence decay (Ossler et al., 2001b, Ossler et al., 2001a), a single exponential has been found to be satisfying in all examined cases; its decay constant gives the fluorescence decay time, typical of the fluorescing species. It is worth noting that by using a single exponential the two characteristics times of fluorescence decay obtained with the monochromator set-up and with the ICCD camera set-up, i.e. τ_F and τ_F' , are numerically coincident.

The results obtained with the oscilloscope confirm the ICCD measurements particularly for long living signals (>5ns). For short decay times (<5 ns), oscilloscope measurements result more reliable. Overall, the comparison generally confirms the possibility of using the ICCD camera to obtain information on time resolved signals at least for longer lifetimes. In this sense, the use of ICCD to evaluate decay times results easier and allows to perform both spectral and time-resolved measurements with a single experimental procedure.

6.3. Ex situ characterization: Differential mobility analysis

Even if the non-intrusive techniques give the best reliability, in some cases a sampling procedure is necessary to use some advanced systems of measure which give more information about particles. Differential mobility analysis is just of the possible detection systems that can be used to

obtain information about particle size distribution function. However after almost ten years of research, it is well established technique that can be reliably used for this kind of studies.

6.3.1. Brief description of DMA

Differential mobility analyzer, or DMA, is a detection system based on two simple principles: separation of particles forming a mono-disperse aerosol and counting of particles present in this aerosol.

Separation system is based on the mobility of the particles within an electric field. It means that this system is generally composed by a charger to provide a well-known steady-state level of charge for particles and an electrostatic classifier. The charger can be a unipolar charger, furnishing a positive charge to the particles, or a bipolar-neutralizer charger. The latter furnishes a steady state level of charge to the particle which is in agreement with Fucks theory for this phenomenon (Alonso et al., 1997b). This allows to determine the distribution of charge and taking it into account for further considerations.

Electrostatic classifier can be found in different geometry. However for sake of simplicity here will be referred to cylindrical geometry which is the one used in the present study. In this configuration an electric field is generated between two coassial steel cylinders. This electric field which is radially oriented acts on charged particles that flow trough. Charged particles change their trajectory according to laws of interaction between charges and electric field. The move of the particles is strongly dependent from the electrical mobility diameter, which is mostly equal to the aerodynamic diameter. With an opportune opening at the end of the cylinders and by varying the electric field applied it is possible to obtain from a poly-disperse aerosol many different mono-disperse aerosols according to the law of Millikan-Fuch for spherical particles:

$$Z = \frac{q \cdot C_c(Kn)}{3 \cdot \pi \cdot \mu \cdot d} \qquad (6.10)$$

The mono-disperse aerosol is then sent to the particle counter, which gives the number of particles per volume. The particle size distribution function can be reconstructed by analysis of single mono-disperse aerosols.

The counting systems can be a Condensation Particle Counter (CPC) (McMurry, 2000), or by an Electrometer (Flagan, 1998), in the case of the EMS. The first one is based on optical counting of the particles the second one is substantially a very sensitive ampere-meter which measures the current associated to the aerosol. CPC counts the particles after they pass through a chamber in which a

supersaturated atmosphere of a volatile alcohol, generally butanol, is created in order to let particles grow and thus more easily be counted. Obviously this system depends in some way from the type of particles, the level of supersaturating and the way particles grow; however it has been demonstrated to be quite reliable for a wide range of conditions. On the other hand, electrometer can suffer of some errors due multiple charge counting and moreover it has a higher lower limit of detection with respect to CPC due to very low current associated to nanoparticles. Generally CPC is able to count very low concentration, down to few particles per cubic centimeter, whereas for particles as small as 2nm electrometer needs a concentration of 10^6 particles/cm^3 to give reliable results.

6.3.2. Sampling systems

Beside on instrument errors, lot of attention has to be paid to the errors due to sampling system. It is something common to all off-line technique due their perturbative nature. However many adjustments are possible in order to minimize the sampling effect on the sampled material. The possible artifacts rely generally in two points: the perturbation on the flame and the effect on the material within the probe. The first one is almost impossible to avoid, since the insertion of a sampling system in the flame cause somewhat perturbation. However the perturbation can be minimized by reducing the size of the probe. Moreover it is possible to take into account and evaluate the perturbation of the probe with a modeling attempt. Through years many different probes have been tested in order to understand which is the most suitable (Zhao et al., 2003, Abid et al., 2008, Abid et al., 2009, Maricq et al., 2003, Kasper et al., 1997). The horizontal probe although causes a large perturbation of the local temperature (De Filippo et al., 2009, Abid et al., 2009) is very useful to prevent artifact within the sampling line. In fact, as described below, this kind of probe allow to have a dilution ratio up to 10000 and thus instantaneously freeze the sample volume, preventing undesired reactions. The short residence time and high dilution also allow to have no change in particle size distribution along the line preserving the original shape present in flame.

6.4. Differential mobility analysis – Experimental apparatus

In this chapter a description of the experimental apparatus used for the DMA analysis will be given.

6.4.1. TAPCON 3/150 - Vienna type DMA

The tapcon EMS was the last development of the previous version distributed by the Aerosol Measurement Division of Hauke, also known as Wien Type DMA or “Vienna” DMA in the literature.

The EMS was equipped with a bipolar radioactive (Am-241) diffusion charger (Winklmayr et al., 1991) and a DMA 3/150, characterized by a superior flow profile to furnish a clean size separation, low diffusional losses and, in principle, a wide range of applicable aerosol (1-10 L/min) and sheath gas flows (10-50 L/min) depending on the critical orifices in the flow control unit. With the aerosol flow at 5L/min and the sheath flow at 50 L/min, the particle size regions achieved by the instrument were 0.6-28 nm and 2-100 nm with high voltage respectively at 1250 V and at 12500 V. The highly stable gas flows were assured by critical orifices rather than electronic mass flow controlling devices. The classified particles were measured by a Faraday Cup Electrometer (FCE-08) and the EMSSYS operating software converted the measurement data to the size distributions and displayed on-line, besides controlling the different hardware components of the EMS system. The size distributions were calculated as dN/dlnD, including the size dependent charging probability in air for single charge and a correction function reflecting the slip correction and the instrument resolution (transfer function). Correction for instrument losses was not included and impactor was not used. Table 6.1 reports details of the used instrument.

	tapcon EMS
Mode	VIE-09
Bipolar Ionizer	Am-241, t1/2 = 458.6 years, 3.24 mCi, α-radiation
Classifier	L=109mm, R1=25mm, R2=33mm (DMA 3/150)
Flow rates	Qa= 5 lpm, Qsheath= 50 lpm
Sensor	Faraday Cup Electrometer
Nominal size range	0.6-28 nm
Scan time	170s

Table 6.1: Tapcon DMA features

6.4.2. Horizontal probe

Ideally, in order to study the flame-generated particles as they exist and evolve unperturbed in the flame, it is necessary to use a sample device able to immediate dilute, quench and transport the

sampled aerosol to the analyzer in a way that preserve the salient features of the nanoparticles, thus effectively and systematically eliminating particle-particle coagulation processes, diffusive wall losses, thermophoresis and condensation. Such a system does not yet exist but, over the years, very efficient sampling devices have been designed and experimentally tested to reduce and minimize sampling artifacts. In 1997, Kasper (Kasper et al., 1997) developed an in situ sampling probe for flames, made of a straight stainless tube with a small orifice for sample intake. The probe was placed horizontally above the burner and the flame gas sample was rapidly diluted by nitrogen gas in the probe, with the main purposes to quench chemical reaction, prevent the particles from coagulating or growing through condensation, and therefore avoid alteration of particle size distribution during the sampling process (Figure 6.7). Compared to the quartz microprobes used in the past, the advantage of this probe was the possibility to sample for enough time without suffering too much from the soot clogging of the orifice. In 2003 two independent studies by Maricq et al. and Zhao et al. furnished further experimental information to characterize a sample probe similar to that of Kasper

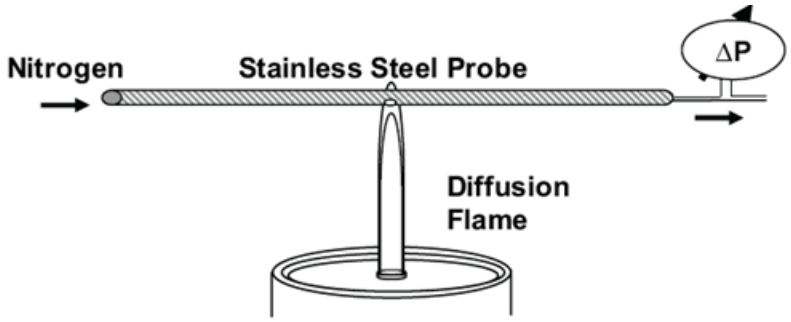

Figure 6.7: Sampling device for a diffusion flame, adapted from Kasper et al (1997)

The pinhole (diameter=0.8mm) was positioned along the centerline of the flame, facing downward toward the burner surface. The pinhole size yielded large dilution ratios (DR> 10000), immediately after the flame sample enters the probe. This nitrogen flow is 3-4 orders of magnitude greater than the flame sample in order to avoid the high concentration of particles and to prevent particle-particle coagulation and study flame-generated particles as they exist in the flame . The absence of coagulation is guaranteed in the moment in which the size distribution is almost constant, even if the dilution ratio changes: this particular condition is named Critical dilution. It is clear that the time of residence of the sample into the probe will be shorter both when the cooling gas velocity will be higher and when the sampling line length will be shorter; so doing the possibility of coagulation will be lower.

The residence time into the DMA does not depend on the dilution flow because the inner flow of DMA is necessarily constant that is 5 l/min, and for this reason the DMA residence time is always 2.13s.

The Reynolds number, relative to the pinhole inner flow depends on the flame velocity. It is possible to calculate the entrance flow value (the required length so that the flow becomes stationary):

$$L_e = 0.06 \cdot \mathrm{Re} \cdot d \qquad (6.10)$$

where Le is the entrance flow, Re is the Reynolds Number and d is the pinhole diameter. So the total residence time is a function both of the sampling flow and of the dilution flow.

Particles smaller than 20 nm are lost to the surfaces mainly by diffusion. Equations exist to calculate these losses in laminar and turbulent flows in tubes. These calculations assume that every collision of a particle with a surface results in a particle loss, which agrees with experimental observation for NaCl particles as small as 2nm at room temperature (Alonso et al., 1997a). For laminar flows, the particle penetration, P, defined as the number concentration of particles exiting the tube length, L, can be calculated using the classical formulas expressed as the sum of the first terms of a series:

$$P = 0.819\exp(-3.657\zeta) + 0.0975\exp(-22.3\zeta) + 0.0325\exp(-57\zeta) \quad \text{for } \zeta \geq 0.0312 \qquad (6.11)$$

$$P = 1 - 2.56\zeta^{2/3} + 1.2\zeta + 0.177\zeta^{4/3} \quad \text{for } \zeta < 0.0312 \qquad (6.12)$$

where ζ=πDL/Q,, D is the particle diffusion coefficient and Q the aerosol volumetric flow rate through the tube (Alonso et al., 1997a).The pinhole can be considered like a pipe (d=0.8 mm and L=1 mm) thanks to the ζ parameter it is possible calculate the amount of particle losses for each sample flow. It is easy to understand that the losses decrease both when the sample flow increase and when the pinhole dimension increases. In the same way it is possible to calculate the losses in the probes.

There are also some losses in the DMA (in particular into the ionizer and the electrostatic classifier) but, for the moment, no calculation is possible yet because of considerable geometric complexity.

For turbulent flows, the particle penetration can be estimated by the following equation

$$P = \exp\left(\frac{-4V_{dep} \cdot L}{D_{in} \cdot U}\right) \qquad (6.13)$$

where V_{dep} is the deposition velocity, Din the inner diameter of the tube and U is the average velocity of the aerosol.

Estimated particle losses with Equation (6.13) in the turbulent flow of the sample line after dilution can be considered negligible (Zhao et al., 2003) or insignificant compared to those in the orifice (Sgro et al., 2009), where the flow is laminar and calculated with Equation (6.11) and (6.12). However, the analysis of particle losses in the orifice requires further comments. The temperature of flame products entering the probe orifice was estimated as Torifice =1000 ± 250K, where the large uncertainty depends on the fact that the temperature profile is steeper within 2mm ahead of the probe. Then, the observation that flame generated particles smaller than 5 nm, at least at high temperature, adhere to surfaces less than larger particles even when they are in higher concentration at flame temperatures suggests that while their mobility is higher, they may escape collisions with surfaces by thermal rebound (D'Alessio et al., 2005). Therefore, the effect of particle rebound has been taken into account considering that the number of collisions with the walls producing losses of particles is equal to the number of collision multiplied by the particle sticking efficiency, γ_{SD}, evaluated by the interaction potential of particle with orifice walls, similarly to the interaction with mica disk as discussed in (D'Alessio et al., 2005) which depends on particle size, temperature and chemical composition.

Figure 6.8 shows the estimated particle penetration in the orifice used to correct the size distributions measured by the DMA for particle losses. Assuming 1000 K as the temperature of the orifice, penetration was calculated in two ways: P1, assuming no thermal rebound (γ_{SD}=1), andP2, accounting for a size-dependent sticking efficiency during particle-wall collisions (γ_{SD}).

The minimum in the penetration curve calculated with γ_{SD} occurs because particle mobility (and so the number of collisions with the walls) increases while the sticking efficiency (or number of collisions that result in a loss of particles) decreases with decreasing particle size.

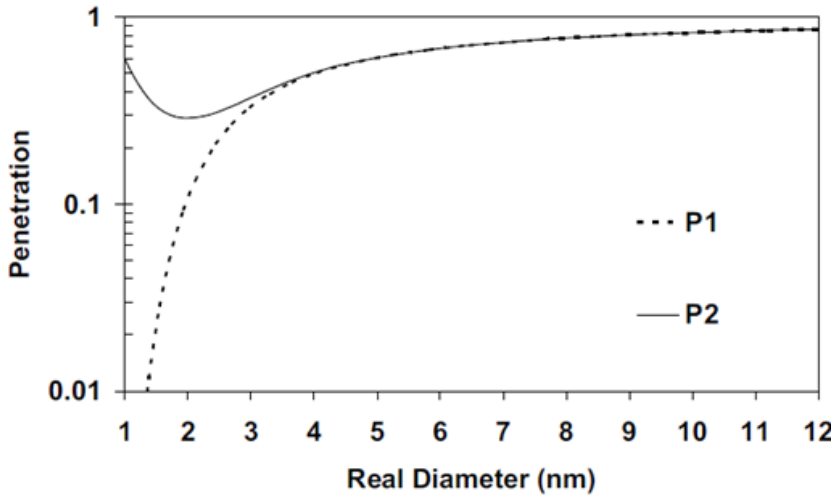

Figure 6.8: particle penetration inside the orifice calculated assuming no thermal rebound P1(γ=1)and assuming a size dependent sticking efficiency P2 (γ_{SD})

Particle losses were estimated ~67% for 2nm particles and ~41% for 5nm particles. Horizontal axis refers to the real or actual particle diameter. Indeed, the presence of particles rebound during penetration of nano-sized particles in laminar flow through tubes is still under debate (Alonso et al., 1997a). In any case, in the size range below 3 nm, the size distributions corrected for losses assuming γ_{SD} will be only marginally different in shape from the uncorrected size distributions.

In contrast, corrections assuming no thermal rebound (γ=1) would produce a dramatic change of the size distribution which would become a tail of a distribution that is below the lower size detection limit of the classifier.

Finally electrostatic losses were minimized by keeping all of the sampling lines in contact with particles conductive and at the same potential. Instead, due to the lack of knowledge about the thermal gradients across the probe orifice, it was difficult to quantify thermophoresis losses and they were not considered. However, since the thermal gradient between the probe wall and the sampled gas, at least at the orifice inlet, seems to be minimal, and, assuming that this remains constant as the nanoparticles travel across the 0.5 mm of the wall thickness, thermophoretic losses can be considered negligible.

7. Modeling aspects

In this chapter details of modeling attempts of particle formation prediction will be presented. Starting with a short comment on gas phase kinetic, its role and main challenges, a brief overview on different approaches for particle modeling will be furnished. After that, the attention will be paid to the sectional method which has been developed during this work. Main features of the model will be presented, clearly stating the wide possibility of appliance of this model. Model will be a key step to understand processes and main feature of particles in flame.

7.1. Gas phase kinetics

As clearly stated in the Chapter 4, gas phase kinetic is of fundamental relevance for getting correct prediction of particle formation and growth in flame (D'Anna, 2009). Moreover incorrect gas phase kinetics could lead to wrong conclusion, underestimating or overestimating some reaction pathways.

On the other hand, many efforts have been spent in this field in order to have a precise tool to apply in several conditions. Although the behavior of some reactions is still under debate in the limit of high and low pressure (Li et al., 2004), the atmospheric conditions are quite well managed by scientific community. In literature, large number of comprehensive kinetic scheme are presented (Sheen et al., 2009, Livermore, Ranzi et al., Frenklach et al., 2011). They all rely in a short error bar, at least for the major species involved in combustion process. Ethylene, methane, acetylene, benzene and their related radical and stable species are quite well determined in terms of formation and evolution during combustion conditions. However, small differences in gas phase kinetic are still present. During this work gas phase model designed by D'Anna has been used (D'Anna). The use of the same model for all the fuel and the combustion conditions is quite useful in order to discern which are the main pathways involved.

Details about this mechanism can be found in literature. However, hydrocarbon oxidation and pyrolysis is modeled with a detailed kinetic mechanism built onto the GRI mechanism for C1 and C2 species (Frenklach et al., 2011). In aliphatic fuel flames acetylene and methane are the most abundant, gaseous, unburned hydrocarbons and benzene is the first product of the molecular growth process (Ciajolo et al., 1994, Ciajolo et al., 1996). Benzene formation is considered to occur by the addition of n-C4 radicals to C2H2 (Frenklach et al., 1985) and the self-combination of propargyl radicals (Miller and Melius, 1992a). The sequential addition of C2H2 to phenyl radical (HACA mechanism) (Frenklach and Wang, 1991) and the combination of resonantly stabilized radicals, RSFR (Castaldi et al., 1996, Colket and Seery, 1994), are the pathways considered for the growth of aromatic cycles up to pyrene.

7.2. Starting point for modeling nanoparticles

Compounds with molecular weight larger than pyrene become very difficult to be modeled since their high number of isomers. Many approaches have been proposed through years. All of them had to face against the computing capacity. If in the beginning only one-step reaction could be used to model soot total amount, nowadays the improved computing capacity allows to have a lot of information on particles through the implementation of quite heavy codes. The next challenge will be probably an efficient and effective coupling between detailed kinetic and turbulence models. For gas phase reactions, reduction and skeleton analysis seems to be the most correct way to proceed. An equivalent universally accepted procedure for the reduction of code size for particle prediction has not been found yet, even because particle formation and growth is not completely understood (D'Anna, 2009).

Chemical approaches such as ab initio calculation (Kubicki, 2006, Kubicki, 2005) and molecular dynamic (Schuetz and Frenklach, 2002, Herdman and Miller, 2008) has been used to simulate single step reaction and to understand if this step can be a key one in particle formation. However, these methods are far to be applied the way they are in combustion modeling. However this issue has stimulated the scientific community to produce some numerical tools, suitable for very easy fluid-dynamic conditions such as laminar one-dimensional configuration, which can be useful to understand and predict particle feature in flames. Some methods have risen as the most efficient for soot prediction: method of moments, other methods on Monte Carlo approach and discrete sectional method based on lumped species. Both methods are the attempt to solve Smoluchowski problem described more the 90 year ago (Smoluchowski, 1916). Hereafter a brief description of different approaches is furnished; for Monte Carlo method, the hybrid approach of the AMPI code, which contains also molecular dynamic approach, is presented.

7.2.1. Method of Moments and Monte Carlo approach

Method of moments has been introduced by Frenklach in the 1985 as a possible solution to Smoluchowski problem (Frenklach, 1985). This method uses the moments of particles distribution instead of trying to get analytical or numerical solution of the Smoluchowski equation. As stated from the first paper about this topic the knowledge of all the moments of size distribution is equivalent to the knowledge of size distribution itself. Due to computational costs and feasibility in the first period only the first moments have been taken into account and the information gained stopped at total amount and particles size distribution. However, some problems were encountered. Particle size distribution was supposed a priori and this makes the approach less general. To overcome this problem a closure of the problem with interpolative method was proposed (MOMIC) (Frenklach, 2002a). This interpolative method consisted in the determination of fractional order moments by

using an interpolation between whole-order moments. However this attempt was not the only tried to use make the method of moments more reliable. In fact in the 1996 Frenklach propose to use a stochastic approach (Monte Carlo) to proceed in the choice of event to be considered in particle evolution (Frenklach, 1996). Practically, the occurring of a certain event such as acetylene addition or coagulation was determined randomly on the base of probability. This method was successfully tested and further developed by several research groups.

This method has been firstly used to predict the state of aggregation and differences between single primary particles and aggregates. Finally, the use of method of moments both with an interpolative closure and with a Monte Carlo approach has given the possibility to investigate also turbulent flames and real combustion systems due its relatively computational lightness. Unfortunately only recently this method has been used to gain more information on particle features such as chemical composition and internal structure.

Lately the Monte Carlo approach was used in order to perform a simulation on a statistical relevant number of particles. These resemble of the real particle situation and thus avoid some closure problems that still concern the solution of method of moments. (Balthasar and Kraft, 2003, Balthasar et al., 2002, Violi et al., 2004)

Incidentally, especially in the years of development of method of moments, very often this was compared with results coming from discrete sectional approach that was considered more accurate even if more effective in computational time consuming.

7.2.2. MC-MD method

Probably the most interesting develop of the Monte Carlo approach for method of moments is the combination with molecular dynamic. This method was born to take into account details of chemist of incipient particles and after that it was called Atomistic Model for Particle Inception (AMPI) code. The molecular dynamic calculation is performed together with Monte Carlo simulation. The code is able to make these two different approaches coexist. Kinetic Monte Carlo simulation generally ay on quite long time scale compared with molecular dynamic which takes into account time steps in the order of vibrational period of the molecules, i.e. picoseconds. The results are quite interesting, because atomistic scale of the structure, such as bonds, bond angles, and dihedral angles is preserved. This code has been tested in simple flame configuration and to evidence the role of single step, e.g. inception process, in particle formation. Moreover the use of molecular dynamic calculation within the code introduces an element of possible error, due to the need of expressions for potential of interactions. This issue has been covered in literature for similar molecules by different research groups; however a universal agreement on this point is still far to be achieved. This makes the AMPI

code at same time an interesting tool to understand particle evolution and a border line research for developing the code itself.

7.2.3. Sectional method

Sectional approach is one of the possible solutions to Smoluchowski problem. In fact, to solve the population balance problem when an analytical solution is not possible probably the first approach is to discretize the domain and try to get and approximate solution. The limit of this approach would be the use of an infinite number of sections to get the continuous solutions. In the first formulation the Frenklach and Kazakov (Kazakov et al., 1995) and successively developments simulation of aerosol dynamic was performed separately from gas phase kinetic calculation. Pope and Howard develop a numerical tool to fully couple the gas phase results with particle evolution (Pope and Howard, 1997). It uses lumped species in order to incorporate particle dynamic. Particles are divided in classes and each one is treated as in gas phase and elemental reaction step can be written. This allows to take into account lot of chemical detail of reaction steps which otherwise would be lost.

This method allowed in the beginning to have information on total amount of soot and particle size distribution. It has been developed by several groups and tested in many flame configurations for different fuels. This wide range of appliance makes this approach one of the most consistent for particle prediction. However since the first attempt was proposed, in 1997, for more than ten years the development of the sectional method relied in the testing previous versions of the code in different conditions. However despite of large help in understanding particle inception and growth mechanisms no information about chemical composition and internal structure was give.

Finally, a multi-sectional approach was developed, as a part of this work. Details on this enhanced method will be furnished further on and are already present in literature.

7.3. Advanced Multi-Sectional Method description

The Advanced Multi Sectional method for particle description in flame is the last development of the discrete sectional approach theorized sin the 1980's and fully coupled with gas phase kinetics in the late 1990's.

The discretization of particles comes after the assumption that pyrene is the largest molecules that can be treated punctually. For larger molecular weights, the high number of compounds makes almost impossible the specific description of each species. The discretization implies to lose some details with respect to continuous approach. However, numerical tests have been conducted to avoid

artificial restriction due to finite number of sections. The upper and lower limit of discretizations are always maintained enough large to be effectively empty.

The kinetic expression can be written in principle for each lumped species. However particles react in similar way, depending on some parameters, such as size, chemical composition and morphology. Kinetic expressions will be tailored on particle features, assuming some specific dependence on these parameters. If these dependences are chosen on the base of physical meanings their validity could be wider. This approach tries to get more general expression for particle reaction avoiding ad hoc kinetic rates used for matching experimental data.

7.3.1. Particle size distribution

The first discretization has been historically and also conceptually made on the molecular weight. In fact, looking at the total particulate matter it is possible to discern particle classes on the base of their mass. Assuming constant density and sphericity for these particles an equivalent diameter can be obtained for each class. According to this discretization, each section is defined by the mass. The knowledge of the amount of particles for each section means to know the total amount of particulate matter and the particle size distribution. This discretization was practically made by defining each lumped species, also called BINs, in terms of content of carbon and hydrogen atoms. In this first version the H/C ratio for each species was kept fixed at 0.5. However further versions of the model preferred to use a different H/C ratio for each particles fixed a priori on the base of experimental evidences. From a computational point of view, there is no difference, because in both cases H/C ratio is not calculated and does not give more information about particle evolution.

Kinetic expression used for particle reactions are written on the base of similarity with gas phase PAHs kinetics. In fact the reaction rates are in the Arrhenius modified form, which allows to have a pre-exponential factor, a temperature power-law coefficient, an activation energy and a particle correction factor. To avoid large errors in evaluation of enthalpy and entropy coefficient for particles forward and backward reactions are written separately and considered both irreversible.

Pre-exponential factor, temperature power-law coefficient and activation energy are mainly taken from the gas phase kinetics of naphthalene and pyrene. Only for some specific reactions typical of soot particles, i.e. unimolecular decomposition and its reverse reaction, an evaluation has been made. The particle correction factor has been considered to take into account the influence of particle features on reaction rate. In the first discretization this factor accounted only for the increase collisional section. Practically the reaction rate was dependent on the 2/3 power of the reduced mass of reacting species. Later also a linear dependence from the fixed equivalence ratio has been accounted for.

Finally, for each section two classes of compounds is considered the stable species and the correspondent radical. These species differ in composition by a single H atom. The formation of radicals is fundamental for the correct prediction of particle formation. However despite of large number of possible radical for each lumped stable species only a generic class of radicals was considered. Particle to particle coagulation was described as completely coalescent and particles were considered always spherical. A size and temperature dependent coagulation was introduced and became fundamental for the correct description of particle size distribution.

Inception, i.e. gas-to-particle transition, was modeled by considering both the chemical and the physical pathway. Polymerization route involving stable and radical PAHs was considered to form the first lumped species. On the other hand stacking of pyrene was considered enough efficient to form stable dimers which belong to particle section.

7.3.2. Chemical composition of particles

To take into account chemical composition another discretization is needed (Sirignano et al., 2010). In fact, experimental evidences already have suggested that particles close to molecular size have features very similar to large interconnected PAHs. On the other hand large soot aggregates exhibit a graphitized structure with very large aromatic islands. In the version of the model presented so far the particles were described in terms of molecular weight, or, more correctly, in terms of carbon atoms and H/C ratio. This latter was fixed a priori, as a constant or a function of molecular weight. However, in order to use the model to deep understand the particle formation process and to explore also unknown combustion conditions a more general model is needed. In particular, in some conditions, it is possible to form very small particles with chemical characteristics similar to graphitized soot and large aggregates in which the structure is not so packed. Model has to be able to predict all possible situations.

For what stated so far and for the building process of the model schematized before, it is logical to devote attention to the discretization of H/C ratio. In this case the upper and the lower limit of this discretization are fixed by physical constraints. H/C ratio can reach 0 as bottom limit value, e.g. fullerene structure or similar; on the other hand H/C ratio equal to 1 represent an enough large value for a resemble of PAHs. Although these limits of H/C equal to 1 and 0 seems to be not realistic values since it is quite hard to find stable clusters of benzene (H/C = 1) or total graphitized carbon with no hydrogen (H/C = 0), however they are necessary to avoid numerical constriction of the scheme. Flame simulations have shown that these classes contain trace amounts of species and do not affect the results in terms of concentration, molecular mass distribution and H/C.

With this discretization each class is now defined by carbon atoms and H/C ratio, both variable within a certain range of values. Fig. 7.1 reports a schematic representation of the species belonging

to the five H/C particle classes for the first four carbon sections (BINs 1 to 4). In this range of molecular weight it is still possible to find corresponding PAHs in terms of H/C ratio. Particles with largest H/C (0.85 < H/C < 1) are mainly clusters of benzene and of biphenyl-like compounds. The class of particles with mean H/C of 0.7 (0.6 < H/C < 0.85) are essentially poly-phenyls, oligomers of small aromatic hydrocarbons and clusters of small polycyclic aromatic hydrocarbons. Clusters of oligomers of small aromatic, pericondensed aromatic hydrocarbons and PAHs of the acene series (polycyclic aromatic hydrocarbons made up by linearly fused benzenic rings) are representative of the particles with mean H/C ratio of 0.5 (0.35 < H/C < 0.6), whereas large molecular weight pericondensed aromatic hydrocarbons and their clusters belong to the H/C = 0.2 class (0.1 < H/C < 0.35). Finally very large, graphene like structures belong to the H/C = 0 particle class. Grey graduation in Fig. 7.1 is representative for the five different classes of H/C from 0 (dark grey) to 1 (white), as a possible discretization chosen for the model.

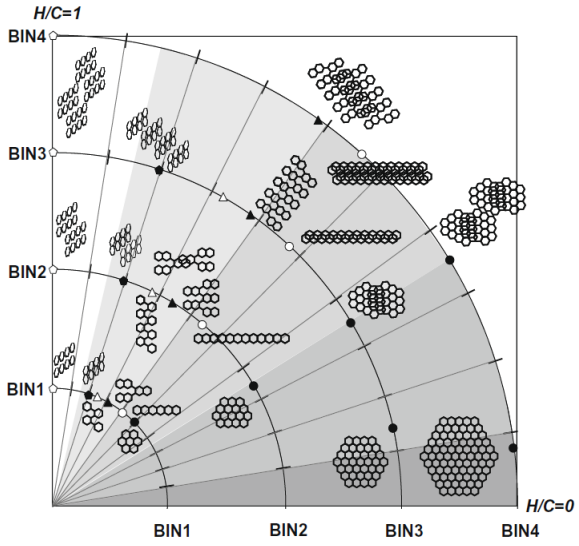

Fig. 7.1. Distribution of large species as a function of mass and of H/C ratio. Model discretization is also reported: From BIN1 to BIN4 it ranges from 24 to 193 Carbon atoms; Grey graduation is representative for the five different classes of H/C from 0 (dark grey) to 1 (white). Dots are representative of classes of compounds: stacks of benzenes (◊), stacks of naphthalene (♦), poly-phenyls (Δ), polynaphthalene (▲), PAHs of acene series and stacks of acenes (○) and pericondensed PAHs (●).

When this discretization is added, reaction rate can be written taking into account chemical composition of particles. The hydrogen content modify the capability of particles to form radical and then to give growth reactions. Moreover particles with different H/C ratio act differently in coagulation process. The more is graphitized the structure the higher is the coagulation efficiency for a given molecular weight. These considerations have to be transposed as reaction rate parameters.

Chemical composition of particles has been taken into account modifying particle correction factor introducing a linear dependence on the H/C ratio. This dependence has been introduced for all the reactions in which an H atom is extracted from the particles. As example, this means that particles with a H/C ratio of 0.75 will react three times faster of particles with same carbon atoms but with H/C ratio of 0.25. Analysis of evolution of particles in flame has showed that the molecular growth by acetylene and gas phase PAHs is not able to explain the aromatization of the particles. In order to match this process a dehydrogenation process has to be taken into account. This process was already known in literature but only a lumped kinetic was proposed and very a few details on the process where furnished. During this thesis a mechanism for particle dehydrogenation has been proposed and kinetic expressions have been written for this. Dehydrogenation channel is built on the consideration that, due to the complexity of the structures for increasing number of C atoms, the radicals formed through the attack of an H atom cyclize to form a closed aromatic ring. The limiting stage is the rearranging of the structure to expel an H atom and form a new stable species with a lower H/C ratio and consequently higher aromaticity. Activation energy of 25,000 cal/mol is used and the dependence on the number of hydrogen atoms present in the structure is considered. The sensitivity of particle formation on this reaction a change of values has been tested ranging from 20,000 to 30,000 cal/mol. The comparison with experimental data available in literature has showed that prediction of H/C ratio is largely missed if these changed values are used. It is interesting to note that H/C ratio strongly influence the total amount of particles. In fact a small value for activation energy favors the dehydrogenation process and thus reduces the possibility to have radical and then molecular growth. On the other hand a too large value of activation energy enhances particle production due to the increased possibility to have radicals. A correct prediction of dehydrogenation process is mandatory for particle prediction in flame.

Coagulation efficiency was written on the base of D'Alessio and coworkers consideration (D'Alessio et al., 2005). One of the main assumptions was that particles interact each other on the bas e of van der Wall attraction which is linked to Hamacker constant. This physical parameter returns the strength of the attraction of the aromatic island. Generally the larger is the aromatic island the higher is the attraction and thus the Hamacker constant. Experimental values for benzene and graphite are available. These values have been considered for the dependence of Hamacker constant on the H/C of lumped species. In fact value found for benzene was assigned to class with H/C = 1, whereas value of graphite was assigned to class of particles with H/C = 0. Linear interpolation has been used for intermediate classes.

Rx1	$A_i + H \leftrightarrow R_i + H_2$	8.85E13 $T^{0.5}$ exp(−16,000/RT) $n_C^{2/3}$ H/C
Rx2	$A_i + OH \leftrightarrow R_i + H_2O$	8.85E13 $T^{0.5}$ exp(−4650/RT) $n_C^{2/3}$ H/C
Rx3	$A_i \rightarrow R_i + H$	6.00E14 $T^{0.5}$ exp(−113,100/RT) n_C H/C
Rx4	$R_i + R_i \rightarrow A_i$	8.00E12 $T^{0.5} n_C^{1/6}$
Rx5	$R_i + C_2H_2 \rightarrow A_i$	3.00E6 $T^{1.787}$ exp(−3262/RT) $n_C^{0.616}$
Rx6	$R_i + A_i \rightarrow A_i + H$	2.00E13 $T^{0.5}$ exp(−15,000/RT) $n_C^{1/6}$
Rx7	$A_i + OH \rightarrow A_i + HCO$	3.00E12 $T^{0.5}$ exp(−10,600/RT) $n_C^{0.623}$
Rx8	$R_i + O_2 \rightarrow R_i + CO + CO$	4.30E11 $T^{0.5}$ exp(−8000/RT) $n_C^{2/3}$
Rx9	$R_i + H \rightarrow A_i + H_2$	8.85E13 $T^{0.5}$ exp(−10,000/RT) $n_C^{2/3}$ H/C
Rx10	$A_i + H \rightarrow A_i + H + H_2$	6.00E14 $T^{0.5}$ exp(−25,000/RT) n_C H/C
Rx11	$A_i + A_k \rightarrow A_{i+k}$	2.00E13 $T^{0.5}$ $\gamma_{COAG} n_C^{1/6}$

Table 1 Ai is the stable lumped species and Ri is the radical one. n_C is carbon number of the reactants except in Rx 4 and 6 where it represents average carbon number of the two reactants; H/C is the H-to-C ratio in the specie. γ_{COAG} is the coagulation efficiency according to D'Alessio (D'Alessio et al., 2005).

7.3.3. Morphology description

The term "particles" was used so far for the definition of lumped species in contraposition to gas phase compounds. Looking at the description of all the processes occurring after large gas phase PAHs formation and feature of compounds which cannot belong to gas phase, this term appears too generic, although the easiest and most intuitive. On the other hand, differentiation between real particles and other compounds is based not only on chemical composition. On the contrary chemical composition can often lead to wrong conclusion on features of compounds. Moreover the model does not account for other discretization and thus the use of a generic definition appears suitable.

In order to gain more information on internal structure of particles another discretization is needed, morphology of lumped species has to be taken into account (D'Anna et al., 2010). Morphology is strictly linked with state of aggregation of compounds. Structures that grow only by chemical reactions can form a per-condensed aromatic hydrocarbon if acetylene is added or aromatic aliphatic linked hydrocarbon if a sigma bond is formed. The introduction of a sigma bond and thus the possibility to rotate make the resulted structure loose. However, no interaction out of plane is involved even if the planarity is lost. These structures are referred as two dimensional ones due to these considerations. They can be also called molecules since no large differences with gas phase

compounds can be noticed. When coagulation acts on these structures, both PCAHs and AALHs, a three dimensional structure is formed. These structures belong to the cluster definition. Unfortunately this definition accounts both for clusters as small as dimers formed by two molecules and for very large structures formed by hundreds of molecules. The correspondent molecular weight can range from a few hundreds up to millions of atomic mass units. The characteristic that these structures have in common is the sphericity, or, more generally, the possibility to be identified as a unique specific entity. In fact after coagulation event, within the cluster the rearrangement of the structure makes impossible to distinguish the original components forming a new entity. Coagulation that leads to cluster formation is also called coalescent coagulation for it similarity with liquid droplets. Clusters are probably the compounds that can be most correctly referred as particles

However as the molecular size increases, clusters form a more rigid structure, which starts having a solid state character. As a consequence of this process, also driven by dehydrogenation reaction, clusters act differently during coagulation process. Coalescence can be alternatively seen as sintering process in which the sintering time scale is shorter than contact time. Contact time can be as long as necessary to give a stable rearrangement of the structure. However, this rearrangement has not to pass through a coalescent-sintering step. If the structure is rigid enough to maintain its own shape the final will not be a unique new cluster but an agglomerate of clusters. This aggregating coagulation is at the base of the formation of chainlike structures, which are also the final form of soot particles. As for the coalescence, aggregation can be seen as a sintering process in which the sintering time scale is longer than contact time. The sintering properties of clusters involved in coagulation depend on chemical composition and molecular weight. Clusters as small as 2nm have high capability to give coalescent coagulation; this can explain why they are always found as single particles. However, 40 nm are the largest size of single particles founded in flame whereas larger compounds are found only as aggregates.

On the base of these considerations three different types of particles are counted for in the model: *Molecules*, *Clusters* and *Aggregates of Clusters*. Two coagulation reactions have been written for coalescence and aggregation. Coalescence can lead from *Molecules* to *Clusters* and from *Clusters* to larger *Clusters*; aggregation can lead from *Clusters* to *Aggregates* or from *Aggregates* to large *Aggregates*. Fig. 7.2 reports contours of the ratio of the agglomeration-to-coalescence regimes at 1800 K for low (lower than 0.25) and high (larger than 0.25) H/C species. It appears that particles with an nC of 10^5 (equivalent size of about 10 nm) have a rate of coalescence higher than that of agglomeration. This behavior is reversed for structures with nC larger than 10^6 (equivalent size of about 20 nm). For particles of 10–20 nm, coalescence and agglomeration rates are similar which means that these particles can coalesce or agglomerate with the same probability. Sensitivity analyses have been conducted by changing the size and H/C ratio dependence of the coalescence rate. The coalescence-agglomeration ratio does not drastically affect the final concentration of the particles but it does determine the size of the primary particles which constitutes particle agglomerates.

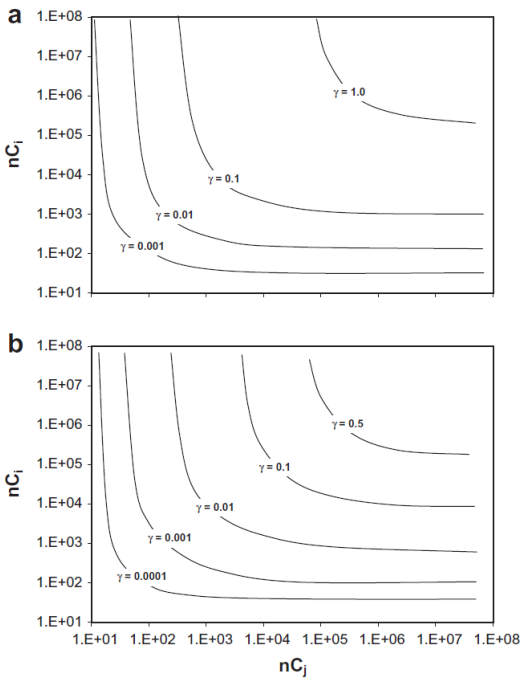

Fig. 7.2 Computed coagulation efficiency γ at 1800 K for pairs of aromatic compounds having C_i and C_j carbon numbers and (a) low (H/C < 0.25) and (b) high (H/C > 0.25) hydrogen content..

Fig. 7.3 reports a general sketch of particle formation according to sectional discretization and experimental evidences.

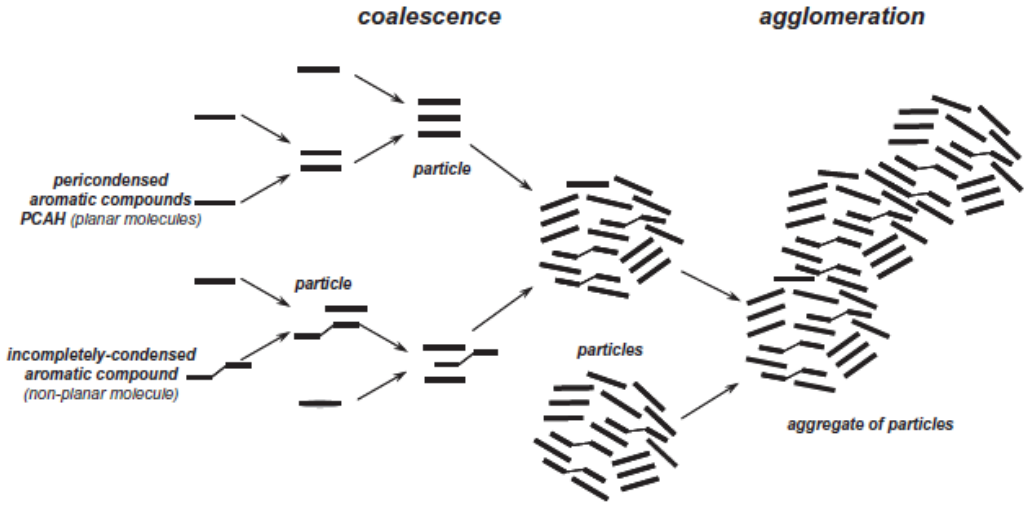

Fig. 7.3. Schematic representation of particle formation pathways).

Since three different types of compounds are defined it is possible to consider oxidation-induced fragmentation described in chapter 4.5. Before morphological discretization was used, it was impossible to clearly describe numerically this process since no difference was operated on chain-like structures and single particles.

Since hydroxyl radical and molecular oxygen have been identified to be the dominant oxidizing species of soot in flames, oxidation has been generally modeled on the base of kinetic expression for these species. In principle both surface oxidation and oxidation induced fragmentation involve the same process. In fact, in both cases the event can be generally schematized as a carbon extraction from soot particles. The main difference relies in the fact that during fragmentation the carbon extraction is in such way critic and strongly affects the internal structure of soot species. This leads to a breaking up of the particle producing smaller fragments. The activation energy of the oxidation by OH is estimated from similar reactions for benzene and PAHs and the collision frequency accounts for the size of the particles involved. Oxidation by O2 molecules uses the rate constant of naphthyl + O2 accounting for the increase of collision frequencies of Xu (Xu et al., 2003). These expression and in particular values for activation energy are considered equal in both surface oxidation and fragmentation whereas different collision frequency factor and other parameters have been considered.

Since fragmentation was not taken into account in the previous version of the model, some considerations have led to the definition of fragmentation process in terms of reaction rates. In particular criticism of carbon extraction in fragmentation process is here described.

Particles are held together in form of aggregates or single primary particles by physical interactions of the aromatic compounds within structures and by internal cross-linking. A reduction of the dimension of the aromatic edges (responsible for physical interaction) or the destruction of the internal cross-linking for effect of the oxidation process can weaken the structure and aggregates or single particles can break apart.

Since the model separately accounts for aggregates and primary particles different fragmentation processes have to be considered.

Fragmentation is considered forming two new entities of equal mass. This process will involve aggregates with large sizes able to contain a large number of primary particles. However, successive splitting up of large aggregates can lead to small aggregates formed only by two primary particles. In this case an eventual fragmentation will form primary particles. Fragmentation can involve also primary particles. In this case internal burning leads to fragment single particle into smaller clusters. This process can continue producing very small fragments.

These simple considerations describe all the fragmentation process. Schematic sketch reported in Fig.7.4 can help to figure out the processes described. It is worth to note that growth and fragmentation appear as different direction in the same evolution path.

Since fragmentation is related to an internal burning of soot, molecular oxygen is considered to be less reactive than OH and hence the only species able to not react on the surface and diffuse towards the points of contact of the primary particles. Larger aggregates have an higher number of contact points and their oxidation-induced fragmentation is considered to be more likely as the size increases. A linear dependence with size of aggregates is considered in this paper.

Aggregates composed by two primary particles are hard to be found, especially with sizes less than 20nm. This suggests that the capability of these aggregates to maintain their shape is weaker with decreasing size. In other words, aggregates of very small sizes are considered be have an high capability to undergo fragmentation process and produce primary particles.

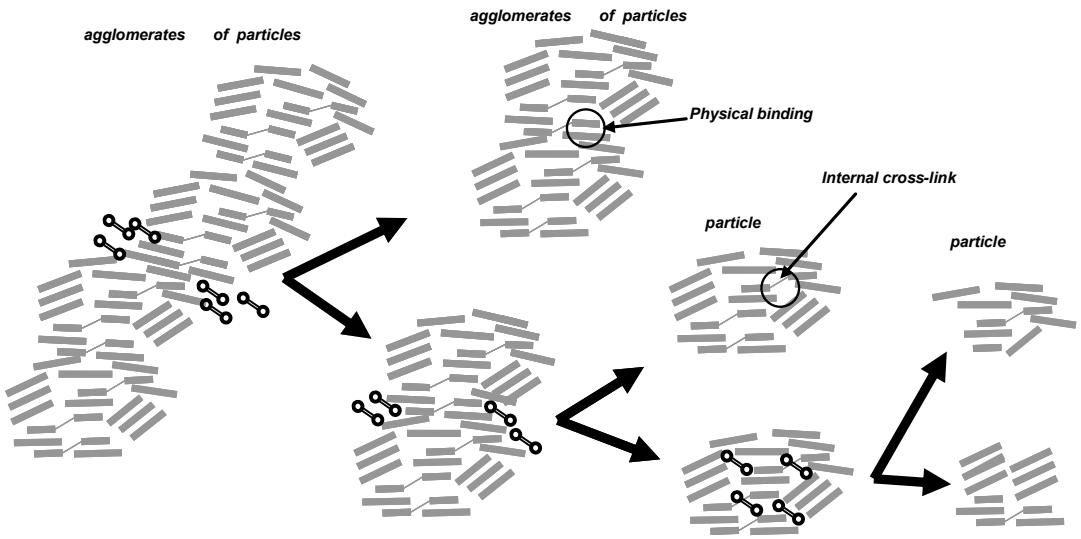

Figure 7.4: Schematic sketch of soot fragmentation; Oxygen molecules are reported in black

As stated before, fragmentation of primary particles is related to the weakening of internal forces, mainly constitute by physical interaction and cross-linking. The strength necessary to maintain together the particle increases as the size of the particle increases. As a consequence, primary particle fragmentation has been considered to linearly increase with particle size itself.

The kinetic expressions used for fragmentation are reported in equations 7.1-3 as a function of the O2 oxidation rate:

$K_{Frag\ A=>A}=K_{Oxy}\ \gamma_{0\ A=>A}\ N_C$; $\gamma_{0\ A=>A}$= 1E-13 (7.1)

$K_{Frag\ A=>P}=K_{Oxy}\ \gamma_{0\ A=>P}\ N_C^{-1}$; $\gamma_{0\ A=>P}$= 1 (7.2)

$K_{Frag\ P=>P}=K_{Oxy}\ \gamma_{0\ P=>P}\ N_C$; $\gamma_{0\ P=>P}$= 1E-4 (7.3)

where A is for aggregates and P is for particles

Size dependence is accounted for through the number of C atoms (NC) in the expression of the kinetic constants

Fragmentation model is generally based on morphological consideration on the processes involved. The rate constants used in the equations 7.1-3 are not coming directly from gas kinetic considerations and can be affected by uncertainties. However, even if the absolute value can strongly affect the total soot burnout rate, the effect on particle size distribution function is determined just by the ratio between different fragmentation processes

Typical values of the oxidation rate with respect to fragmentation for selected numbers of C atoms in the aggregates/particles are reported in table 7.2.

Nc	D, nm	K_{Oxy} / $K_{FragA=>A}$	K_{Oxy} / $K_{FragA=>P}$	K_{Oxy} / $K_{FragP=>P}$
10^4	7	1.E+09	1.E+04	5.E-01
10^6	40	1.E+07	1.E+06	5.E-03
10^8	160	1.E+05	1.E+08	5.E-05

Table 7.2. Ratio between oxidation rate by O2 and different fragmentation rates; Nc is the number of carbon atoms.

7.3.4. Numerical aspects

Hereafter numerical details of the discretization operated. Molecular weight is discretized considering that Species with molecular masses larger than 300u are lumped into classes of compounds defined by a carbon number, which ranges from 24 to $4*10^8$ and an H/C ratio for each

carbon number which ranges from 0 to 1. Twenty-five sections are used in a geometric series of carbon number with a ratio of two between sections. Five sections are used for H/C variation, namely 0, 0.25, 0.50, 0.75, 1. Overall 125 lumped species for the stable form and 125 for radicals are modeled. It is assumed that only one radical species corresponds to each stable species. The current model introduces another discretization which accounts for the level of agglomeration of the compounds. Three entities are defined: single molecules, clusters or particles and agglomerates of particles. In all cases the numbers of C and H atoms are taken into account. For all these entities, radical formation, oxidation by hydroxyl radical and O_2 molecules and dehydrogenation reactions are considered.

8. Reactor analysis: time scale and operative temperature history

In this chapter hints about time scale and mixing conditions for the reactors used during the thesis periods will be furnished. In particular premixed flame and diffusion flame will be analyzed.

8.1. Premixed flame configuration

Premixed flame is one-dimensional reactor which is possible to consider in principle at a plug flow reactor. When operated in laminar conditions, it is also possible to stabilize a flat velocity profile instead of a parabolic one. This allows to have one dimensional feature and thus a correspondence between spatial coordinate and residence time. In this configuration, this flame results quite accessible for experimental and numerical studies. In particular, due to the very low level of complexity of fluid-dynamic conditions, these flames result an important reactor in order to investigate kinetic aspects.

8.1.1. Temperature history in premixed flame

In premixed configuration fuel and oxidant are intimately mixed before the flame front. After a zone of preheating they reach the maximum temperature and then the post combustion zone. It would be an error to think that flame front is the only zone interested by chemical reactions. The preheating zone can reach temperature higher than 1000K becoming a zone in which decomposition and low-temperature oxidation can take place. Due to the high reactivity of the fuel, such in the case of flame of aromatics, this zone becomes fundamental for the formation of high molecular mass compounds. The convective flow brings the partially-reacted mixture toward flame front, where the higher temperature and large presence of ions and radicals strongly enhance the reaction rates. After this point main gas phase compounds have been already formed in large amount and intermediate of reactions are consumed. However the temperature in the post combustion zone does not dramatically decrease and the drop is usually within 200K. Temperature is generally still above 1500K and reactive species such as OH, H radicals, acetylene and eventually PAHs are present in large quantity. In this environment molecular growth process, described before, starts with inception and continues with soot loading and coagulation. Temperature history is quite similar for almost all the hydrocarbon flames, although a preliminary analysis of gas phase combustion products has to be done before looking at further processes.

8.1.2. Residence time in premixed flame

Together with temperature history residence time can give information on the time scale of the processes involved. Generally gas spent in the preheating zone less than 10ms which is almost the same residence time spent in the flame front. This residence time is quite small, suggesting that in this zone just very fast reactions take effectively place, typically oxidation ones. In other words, for many configurations, the flame front can be seen as a starting point for processes with renewed initial conditions, i.e. high temperature large radical and unsaturated species concentration. In other cases pathways that lead to the formation of large molecules can start already in these zones. The post combustion zone starts just after the flame front, .i.e. generally 2-4mm above the burner. It extends conceptually until the emission in the atmosphere. However, due to experimental limitations the studies are conducted up to 20-25mm above the burner. Correspondent residence time is in the order of tens of milliseconds. This time scale results enough large for giving place to inception and growth process.

In premixed conditions, the flame evolution follows the stream line and the products are formed through a specific and unique pathway. This uniformity in precursors pathway and thus in particle formation links the particles present in the flame to the position along the flame axis. In this case different processes appear clearly separated and thus their investigation becomes easier.

8.1.3. Numerical investigation of premixed flame

Implementation of a detailed scheme for the prediction of a premixed flame needs to have some link with experimental details. In fact, due to heat exchange with the burner and the surrounding environment temperature profile of the flame is typical of the specific burner. Moreover the presence of soot particles can cool down the flame due to strong emission. These considerations make mandatory the use of an experimental temperature profile to perform a correct simulation of the premixed flame. This means that energy equation is not solved for this flame.

8.2. Opposed-flow Diffusion flame configuration

In the opposed flow diffusion two opposed nozzle feed fuel and oxidant separately. The flame is quasi one dimensional since each plane of the flame can be assumed at same conditions of temperature and species concentration. The spatial coordinate is the distance between nozzles. A stagnation plane is always possible to be individuated together with a flame front where a maximum of temperature is located. Flame front can be stabilized in the oxidant side, with respect the stagnation plane, or in the fuel side. The post combustion zone in the first case extend both in fuel and oxidant zone, whereas in the latter is confined in the fuel side. Convective fluxes are very peculiar since they are opposed in the two different side both pushing the material toward stagnation plane.

Diffusion smoothens the profiles of temperature and species acting both toward oxidant and fuel nozzle.

8.2.1. Temperature history in opposed-flow flame

Temperature in opposed-flow flame strongly varies with the position along the distance between nozzles. In flame front zone temperature can be as high as 2000K, whereas in the fuel side, where pyrolytic conditions are present, temperature can be as low as 700-1000K. This great variation associated with very peculiar stream lines does not allow to consider that in this flame only one particular pathways of reaction is favored. As a consequence attention has to be paid to all pathways especially for particle formation. Moreover temperature depends on initial condition of the fed gases in terms of velocity and concentrations: strain rate and position of maximum temperature can significantly change temperature history of the flame.

8.2.2. Residence time in opposed-flow flame

Similarly to temperature history residence time strongly depends on the initial conditions in particular velocity field. However in laminar flames velocity of fed gases can vary in a range in which the strain rate still allows to the flame to be sustained. However, the distance between the two nozzles is small, generally less than 2cm. This implies that also the post combustion zone residence time is comparable with those found in premixed configuration.

8.3. Coflow Diffusion flame configuration

In the coflow diffusion flame configurations the one-dimensional feature is lost. Flame is developing both in axial and radial direction. For each axial position along the flame, a radial profile of temperature and species concentration can be determined. This makes harder both the investigation with experimental equipment and numerical tools. However, the study of diffusion flames is mandatory to achieve reliable results. These flames are more similar to real combustion systems in which the premix condition is not always achieved and in many cases it is not desired.

8.3.1. Temperature history in co-flow flame

Temperature history in diffusion flame is strictly linked with streamlines. The combustion is controlled by the diffusion of fuel in oxidant and vice versa. On the other hand, the convective flux moves toward upper zones, in which different temperature condition can be created. When fuel is sent in the inner side and oxidant is sent in the annulus – “normal” coflow flame – flame front is located in the outside and the post combustion zone relies in the inner part of the flame. In this case temperature of the flame front can reach values as high as 2000K whereas the inner part is much colder, generally down to 500K. In the “inverse” diffusion flame the air is sent in the inner side and

the fuel is sent in the annulus. In this configuration, the post combustion zone is not confined by the flame front, which is located in the inner part of the flame. In the normal diffusion flame, the convective stream lines pass through the flame front in the top of the flame. This passage can induce an oxidation of unburned hydrocarbons and also of particles produced in the inner part of the flame. This process can make the flame sooting but not smoking. However, as for opposed flow configuration, different particle formation pathway can be simultaneously active ant thus the particles resulted having intermediate properties in dependence of the peculiar flame history.

8.3.2. Residence time in co-flow flame

Differently for previous flame reactor coflow flame is characterized by substantially longer residence time. In fact lab scale diffusion flames are in the order some centimeters in height. Looking at streamlines in a normal co-flow flame, the convective flux moves longitudinally with respect to the flame. This means that the outer part of the post combustion zone will be relatively close to the maximum temperature zone from the bottom to the tail of the flame, in a similar way to the very first part of post combustion zone in premixed configuration. The inner part of the post combustion zone instead is relatively far from the most reactive zone and the temperature is almost always below 1000K. The tail of the flame, where the streamlines converge, unify the two zones and let them both pass through the flame front again. In the inverse diffusion flame the situation is quite similar except for the fact that the streamlines move toward the outer part and there is not closure of the flame on the top. In both configurations, residence times are almost one order of magnitude larger making the molecular growth process and the coagulation more effective. Moreover most of the particles are relatively close to high temperature zone than in other flame configurations. This can affect their evolution and final feature.

8.3.3. Numerical investigation of co-flow flame

Numerical investigation of co-flow flame is generally much more onerous. As for the opposed flow flame and differently from premixed flame, the energy equation has to be solved. Moreover, the two dimensional configuration slows down the calculation requiring a larger spatial domain discretization - a second power increase of cell number in principle. Probably the stiffest point is related to the effect of soot on temperature balance. Radiation has to be taken into account: in the opposed flow configuration, the small dimensions and the relatively high strain rate make this term almost negligible. In coflow configuration, an error on soot radiation can turn into a large error in temperature. This again can affect the total amount of soot predicted starting a loop which can lead to very wrong conclusions. That’s why a check with experimental data and sensitivity analysis on the radiation coefficient used for soot has to be done in order to avoid large numerical errors.

9. Production and characterization of tailored nanoparticles

In this chapter results obtained both with experimental techniques and modeling will be presented. Particles will be investigated not only on the aspect of production rate but also looking at their physical chemical characterization. Results for flame reactors will be presented first, later based on the knowledge gained on these reactors a different approach will be described. This approach is based on the study of the evolution and eventually the formation of particles in medium temperature regime. Hereafter some preliminary results will be presented discussing eventual developments of this technique.

9.1. Flame reactors

In traditional flame reactors many parameters have been studied such as temperature, fuel nature, equivalence ratio, premixing ratio. In this work some of these have been investigated; here the effect of equivalence ratio and the fuel structure on the production and main features of the particles will be presented for premixed flame, the effect of the mixing and temperature history in the opposed-flow flame and finally the role of oxidation-induced fragmentation in coflow flame.

9.1.1. Premixed laminar flame

For their one-dimensional feature and the relatively high experimental accessibility, premix flames and the effect of key parameters on particle formation are widely studied. Usually temperature effect on both total amount and nature of produced particles has been always looked with great interest (Alfè et al., 2010, Ciajolo et al., 1996, Kent and Wagner, 1985, Glassman and Yaccarino, 1981, Alfè et al., 2009). This is probably due to the research of a single parameter which can help and lead in the world of combustion generated particle. Although many correlations have been found between maximum temperature and particles, this point of view appears overtaken. In fact, nowadays the main issue is no longer only total soot amount reduction in real combustion systems, but also preventing the formation of large numerical concentration of small nanoparticles. Moreover for these compounds the effects on health and climate are far to be completely understood. This task cannot be faced approaching the problem looking just at temperature effect. Together with temperature other parameters have to be investigated. According with these statements in this work less attention to the effect of temperature has been paid, focusing on other

less investigated parameters. However experimental techniques and especially numerical tool can be easily applied to the study of temperature or other parameters in further works.

Role of equivalence ratio

A benchmark of classical combustion view is that for an equivalence ratio, Φ, equal to 2 soot starts being produced. This point, also known as soot threshold, has been quite verified for aliphatic hydrocarbon flames whereas slight disagreement has been found for aromatic flames in which soot appears at lower Φ. This statement only takes into account large aggregates which were the first detected in flame. For Φ close to stoichiometric, i.e. in less rich conditions, it is possible to have a particle-free flame. However recent studied clearly demonstrated that there is a zone of equivalence ration in which nanoparticles are produced in absence of soot aggregates.

An analysis of flame with equivalence ratio slightly below soot threshold, conducted with differential mobility analysis DMA by different groups in the world, has showed that these particles appear as unimodal size distribution between 2 and 10nm. However DMA does not furnish details of the chemical features of these particles. Previous experiments on flame with similar conditions showed the presence of UV absorbing compounds able also to give a non-structured UV fluorescence, which cannot be assigned to gas phase PAHs. Nowadays the existence of these particles is well established and there are hints about their chemical features.

Mechanisms of particle formation have been described before; however some particular pathway in particle evolution not well evidenced can help in produce tailored compounds.

Premixed laminar ethylene-air flames have been studied with 0,71 and 0,77 C/O ratios (corresponding to the equivalent ratios Φ of 2,13 and 2,31 respectively) and with cold-gases velocities of 10 $cm \cdot s^{-1}$. The goal of this study is to characterize with optical techniques combustion-formed particles.

From laser induced emission measurements, conducted by exciting in the ultraviolet region of the electromagnetic radiation by the fourth harmonic of the Nd:YAG laser, i.e. a radiation with a wavelength of 266 nm, the attendant presence of the three principal emission phenomena:

- elastic light scattering,
- laser induced fluorescence,
- laser induced incandescence.

Several delay times and several signal acquisition gates has been used to highlight the three principal emission phenomena separately. The attention has been addressed to the fluorescence and incandescence phenomena principally. Spectra have been obtained subtracting the natural emission of the flames.

In figure 9.1 and 9.2 the blue spectra have been obtained starting from zero, such that the maximum value of the scattering. These spectra show the elastic scattering signal at 266 nm and the scattering of the residual second harmonic of the laser, the two peaks at 470 nm and at 513 nm correspond to the emission of the C2, between 270 nm and 450 nm the fluorescence signal is visible. At a delay time of 10 ns, the scattering signal disappears, while the signals of C2 emission and fluorescence are still present and have the same trend but lower intensity than the spectra at zero. At higher delay times the fluorescence signal quenches and at a delay time of 20 ns is negligible.

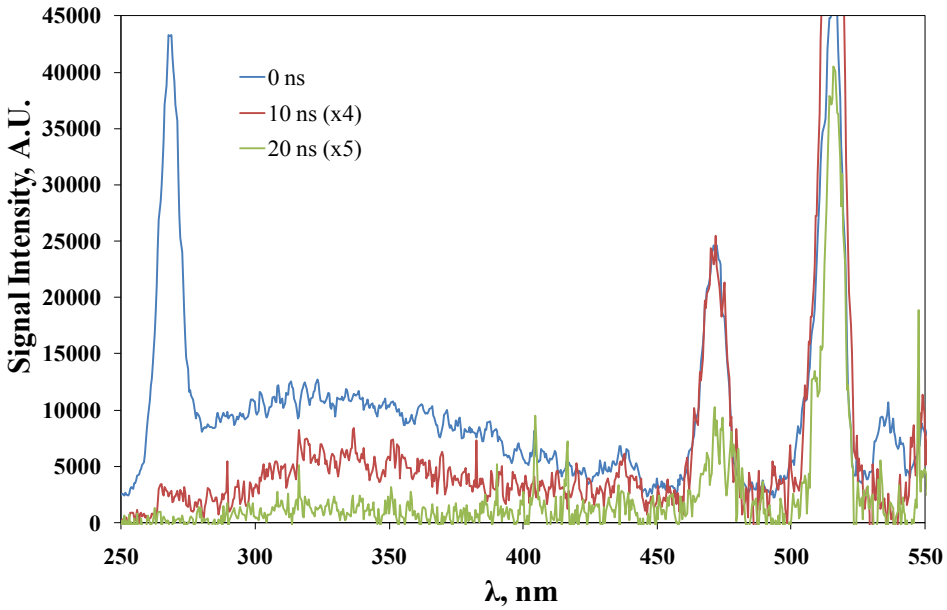

Figure 5.1 Emission spectra, C/O=0,71, HAB=5 mm, variable delay time, camera gate 20 ns.

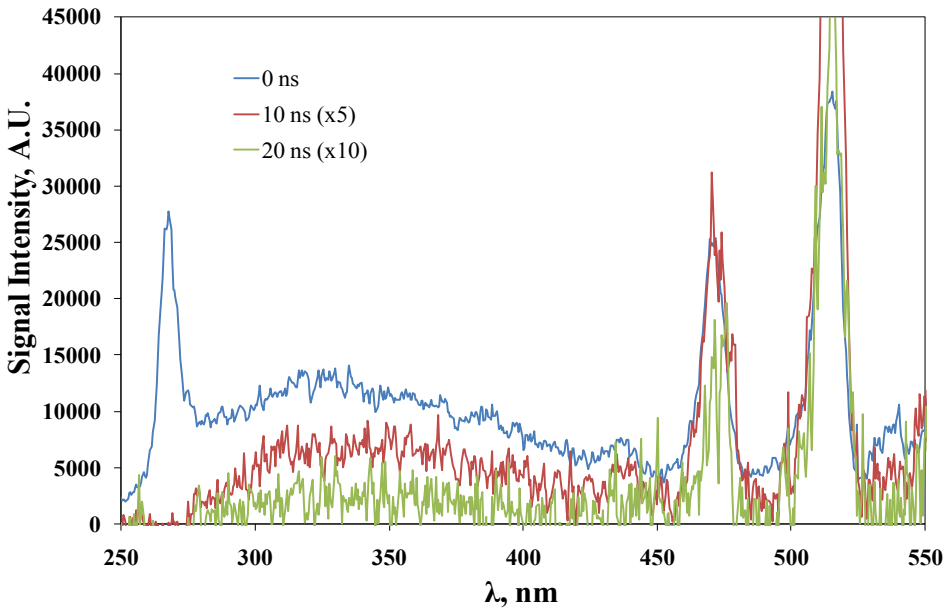

Figure 5.2 Emission spectra, C/O=0,77, HAB=5 mm, variable delay time, camera gate 20 ns.

In figures 9.3 and 9.4 emission spectra at 8 mm height above the burner of the flame C/O=0,71 and flame C/O=0,77 are reported respectively. In the C/O=0,71 flame (figure 5.3), at 8 mm HAB and at a delay time of 10 ns, the fluorescence phenomenon is still distinguishable since small aromatic molecules are still present. Moreover, the incandescence phenomenon is not detected, suggesting that soot particles are still not formed. On the other hand, in the C/O=0,77 flame (figure 5.4), at 8 mm HAB and at a delay time of 10 ns, the fluorescence phenomenon is visible but at this height (i.e. dwell time) the incandescence phenomenon, which follows the blackbody radiation trend, appears noticeable. This signal is the only present at larger delay times.

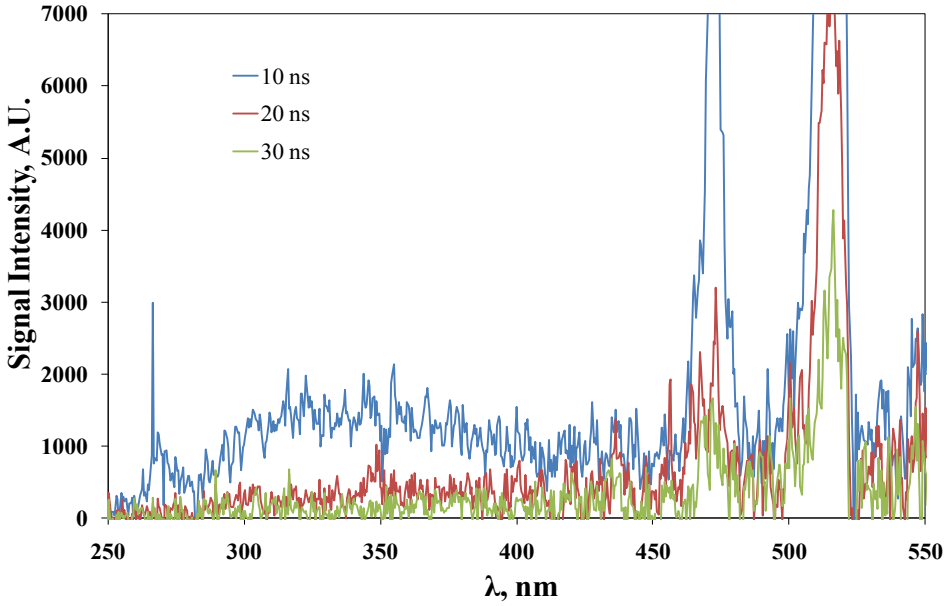

Figure 9.3 Emission spectra, C/O=0,71, HAB=8 mm, variable delay time, camera gate 20 ns.

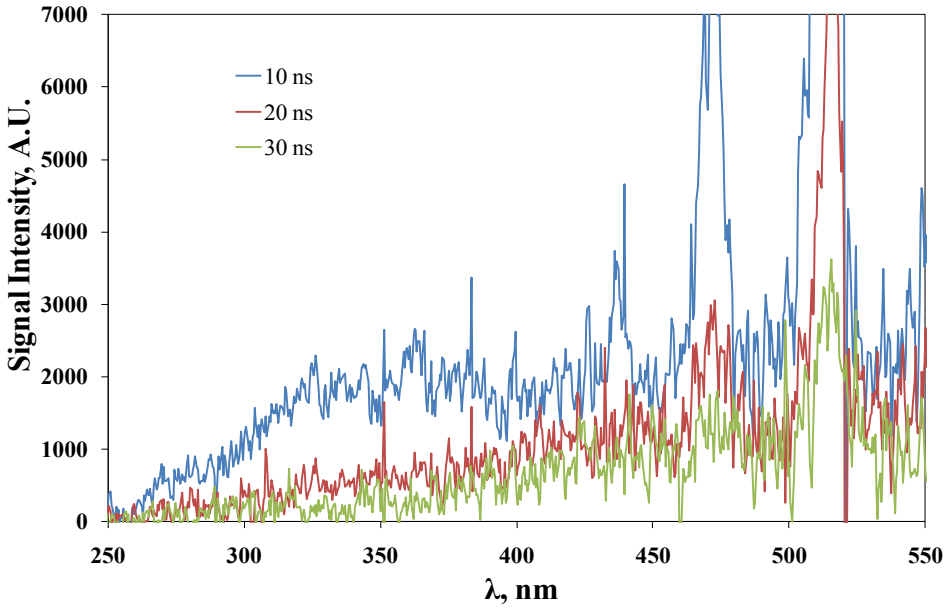

Figure 9.4 Emission spectra, C/O=0,77, HAB=8 mm, variable delay time, camera gate 20 ns.

In figure 9.6 spectra of the C/O=0,71 flame at 14 mm HAB, at different delay times and with a camera gate of 50 ns are showed. The incandescence signal is still weak and a fluorescence signal is still detectable, that is there are still present small aromatic molecules and soot particles are present

in low concentration. In figure 9.7 the emission spectra of the C/O=0,77 flame at 14 mm HAB, with a camera gate of 50 ns and several delay times are showed. The incandescence signal is stronger than the incandescence signal at 8 mm HAB of the same flame (figure 5.6) that means that the presence of soot particles is more considerable.

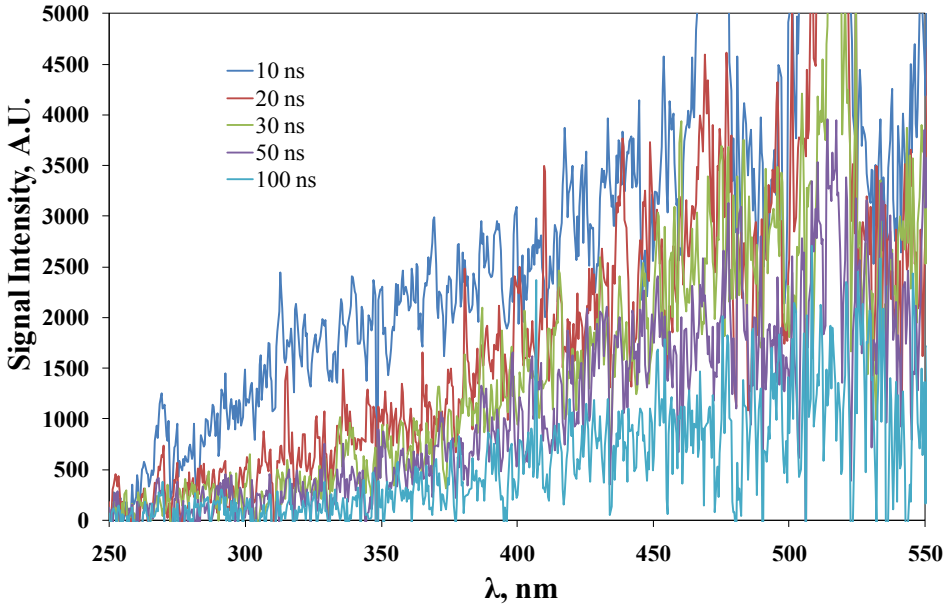

Figure 9.6 Emission spectra, C/O=0,71, HAB=14 mm, variable delay time, camera gate 50 ns.

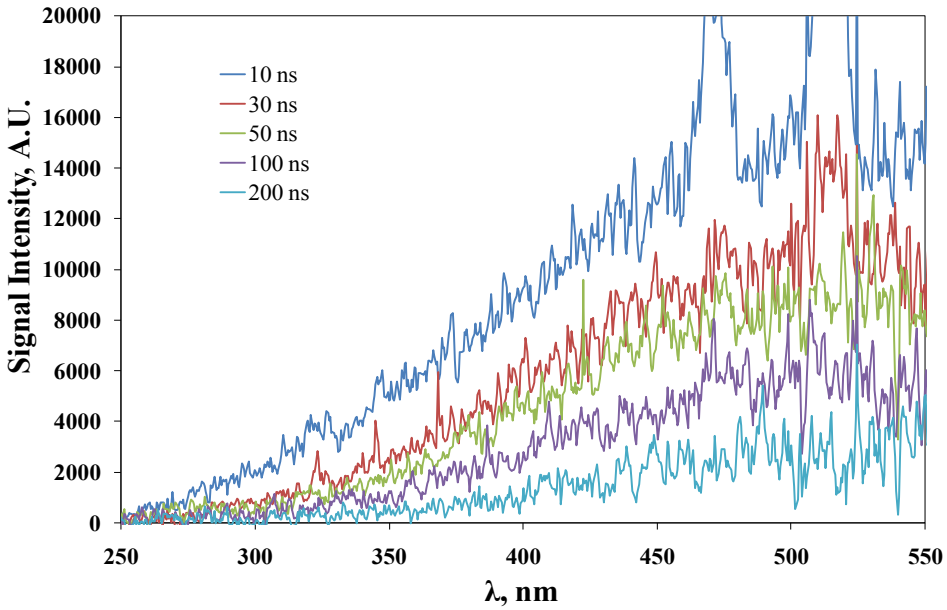

Figure 9.7 Emission spectra, C/O=0,77, HAB=14 mm, variable delay time, camera gate 50 ns.

To compare emission spectra at several heights is possible, fixing the camera gate and the delay time. In figures 9.8 and 9.9 are showed spectra at different heights above the burner for the C/O=0,71 and C/O=0,77 flames respectively with a camera gate of 20 ns and a delay time of 10 ns.

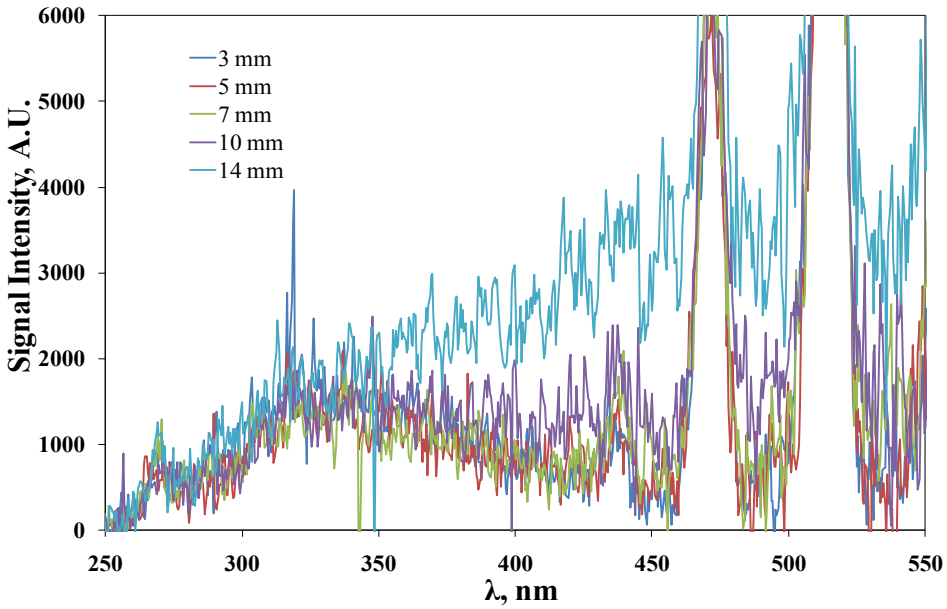

Figure 9.8 Emission spectra, C/O=0,71, 10 ns delay time, different heights, camera gate 20 ns.

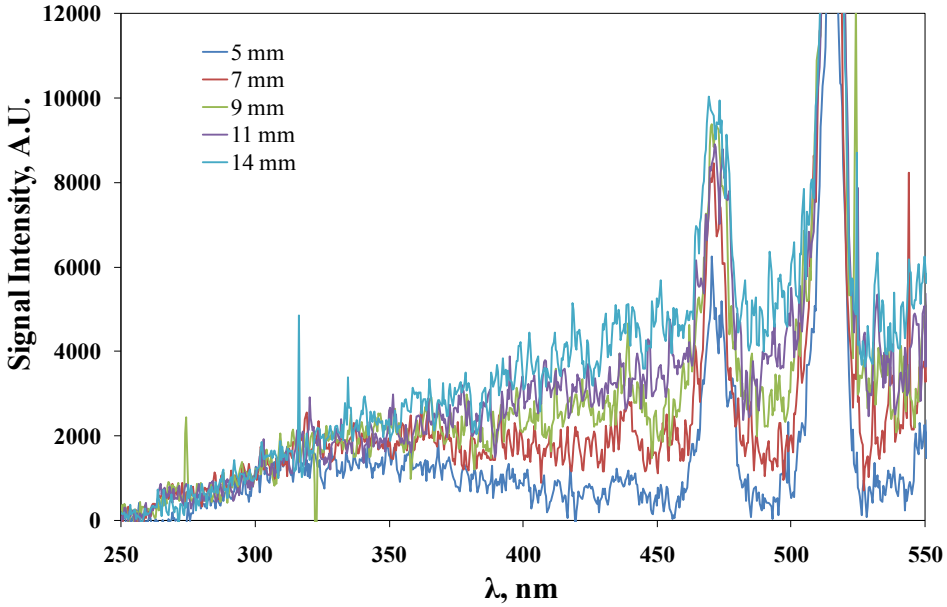

Figure 9.9 Emission spectra, C/O=0,77, 10 ns delay time, different heights, camera gate 20 ns.

From figures 9.8 and 9.9 the beginning of the incandescence phenomenon can be noticed: in the C/O=0,71 flame the incandescence begins to be significant at heights above burner higher than 10 mm, while in the C/O=0,77 flame at 7 mm height above burner the incandescence contribution is clearly visible. In both flames the incandescence signal grows with the height above burner and decreases with the delay time, as showed in the previous figures. In figure 9.10 spectra of the C/O=0,77 flame for a delay time of 50 ns and a camera gate of 50 ns, for several heights are showed.

The trend of fluorescence and incandescence signal for both C/O=0,71 flame and C/O=0,77 flame are reported in figures 9.11 and 9.12 respectively. Fluorescence phenomenon has been considered peaked at 310 nm, 340 nm, 390 nm and 420 nm while for the incandescence phenomenon the signal at a wavelength of 550 nm has been used. In both figures the incandescence values have been reported to the second vertical axis. For the fluorescence phenomena the signal has been taken at a delay time of 0 ns (i.e. zero time) and a camera gate of 50 ns, rather for the incandescence the signal has been taken at a delay time of 50 ns and with a camera gate of 50 ns to avoid the fluorescence signal overlapping.

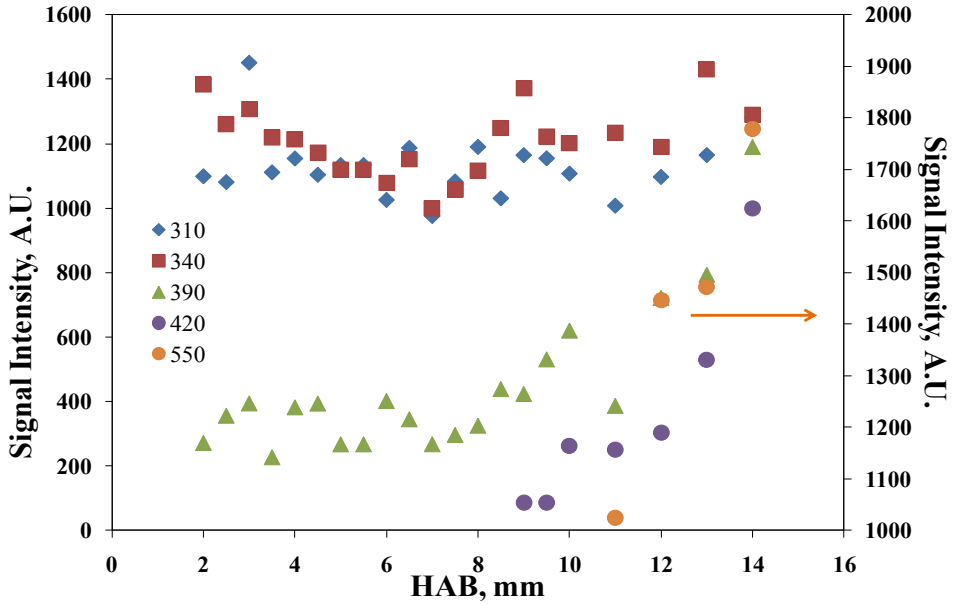

Figure 9.11 Fluorescence and incandescence signals along HAB, C/O=0,71, 0 ns delay time for the fluorescence and 50 ns delay time for the incandescence, camera gate 50 ns.

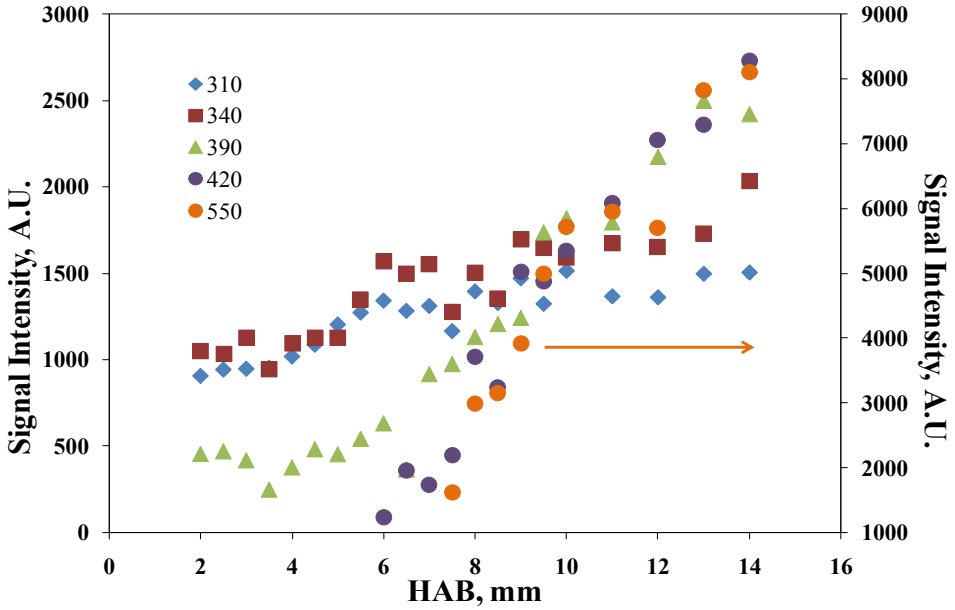

Figure 9.12 Fluorescence and incandescence signals along HAB, C/O=0,77, 0 ns delay time for the fluorescence and 50 ns delay time for the incandescence, camera gate 50 ns.

In the C/O=0,71 flame (figure 9.11) it is possible to notice that the signals at 310 and 340 nm are present all along the flame, while fluorescence at 390 and 420 nm appears above the 8 mm and the incandescence signal appears above the 11 mm. This means that all along the flame small aromatic molecules are present while large aromatic molecules and soot appear only at high heights (i.e. dwell time). Also in the C/O=0,77 flame (figure 9.12) the signals at 310 and 340 nm are present all along the flame but the fluorescence signals at 390 and 420 appear at 5 mm height above burner and the incandescence signal appears at 7,5 mm HAB. In the C/O=0,77 flame, small aromatic molecules are present all along the flame but large aromatic molecules and soot particles appear earlier than in the C/O=0,71 flame.

The trend of the incandescence signal can be verified with the elastic scattering signal (at 266 nm) since the scattering signal is related to the diameter of soot particles raised to the sixth power. Scattering signal trends for the C/O=0,71 and C/O=0,77 flames are reported in figures 9.13 and 9.14 respectively.

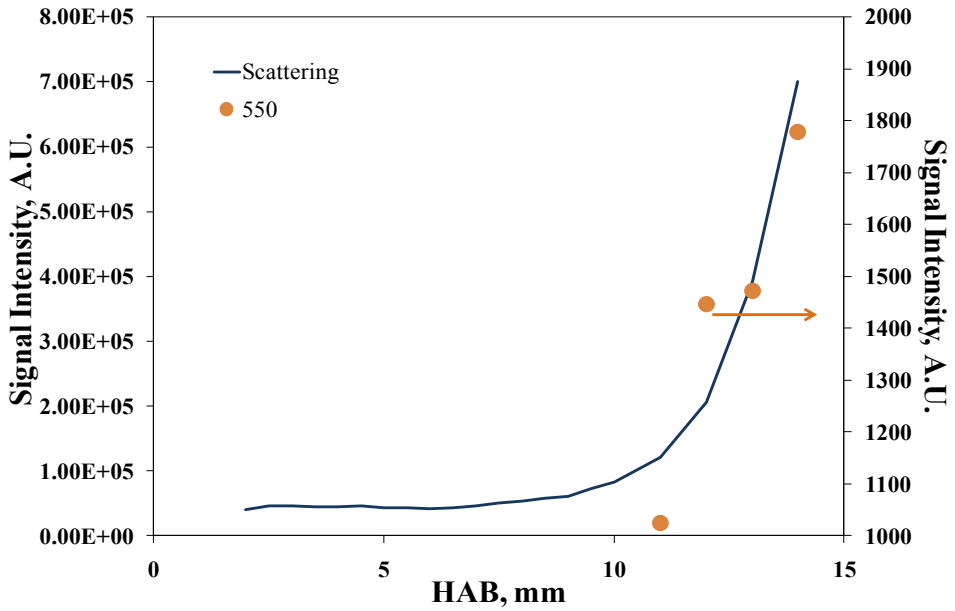

Figure 9.13 Scattering signal along HAB, C/O=0,71, 0 ns delay time, camera gate 20 ns.

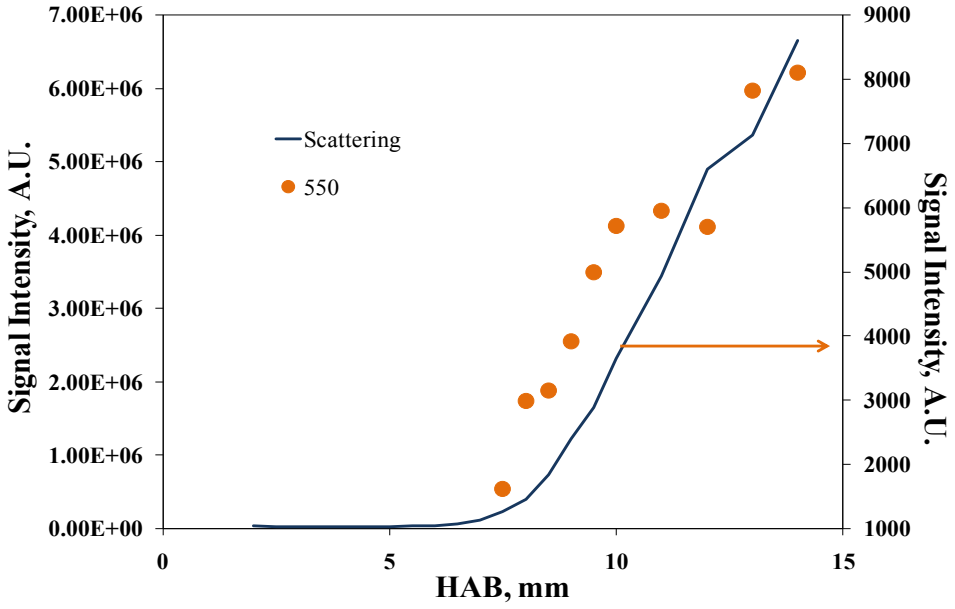

Figure 9.14 Scattering signal along HAB, C/O=0,77, 0 ns delay time, camera gate 20 ns.

A global analysis of these flames suggests that in some combustion conditions when large aggregates are not present some aromatization process is already taking place. As a consequence, the

fluorescence signal is detected at larger wavelength that is related to large aromatic islands within the nanoparticles. As the equivalence ratio increases, this step becomes faster and thus between the UV fluorescence and the incandescence signal the spatial and temporal gaps are reduced. Equivalence ratio in this case seems to be a possible way to tailor the aromaticity of the particles with all the consequences that this change implies.

Role of fuel structure

The role of fuel on the final structure of particles has been partially assessed in literature, perhaps focusing the attention on other parameters. On the other hand, only lately the role of fuel on the soot yield and formation mechanism has been investigated by using the DMA. Again these technique give information on amount of soot and nanoparticles produced close to flame front and in post combustion zone whereas no clue about properties is furnished. However, even separately, both aliphatic and aromatic fuel flames have been optically investigated and information on particle nature has gained. However, since many parameters can influence the mechanisms that control particle formation and evolution a systematic study is needed.

On this point, a comparative experimental and numerical analysis of flames fuelled with different fuels has been conducted. Experimentally the flames were investigated with several techniques in order to simultaneously obtain information on yield, chemical composition, size distribution, and optical properties. Numerically the most advanced discrete sectional methods which is able to model total amount, size distribution, chemical composition and particle structure.

Experiments have been conducted in collaboration with Ciajolo research group. Hints about the experimental characterization will be furnished whereas further details can be founded in literature (Sirignano et al., 2011).

Methane, ethylene and benzene fuel-rich premixed flames have been investigated to study the effect of the fuel structure on particulate formation and on the chemical and morphologic characteristics of the particles. Premixed flames at atmospheric pressure were produced on a commercial McKenna sintered bronze burner (60 mm OD). The burner was water-cooled and the temperature of the cooling water was kept constant at 60°C. An external shield of nitrogen was used to avoid air entrainment. Different cold-gas flow velocities, equivalence ratios and nitrogen dilution were used in order to obtain comparable flame temperatures as shown in Table 9.1, where the flame operating conditions are reported.

Fuel	Cold gas velocity (cm/s)	C/O	ϕ	Fuel (vol.%)	O_2 (vol.%)	N_2 (vol.%)	T_{max} (K)
Methane	5.0	0.6	2.4	54.5	45.5	–	1700
Ethylene	4.0	0.8	2.4	44.4	55.6	–	1730
Benzene	4.0	0.77	1.9	4.9	19.0	76.1	1780

Table 9.1 Experimental conditions of premixed flame investigated for the study of fuels structure effect on soot.

Samplings were performed in order to obtain material for successive off-line measurements. Combustion products, including gaseous, tarry and solid material, were collected from the flames by a water-cooled probe. Total particulate matter was recovered from the sampling line, constituted of an ice-trap and a Teflon filter, and extracted by dichloromethane (DCM) to separate the DCM-soluble species, containing polycyclic aromatic hydrocarbons (PAH) (Tregrossi et al., 1999, Ciajolo et al., 1998), from the DCM-insoluble species. Gravimetric evaluation of the sampled material was conducted in order to obtain soluble, insoluble and by summation total particulate yield. Moreover, on the same material H/C atomic ratio of the solvent-soluble fraction and dry soot were measured by an elemental analyzer.

Here it appears evident that the distinction into two fractions within total articulate matter relies in their solubility in a specific solvent. This is an arbitrary division. However, experimental evidences have suggested that this division and similar separation processes are more general than expected. The soluble fraction is mostly composed by what is also called nanoparticles, i.e. compounds with size less than 10nm and with chemical-physical composition more similar to gas phase PAHs than graphitized soot.

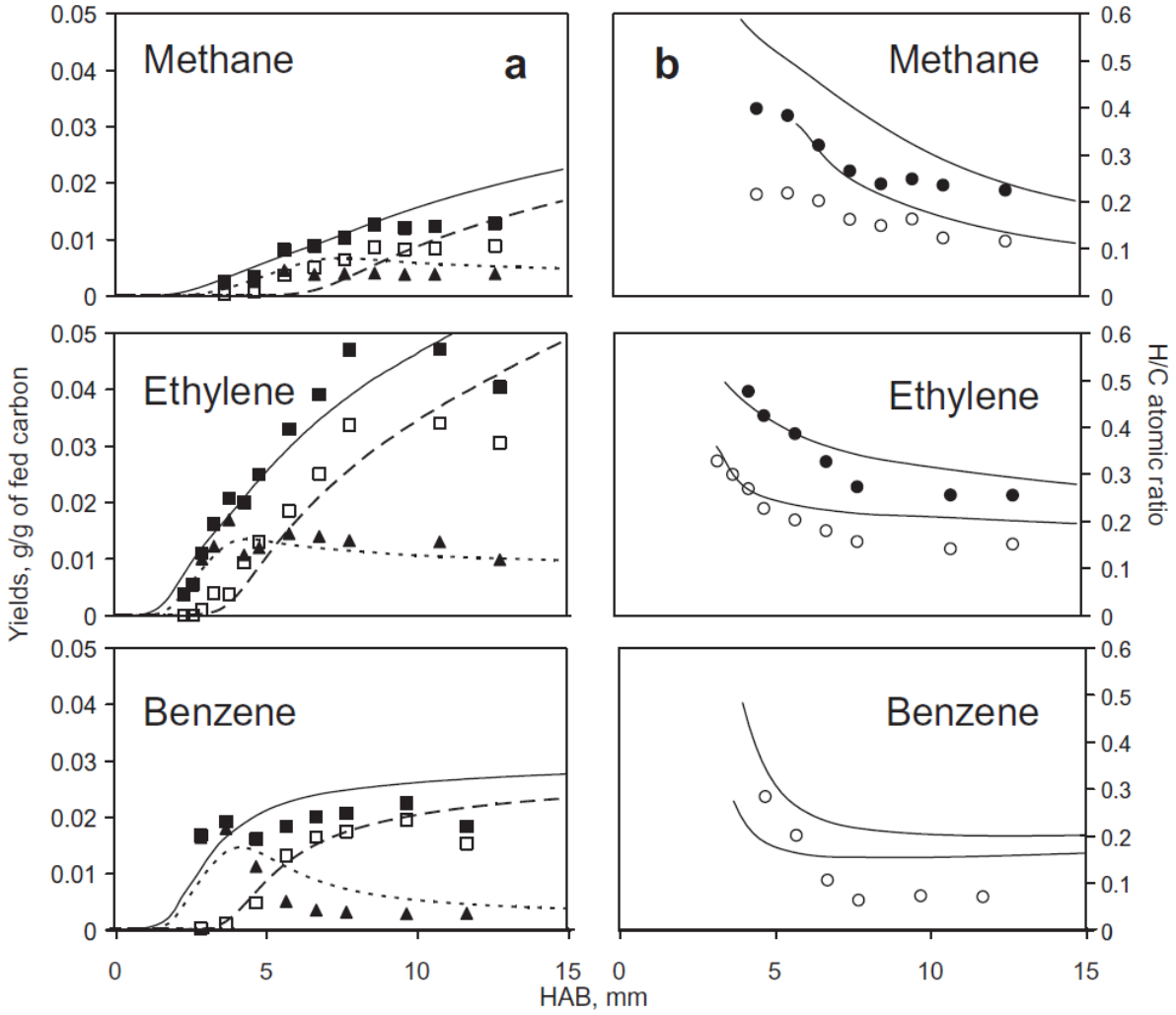

Fig. 9.15. (a) Yields of total particulate matter (■ experiments, __ modeling), soot (□ experiments, __ __ modeling) and solvent-soluble species (▲ experiments, - - - modeling) for the three flames. (b) H/C ratio of total particulate (● experiments, heavy line for modeling) and soot (○ experiments, thin line for modeling) for the three flames

To take into account for the different fed carbon and flame dilutions, experimental data have been expressed as carbon yields and compared with model predictions. On the base of past experimental evidence about the separation of the total particulate, the solvent-soluble fraction has been compared to modeled species with MW <105 u and solvent-insoluble fraction, i.e. soot fraction, to modeled species with MW >105 u. At this point, in order to avoid artifact in the comparison, he only distinction has been done on the molecular weight of the species and thus the summation has been operated on all the three morphological types considered.

Figure 9.15a reports the carbon yields of the total particulate, solvent-soluble fraction and soot fraction measured along the axis of methane, ethylene and benzene flames. The particulate yield increases along the axis of all flames, but a higher formation rate can be observed in the benzene flame. However, in spite of the higher propensity of benzene to form soot, the particulate yield is lower in respect to the ethylene flame due to the higher dilution of the benzene flame (Table 1). The total particulate rise is initially due to the increase of the solvent-soluble fraction yield. After the maximum, the steep decrease of the solvent-soluble fraction occurs in the benzene flame, reaching very low values as soot production rapidly levels-off. Along the ethylene and methane flames the solvent-soluble fraction increases and, after the maximum, it remains quite constant whereas soot exhibits a monotonic increase throughout the flames, although with a lower rate in the final flame region. Model predictions, also reported in Fig. 9.15a, reasonably well reproduce the profile shapes and values of yields, especially for ethylene and benzene flames.

The experimental and modeled H/C ratios profiles of total particulate and soot fraction are reported in Fig. 9.15b to follow the chemical and thermal histories of the carbon particulate. The H/C ratio of the total particulate in the benzene flame could not be evaluated due to the interference of oxygenated aromatic species in the solvent-soluble fraction. The H/C ratio decrease of particulate along the flame axis testifies the occurrence of dehydrogenation/graphitization process leading to the increase of the aromatic carbon network. The model reasonably reproduces this trend, although the H/C ratios are overestimated for the methane and benzene flames. It is worth to remind that the H/C ratio decrease is mainly due to soot fraction rather than to solvent-soluble fraction(Ciajolo et al., 1998), demonstrating that the increase of the extension of the aromatic network primarily occurs in soot particles. At same time the separation based on solvents affinity probably hide slight but progressive and remarkable changes also in nanoparticles which were evidenced with optical technique. H/C ratio of benzene soot rapidly and early decreases, reaching very low values downstream of the flame front, where dehydrogenation process ends. The model is able to reproduce well the fast decrease of soot H/C ratio in the benzene flame.

The different behaviors of the H/C ratio along the three flames can be ascribed to the different flame environments in which particles nucleate and graphitize. Indeed, in benzene flame particles formation occurs already in the main oxidation region, i.e. in the flame front. In this region, located at about 3.5 mm (Fig. 9.15a), the concentration of H and OH atoms reaches the maximum values. The high temperature and radical concentration and the aromatic nature of the fuel strongly favor molecular growth and particle inception. In benzene flame dehydrogenation reactions occur very early leading to the formation of graphitized structures, i.e. mature soot particles, across the flame front. Conversely, particulate formation in the aliphatic fuel flames occurs downstream the flame front, which is located at about 2 mm in both methane and ethylene flames. In this post flame region, the temperature is slightly lower, while the concentrations of H and OH radicals attain the equilibrium values. The temperature and radical concentration decrease inhibits the dehydrogenation causing a

reduced and delayed maturation of soot particles. This is suggested both by the shape of H/C ratio of soot particles and by final hydrogen fraction in them.

Further insights on the particle structure evolution have been obtained by evaluating the MW distribution of particulate matter with Size Exclusion Chromatography, SEC,

Figure 9.16 shows the normalized mass distributions of total particulate experimentally determined at the inception (left side of Fig. 9.16) and in the post-flame region (right side of Fig. 9.16) of the three flames in comparison with the model results. It is worth to remind that the MW distribution of the total particulate has been obtained by re-composition of the SEC chromatograms of the solvent-soluble fraction and soot assuming the same absorptivity measured at 350 nm of the particulate fractions.

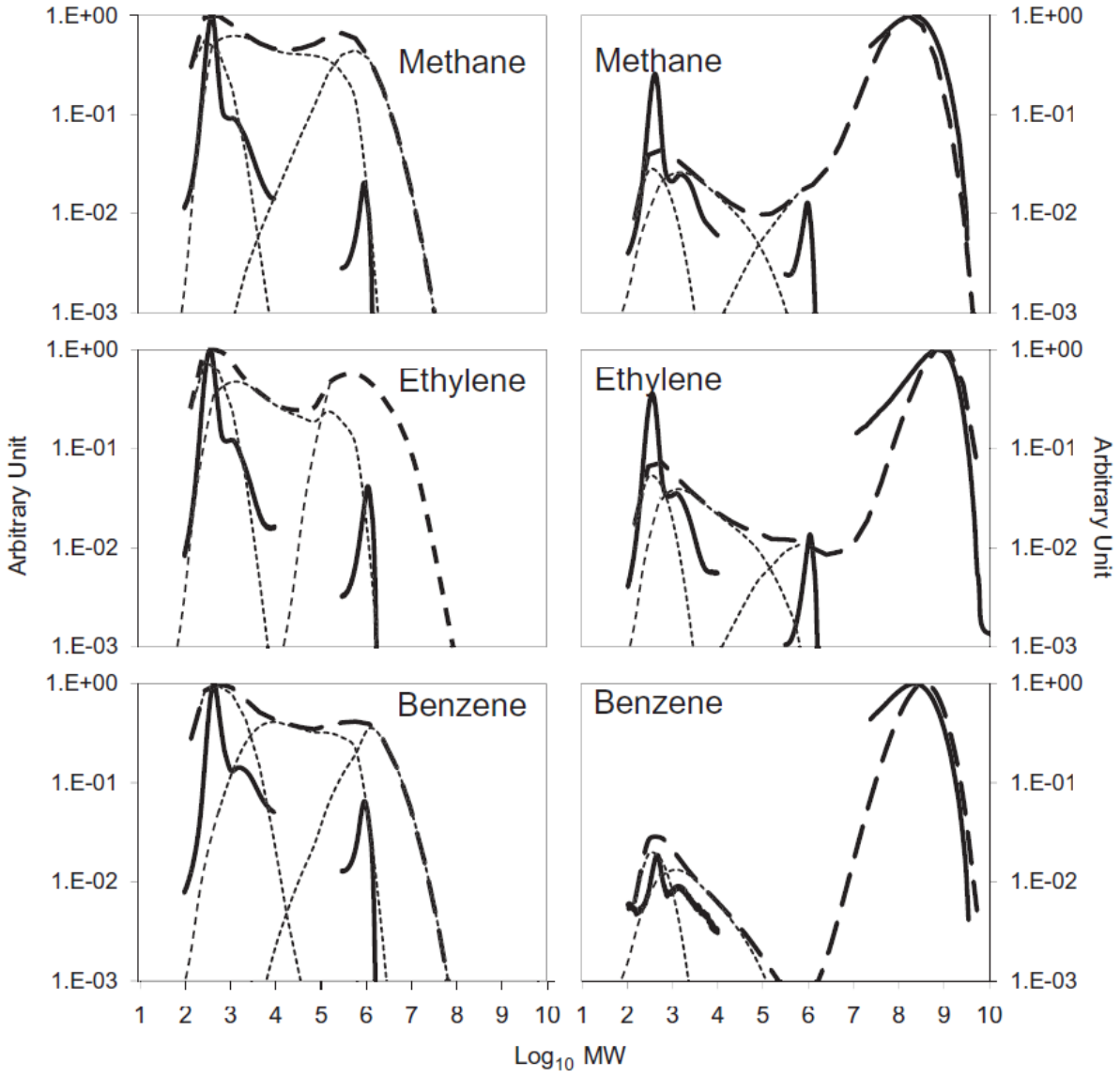

Fig. 9.16. Normalized SEC chromatograms (__) compared with normalized concentration profile of total particulate (__ __) and type1, type2 and type3 compounds (- - -) (see text) at inception (left part) and in the post-flame region (right part) of the three flames.

Overall, the MW distributions show four peaks belonging to species in the 100–1000 u range, in the 1000–5000 u range, in the 105–106 u range and in the 106–1010 u range. At particle inception the first three peaks, mostly belonging to the solvent-soluble fraction, are predominant whereas in the post-flame region the higher MW peak in the 106–1010 u range, due to soot, prevails. Model results are in good agreement with experimental data and are useful in giving information on the nature of the very high MW classes, not amenable to chemical analysis. The modeled first peak

derives from aromatic molecules having masses up to 1000 u (Molecules) in agreement with the mass spectrometric analysis. On the basis of the model prediction, the second peak can be ascribed to clusters of aromatic molecules with MW up to about 5000 u (Clusters), whereas the third peak is due to clusters of about 106 u (Clusters). It is worth to remind that modeled Cluster concentration accounts for all the species which undergo coalescent coagulation; these can range from the small dimer to large primary particles. In fact, these latter constitute the first species which have acquired a solid nature and cannot longer coalesce with other species, but can only agglomerate. The fourth peak is due to agglomerates of these clusters (Aggregates) constituting soot.

The agreement between experimental and modeled data can be used to gain more information about particle formation. Looking at the MW distributions, a remarkable difference can be noticed in the region up to 106 u both in terms of peak position and relative abundance. In particular, the modes of MW distribution in the MW region up to 106 u, which are related to Molecules and Clusters, are still visible at the end of ethylene and methane flames whereas result practically negligible in the benzene flame (left part of Fig. 9.16). Model well reproduces this behavior showing a persistent significant presence of modes around 300, 1500 and 106 u at the end of ethylene and methane flames. Hence, this trend seems to be a peculiar difference from aliphatic and aromatic flames.

To analyze the passage from Molecules to Clusters occurring at soot inception, an optical analysis of compounds with different molecular weight has been carried out at inception. In particular, the optical band gap, sensitive to the mean molecular mass of the largest aromatic units constituting each class, has been has been evaluated on the on-line UV–visible spectra measured on the apex of peaks detected in the MW distribution up to 104 u of particulate at inception. These peaks correspond to Molecules to Clusters in modeled results. Figure 9.17 reports for all flames the MW distribution up to 104 u of particulate at inception (upper part of Fig. 9.17) together with the optical band gaps (Eg) of the Molecules peak and of Clusters peak (lower part of Fig. 9.17). It is noteworthy that in the three flames the Eg values of Molecules and Clusters are quite similar at soot inception.

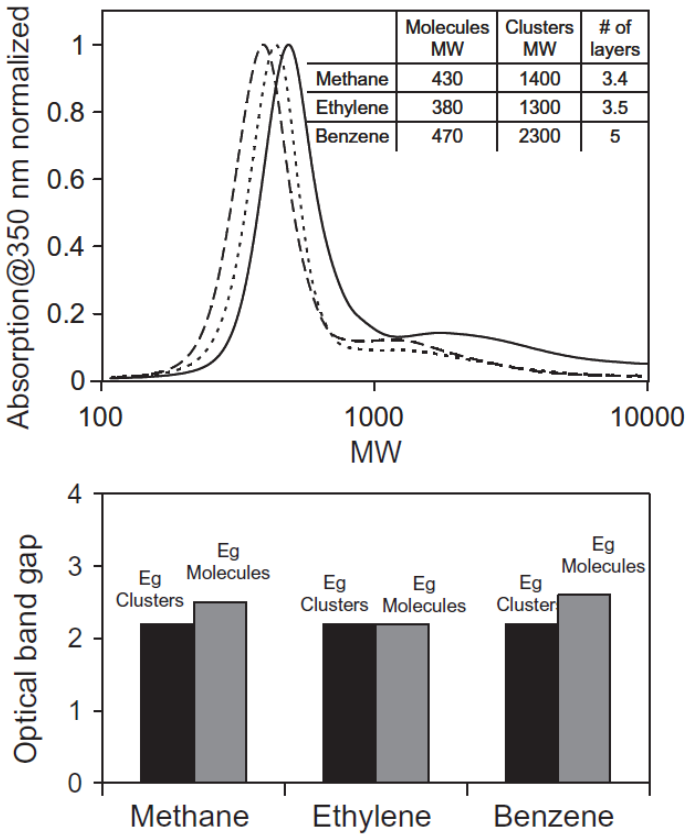

Fig. 9.17. Top: Normalized SEC chromatograms up to 10,000 u at inception for methane (- - -), ethylene (__ __) and benzene (__) flames. Bottom: Optical band gap (Eg) of molecules and clusters separated on the base of SEC analysis at inception in the three flames

This demonstrates that the aromatic units in Molecules are the aromatic units constituting the Clusters. In other words at inception Clusters are the snapshot of the surrounding environment constituted by Molecules. This correspondence is quite interesting because it furnishes a new tool to look at the characteristics of the particles. Moreover more information can be gained from the analysis of the MW distribution. If clusters are formed by molecules totally similar to the surrounding environment it means that a certain number of these molecules can be found stacked in some way within a cluster. Extending this view, it turns out that the ratio of the mean MW of clusters and molecules is representative of the number of molecules staked in the cluster, i.e. the number of stacked layers.

These mean values has been evaluated and reported in the inset of Fig.9.17. Moreover in the same inset in Fig. 9.17, the calculated number of stacked layers per Cluster is reported. A lower number of stacked layers, i.e. a lower degree of stacking can be noted in the clusters found in

methane and ethylene flame whereas this value is remarkable higher Clusters found in the benzene flame.

However, further evaluations can be done looking at MW distribution functions. Instead of using the mean value of the MW distribution, it can be possible to use the function itself. First of all a deconvolution of the distribution has to be operated in order to distinguish Molecules MW distribution and Clusters MW distribution. After this it is possible to consider the ratio between the two MW distribution functions of clusters and molecules. This ratio gives back another MW distribution function which may have a physical meaning: the final result is the distribution of the number of stacked layers per cluster. This calculation can be done both on the experimental MW distribution after the deconvolution and by using the modeled MW distribution for Molecules and Clusters. If this distribution would be shifted toward higher number of stacked layers per cluster, it would mean that the structure is more graphitized.

The results are reported in Fig. 9.18. Model and experimental data are in very good agreement both indicating that the stacked layers number is much lower in methane and ethylene flames in respect to the benzene flame. This means that a relevant higher level of stacking/organization of the precursor particles is obtained at inception in the benzene flame. The more ordered structure of early soot in benzene flame, is consistent with its lower H/C ratio, and causes the higher soot formation rate and the peculiar evolution of benzene particulate properties in terms of size and oxidation reactivity showed by the same group (Alfè et al., 2009, Alfè et al., 2007)

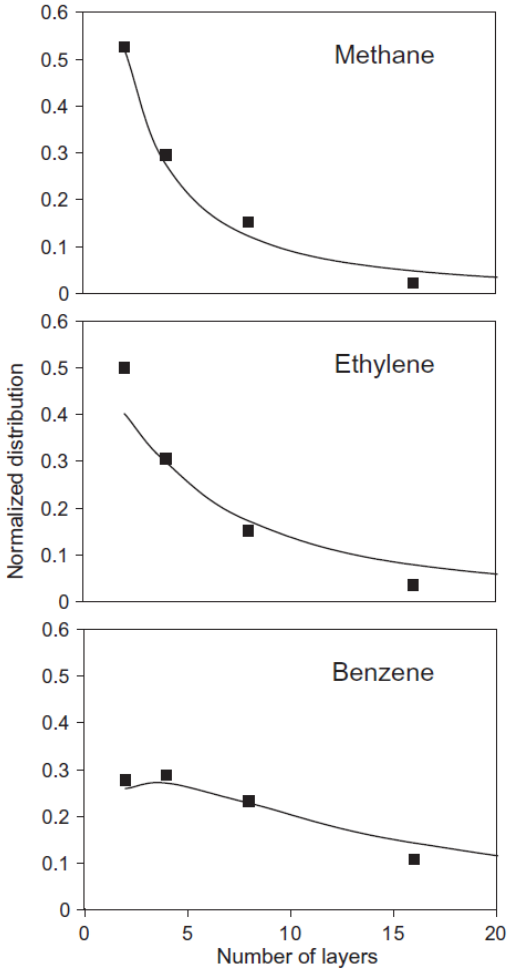

Fig. 9.18. Experimental (dots) and modeled (lines) normalized distribution of number of stacked layers per cluster at inception in the three flames.

In conclusion, in the benzene flame aromatic molecules and nascent soot particles appeared very early in the oxidation region and were no longer detected at the end of flame whereas aliphatic fuels showed both aromatic molecules and freshly-nucleated soot particles persisting downstream of the flame. Elemental analysis and UV–visible properties of the carbon particulate showed that also the graphitization process is earlier and much faster in the benzene flame whereas in aliphatic flames a less ordered structure is produced later on the flame and with a slower rate. Detailed modeling of the carbon particulate yields and properties confirms the differences in the evolution of carbon particulate and its structure in benzene and aliphatic flames, also individuating the classes of species: aromatic molecules and clusters of aromatic molecules responsible for soot inception. Nascent soot particles in benzene flame, earlier formed in the main oxidation zone overlapped with the pyrolysis region of the flame, exhibiting a more organized/stacked aromatic structure. Here graphitization is

enhanced by the high radical concentrations typical of the lame front. As a consequence the coagulation is also enhanced for effect of the increased aromaticity lower H/C ratio) of the incipient particles which result in increasing binding energies of the formed lusters. The inception of particles in the aliphatic flames occurs in the pyrolysis region that is well distinct from the main oxidation region and located downstream of the flame front. Here the temperature is slightly decreasing while the concentrations of small radicals are attaining the e equilibrium values. Both the temperature and radical concentration decreases, turn into the formation of less organized structures subjected to a slower and lower evolution toward larger mature soot

9.1.2. Opposed-flow diffusion flame

Structure of the flame in the opposed flow diffusion flame has been already described in the chapter 8. Several flames have been investigated in this thesis work; however a test case of ethylene/oxygen/argon flame will be discussed. This case has been found to be interesting for evaluating the different pathways that lead to particle inception. Moreover a new technique based on the Time-Resolved Laser Induced Fluorescence has been applied to this flame in order to capture the structure of the particles produced. Model has been applied to this flame substantially confirming and supporting the results obtained with experimental data.

The ethylene diffusion flame was stabilized between two opposed jet nozzles (ID 2.54 cm). The oxidizer stream, containing different amounts of O2 and Ar, was introduced from the upper nozzle; the fuel stream was introduced from the lower nozzle. All gases used were of high purity. Screens were used at the exit of each jet to establish uniform gas flow velocities to generate stable, flat flames. Nitrogen was used to shield and protect the flame from the surrounding air. Using a mild vacuum through the holes in the annular section of the bottom burner, combustion products and shield gas were vented out of the system. Sampling position within the flame was changed by moving the entire burner assembly up or down with respect to the fixed sampling volume using a translation system (0.1 mm). For the ethylene counter-flow diffusion flames stabilized, the fuel stream was fixed at 75% C2H4 and 25% Ar, whereas the oxidizer streams consisted of 22% by volume of O2 and the remaining Ar. The oxidizer and fuel stream velocities were fixed at 16.1 and 13.2 cm/s, respectively. The distance between the two burners was maintained at 1.5 cm. The global strain rate, calculated as follows:

$$K = -\frac{2v_{\mathrm{O}}}{L}\left[1+\frac{v_{\mathrm{F}}}{v_{\mathrm{O}}}\left(\frac{\rho_{\mathrm{F}}}{\rho_{\mathrm{O}}}\right)^{1/2}\right] \tag{9.1}$$

results to be of 37.7s-1 for the flame. The parameter L, v, and ρ are the separation distance of the opposing jets, jet velocity, and jet fluid density, respectively. Subscripts O and F denote the

oxidizer and the fuel stream, respectively. These conditions resulted in flames stabilized on the oxidizer side of the stagnation plane. Position of the stagnation plane was estimated by seeding the fuel stream with 1 μm-TiO2 particles and measuring the scattering coefficient along the flame axis. TiO2 particles give a strong scattering signal in the fuel side which vanishes at the stagnation point where particles are convected away. The stagnation plane is located at about 4.2mm from the fuel nozzle

First of all a sketch of the flame structure is presented in order to clarify the zone of interest within the flame, the temperature, the gaseous species and the streamlines.

In the experimental conditions studied in this work the flame front is located in the oxidizer side of the stagnation plane. Figure 9.19 shows the image of the flame and the measured flame temperature profile (uncorrected and radiation corrected). The two vertical lines in Fig.9.19 represent the location of the stagnation plane, about 4.2mm, and the position of the maximum flame temperature, about 7.8mm. Figure 9.19 also reports the modeled concentration profiles of fuel and oxidant and major gas-phase by-products obtained by using a detailed kinetic modeling of the flame structure. Modeled profiles will help in the identification of the different flame zones.

On the basis of the measured temperature, the computed major species concentrations and the flame fluid-dynamic, three regions can be distinguished in the flame: the fuel side, the stagnation zone and the oxidation zone (colored areas distinguish the three regions in Fig.9.19).

The fuel side (left side in Fig.9.19), in particular the region from 3 to 4mm, is characterized by a relatively low temperature, from 600K up to 1000K, by a high concentration of the fuel (C2H4) and a complete absence of oxygen. The flame shows in this region a fair yellow luminosity.

Across the stagnation plane, i.e. between 4 and 5mm, the flame starts showing an intense yellow luminosity typical of soot particles incandescence and the flame temperature reaches values of the order of 1000-1300K. Major by-products of the combustion process, such as C2H2, benzene and small PAHs, are abundant in this region of the flame. Even benzene and PAH concentrations maximize in this region.

Moving toward the oxidizer side between 5 and 6.5mm, the yellow luminosity changes towards a blue luminosity typical of the main oxidation region of the flame. The concentration of acetylene, after a maximum at the beginning of this flame region, decreases to very low values at the end of this region. The same behavior is shown by the concentrations of benzene and PAHs.

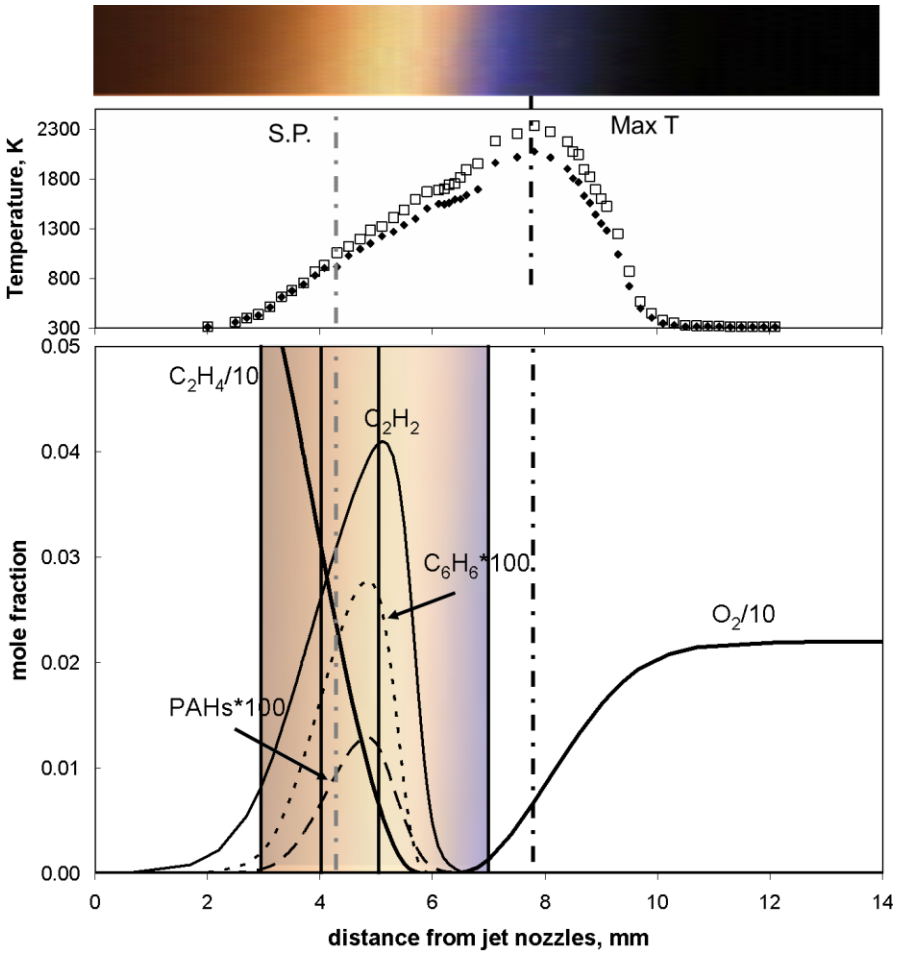

Figure 9.19 Flame image and modeled gas phase compounds and measured temperature profile (radiation corrected, □, and uncorrected, ♦) as function of the distance from fuel jet nozzle. Stagnation plane (S.P.) and maximum of temperature (Max T) are evidenced as dashed-dotted lines. Colored areas and vertical solid lines evidence different flame zones (D'Anna et al., 2009).

Laser Induced Emission measurements were performed using as excitation source the fourth harmonic radiation (266nm) of a Nd:YAG laser. Laser beam was focused in the flame and a beam diameter at focal point of 350µm was obtained. The energy of the laser pulse was kept constant at 0.8mJ with a pulse duration of 8ns. Higher energies of the laser pulse increased species fragmentation and consequently the interference of C2 emission on fluorescence. Conversely, incandescence emission was enhanced. The chosen energy of 0.8mJ gave the better compromise between incandescence emission and fragment interference to fluorescence, in the examined conditions.

To perform spectral measurements, the emitted radiation was detected at 90° respect to the laser beam and was focused onto the 280nm entrance slit of a spectrometer and detected by an intensified CCD camera (Oriel Instruments InstaSpec V ICCD) thermoelectrically cooled, down to -10°C, in order to reduce dark noise. Spectral emission profiles were obtained using a gate time of 200ns synchronized with the laser pulse and by summing the CCD counts over 150 scans. The measured spectra were corrected for the spectral response of the detection system and calibrated against the Rayleigh scattering from cold ethylene at 266nm. Emission signals were measured along the distance between the two nozzles, from the fuel jet to the oxidizer jet. Figure 9.19 reports the intensities of the fluorescence at 310, 340, 390, and 440 nm as determined by deconvolution procedure. The location of the stagnation plane is reported as a vertical dashed line to allow an easier identification of the flame zones.

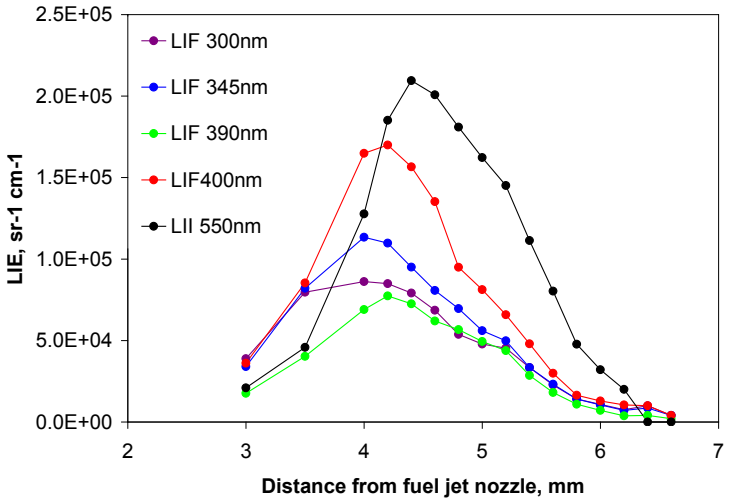

Figure 9.19 Laser induced emission signals at different wavelengths as a function of distance from fuel jet nozzle.

Fluorescence emission is detected along the entire flame, from 3 to 6.5mm. Moving from the fuel side toward the stagnation plane, fluorescence intensity increases. The strongest fluorescence intensity is measured at longer wavelengths; however in the first region of the flame at about 3.5mm fluorescence signals at 310 and 340nm still exhibit a noticeable intensity. Crossing the stagnation plane towards the oxidizer side of the flame, fluorescence intensity reaches the maximum value thereafter it decreases in the oxidation side. In the region approaching the flame front, at about 5.2mm, a shoulder in the fluorescence profile is observed. This is more evident in the UV curves. This shoulder was already detected and even more evident in a previous work, in which the fifth harmonic

of the laser, at 213 nm, as excitation beam was used. The laser induced incandescence signal is also reported in Fig.9.19. Incandescence signal maximizes across the stagnation plane region.

To better evidence the behavior of the fluorescence signals, Fig.9.20 reports the ratio between fluorescence in the UV (310 and 340 nm) and visible (390 and 440 nm), LIFUV/LIFvis. Fluorescence in the visible becomes more important than UV close to the stagnation plane, whereas the UV emission becomes predominant on both fuel and oxidation sides.

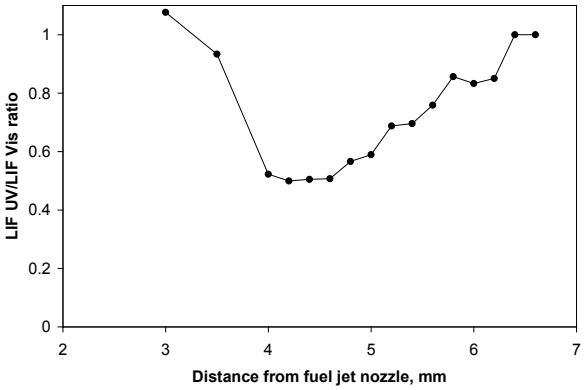

Figure 9.20 UV-to-visible fluorescence ratio as a function of distance from fuel jet nozzle.

Fluorescence spectra and lifetimes can be correlated with the internal structure of the fluorescing species for a fixed temperature and composition of the surrounding gases. Indeed, besides of temperature and composition of the surrounding gases, internal structure of the fluorescing species affects their capability to dissipate energy through non-radiative channels. For example, sandwich-like structures (cluster of PAHs held together by van der Waals forces) or highly-packed small particles should exhibit longer living fluorescence signals with respect to single parent fluorophores. In fact, when single fluorophores are trapped in semi-rigid structures such as sandwich-like structures, they are not able to give roto-vibrational movements and to loss internal energy by other routes than the radiative emission. Moreover, the □-electron interactions between aromatic islands are relevant in these highly-packed structures and induce a shift of the fluorescence emission toward longer wavelength. Conversely, the more loose aromatic moieties which comprise aromatics linked together by □-bonds (aromatic-aliphatic linked hydrocarbons) should exhibit fluorescence spectrum typical of the PAHs of which they are composed and a much lower lifetimes since such configuration favors energy dissipation through other routes (roto-vibrational movements) more than through radiative emission. With increased molecular mass and solid state character of the compounds, internal conversion of the energy acquired by photon absorption increases, the

fluorescence quantum yield becomes negligible and energized particles dissipate energy by thermal emission (Vander Wal, 1996a).

Measurements of the temporal evolution of fluorescence emission are reported in Fig.9.21 for two wavelengths, namely in the UV at 310nm and in the visible at 440nm. The decay times are compared with those of small PAHs at high temperature as reported in the literature (naphthalene and pyrene). In particular the shaded area in Fig.9.21 represents the decay times of small PAHs measured in cell at atmospheric pressure without quenching molecules (Ossler et al., 2001a). Flame temperatures at each point are reported for clearness.

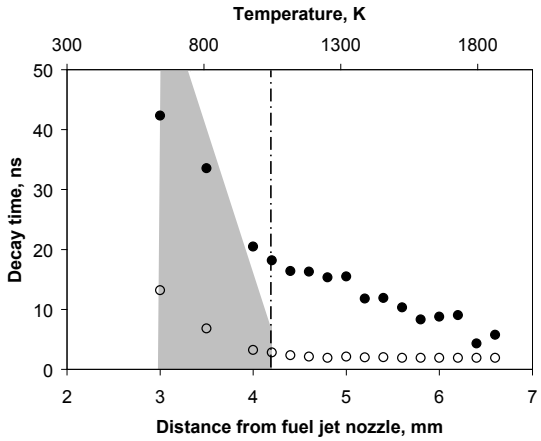

Figure 9.21 Fluorescence decay times in the UV (○ 310nm) and visible (● 440nm) as function of distance from fuel jet nozzle. Fluorescence decay times of gas phase PAHs (naphthalene and pyrene) from literature (Ossler et al., 2001a) are reported as shaded area.

Fluorescence decay times measured in the fuel side are of the order of 20-40 ns, i.e. similar or longer than those of naphthalene and pyrene in cells in the same condition of temperature (Ossler et al., 2001a). The fluorescence decay times rapidly decrease with increasing temperatures, i.e. moving toward the stagnation plane. Across the stagnation plane region, the measured fluorescence decay times are significantly longer than those of small PAHs. It is particularly evident for fluorescence emissions at longer wavelength. In the oxidizer side, fluorescence decay times further decrease approaching very low values typical of small PAHs only at the end of this region. Along all the oxidizer zone, the fluorescence decay times are longer than those of small PAHs but quite shorter than those measured across the stagnation plane.

To evidence the different behaviors of UV and visible fluorescence in various flame regions, fluorescence spectra collected at three different distances from the fuel jet nozzle are reported in Fig.9.21. These positions were selected as representative of the different zones of the flame described above. Moreover spectra at three delay times of the acquisition device, namely synchronized with the laser pulse (top), at 10ns (middle) and at 100ns (bottom) are also reported in Fig.9.22. It is important to underline that to correctly estimate fluorescence signals in the visible, incandescence has to be subtracted from the emission signal.

Fluorescence emitted in the UV below 330 nm has the shortest lifetime despite of the examined flame zone, while fluorescence emission in the visible have longer lifetimes and it is still detectable 100 ns after the excitation pulse in the flame zone at 3.5 and 4.2 mm from the fuel nozzle.

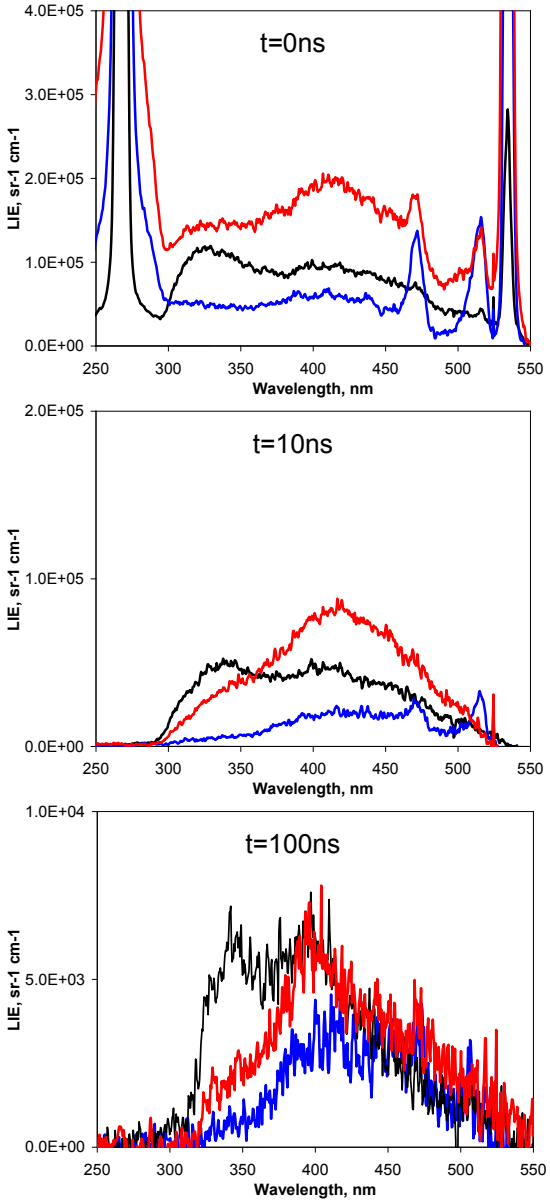

Figure 9.22 Laser induced emission spectra collected with ICCD camera at three different distance from fuel jet nozzle (3.5mm – black; 4.2mm – red; 5.4mm – blue) and for three different gate opening delay times (0ns – top; 10ns – center; 100ns – bottom) from the laser pulse.

The coupling of spectral emission analysis with measurements of the fluorescence decay times furnishes an even more detailed characterization of such species and gives a qualitative view of the processes of aromatic growth and particle formation in an opposed-flow flame.

We have interpreted the emissions signals and the fluorescence lifetimes detected at various distances from the opposed jet nozzle on the basis of the previous considerations.

Fluorescence spectra detected in the fuel side of the flame, i.e. between 3 and 4mm, show considerable signals at 310 and 340 nm with lifetimes comparable with those of gas-phase PAH in the same conditions of temperatures (Figs.9.19 and 9.21). The fluorescence signals at 310 and 340 nm are attributed to aromatic compounds which diffuse from the main flame zone across the stagnation plane or are partially produced in the pyrolytic (fuel-side) low-temperature zone of the flame. Beside the UV band, in the same flame location, fluorescence in the visible is also detected in this flame region (Figs.9.19 and 9.20). It might be attributed to both the formation of higher molecular mass aromatics and to small clusters (dimers or trimers) of PAHs. The latter mechanism is favored by the low temperature characteristic of this region and seems to be confirmed by fluorescence lifetime comparable with that of pyrene or longer.

The longer wavelength fluorescence prevails in the spectra together with a strong incandescence signal (Figs.9.19 and 9.20) moving across the stagnation plane region, i.e. between 4 and 5mm. This zone is characterized by temperatures up to 1300K and a high concentration of gas-phase PAHs, as evidenced by flame modeling (Fig.9.18). This environment promotes PAH clustering more than molecular growth due to the relatively low temperature. In this flame zone, the fluorescence decay times become significantly longer than those of single PAHs indicating that the fluorescing structures are not able to dissipate energy by non-radiative processes despite of the relatively high temperatures measured. Also in this region, the shift of the fluorescence emission toward longer wavelength and the longer fluorescence lifetimes indicate that fluorescing species have more packed structure with strong interactions between the aromatic planes.

In the oxidizer side, emission signals decrease moving towards the flame front and vanish at about 6.5mm. Incandescence and visible fluorescence prevail in the emission spectra in all the region (Fig.9.19) although UV fluorescence becomes more relevant moving closer to flame front after 5.5mm (Fig.9.20), showing the formation of small PAHs in this flame location. Formation of gas phase PAHs is also confirmed by the short fluorescence lifetimes measured between 5.5 and 6.6mm. Small PAHs so formed are transported by diffusive fluxes close to flame front and by convective and diffusive fluxes towards the stagnation plane. In this region PAHs undergo molecular growth processes either by acetylene (pericondensed aromatic formation) and aromatic addition (aromatic-aliphatic linked, bi-phenyl like compounds). The compounds formed in this region exhibit lower fluorescence lifetimes respect to those formed close to the stagnation plane indicating that aromatic-aliphatic linked, bi-phenyl like compounds are favored since these compounds may easier dissipate energy through roto-vibrational channel due the presence of □-bonds inside the compounds. Once formed, the aromatic-linked compounds can lose hydrogen through dehydrogenation processes increasing the level of aromaticity of the compounds and reducing the internal energy dissipation resulting in an increased intensity and lifetime of visible fluorescence as measured at the beginning of this region. The role of oxygen quenching on the shorter fluorescence lifetimes measured in the oxidizer side however cannot be excluded.

In order to support these experimental data the opposed-flow diffusion flame of ethylene has been numerically investigated. In figure 9.23a particulate concentration along the flame axis is reported both as total particulate and, according the division, in Molecules, Clusters and Aggregates. Maximum temperature and stagnation point position has been also reported for clearness. Particles clearly appear on both oxidizer and fuel side. In the oxidizer side, very high temperature region, very fast formation leads to large amount of molecules and clusters and, moving toward stagnation plane, aggregates. This process is mainly due to the high temperature environment, fast radical formation and large presence of species such as acetylene. In the fuel side, the considerable amount of PAH, deriving from fuel pyrolysis and diffusion from the oxidizer side, and small aromatics together with the low temperature make physical process to be dominant. As result, in this region, the amount of molecules is very limited and clusters result almost the only species present. However, across the stagnation plane aggregates show a peak of concentration, remarking this as the zone of maximum particulate production.

In figure 9.23b the H/C ratio of the total particulate and of the three classes is reported. Molecules exhibit a lower H/C ratio in the oxidizer side in correspondence of the high temperature nucleation zone. This result is in accordance with the kinetic mechanism described before: the acetylene addition lead to pericondensed structures and the high temperature favor the dehydrogenation process in the few oligomer–like structure formed. Clusters and, subsequently, aggregates, that are formed starting from molecules, assume the same H/C of these latter.

Moving toward the stagnation plane the decreasing in acetylene addition process make the PAH reactions more relevant and increase the H/C ratio of both molecules and clusters. Looking at the fuel side, clusters with H/C ratio typical of small aromatic are formed, supporting the hypothesis that stacking is the prevalent mechanism in this region. All these particles so formed contribute to the total H/C ratio

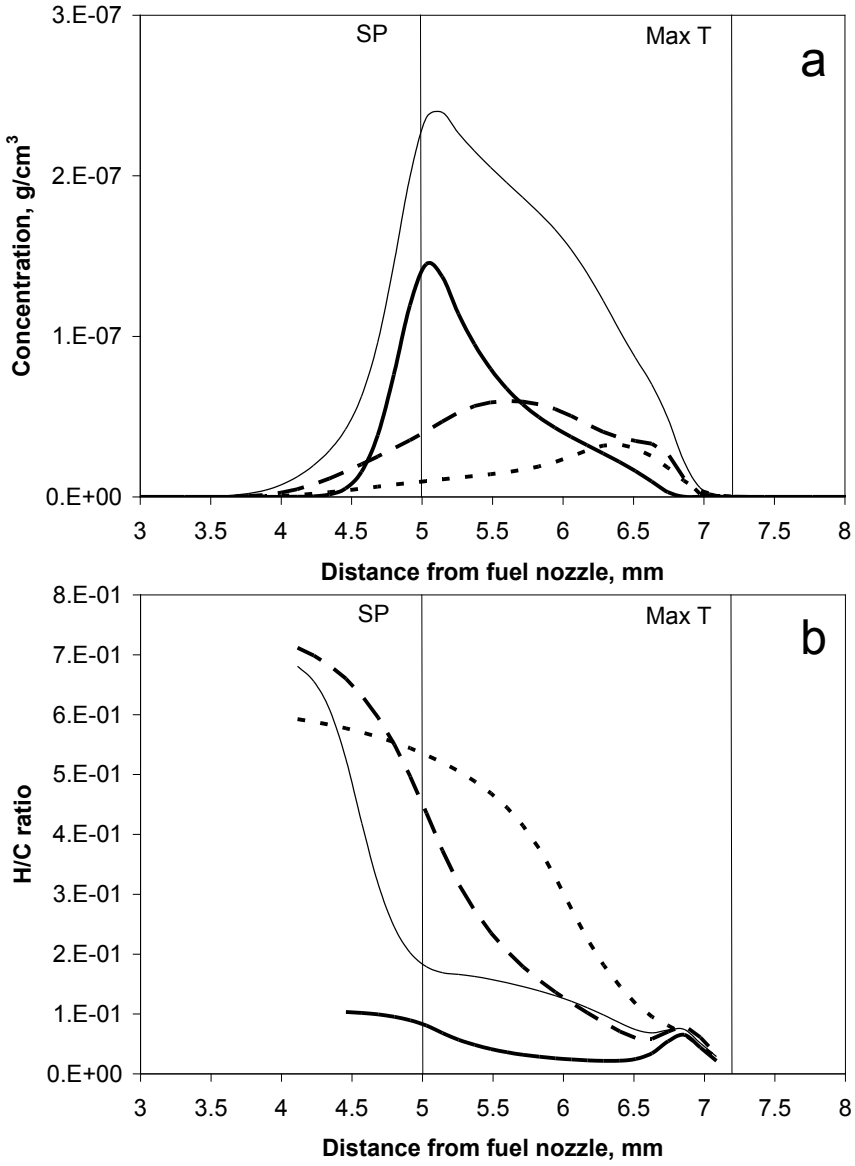

Fig. 9.23 Concentration (a) and H/C ratio (b) of total particulate matter (___ thin line), molecules (- - -), clusters (__ __), aggregates (____ heavy line) along the flame axis. Stagnation plane and maximum temperature position are also reported.

The process of particle inception in counter-flow flames seems to be the result of both a chemical growth and a physical process involving gas-phase and high-molecular mass aromatic coagulation. In the region close to the main oxidation zone of the flames, particle inception is due to a chemical growth mechanism initiated and enhanced by the presence of large concentrations of gas-phase aromatic compounds and small radicals. High-molecular mass aromatics are moved away from the flame zone towards the stagnation plane by convective, diffusive and thermophoretic fluxes crossing region of the flame characterized by the presence of relevant concentrations of acetylene and other aromatics which contribute to the molecular weight growth process forming particles of increasing sizes. Graphitization of these particles and thermal annealing lead to the formation of more aromatic solid structures. Molecular growth is also evident close and beyond the stagnation plane at the relatively lower temperature found in the fuel side of the flame. In this flame region, physical interaction of PAHs is a viable growth process. PAHs can form stacks or add to existing particles since, due to the lower temperature, the coagulation process is more effective than at higher temperatures.

The results obtained for this flame can be extended to other diffusion flames and other combustion systems. In particular, in the fuel zone the evidence of a considerable amount of PAHs and stacking process have to be considered in modeling since it appears determinant in many practical conditions.

It is worth to note that the sketch of particle inception via physical and chemical pathway can be obtained separately by experimental techniques and numerical model. However the coupling of these two tools enforces the validity of results, making them even more general.

Moreover by tuning flame conditions in a diffusion flame it is possible to obtain particles with different features: stacks of PAHs deriving from the physical coagulation of gas-phase PAHs and aromatic-aliphatic linked compounds with different degrees of annealing depending of particle trajectories inside the flame. This possibility appears to be determinant looking at these by-products as a resource for new applications and at the flame as a reactor for the massive and cheap production of new materials.

9.1.3. Co-flow diffusion flame

Coflow flames represent the reactor configuration closer to a real combustion system. Moreover, this flame configuration is particularly interesting due to the presence of multiple zones in terms of temperature and mixing of fuel and oxidant. It is the extension to the non-one-dimensional case of the opposed-flow flame previously described. The main structure of the flame has been described in and large scientific literature on this topic is present.

The main challenge probably relies within the looping effect of the temperature on soot and soot on temperature. In fact, temperature has a strong effect on soot production and a change of

temperature can lead to different amount of soot produced according with general considerations. Moreover a change in temperature profile within the flame can also modify some minor phenomena that can become determinant such as thermophoresis acting on particles and thermal diffusion. A change in soot production can change locally the radiative term in the energy equation balance and thus affect the temperature. This phenomenon makes tricky the evaluation of single parameters on particle formation.

The enthalpy source term because of radiative transfer is from

$$\frac{dI}{ds} = -(k_a + k_s)I + \frac{\sigma}{\pi} \quad k_a T^4 + \frac{k_s}{4\pi} \quad \int_0^{4\pi} I d\Omega \qquad (9.2)$$

where

using the discrete transfer method (D'Anna et al., 2001a). Radiation was modeled as broadband without scattering. The absorption coefficient in this case was related proportionally to the soot volume fraction, respecting the effective of physical process of the flame. The constant of proportionality has been set by matching the predicted with the experimental peak temperature found for this flame. Diffusivities were taken from and Wang and Frenklach (1994); they are binary coefficients in nitrogen, because N2 is the dominant species everywhere. The viscosity and thermal conductivity of the mixture are likewise those for nitrogen.

Moreover, the two-dimensional feature of this flame makes the experimental and numerical investigation quite hard. In this work a normal coflow flame has been firstly studied by Santoro in the 1983. After this work, this flame has been studied experimentally by several research groups using a variety of techniques to measure particulates. This means that this flame is well characterized and in some way it represents a standard flame for approaching the study of coflow flames .

However, in this thesis work numerical investigation of this flame has been conducted. Particle formation has been evidenced and the advanced model allows to distinguish different inception pathways. Moreover information can be gained on chemical composition and morphological aspects of the formed particle and their evolution along the flame. This flame is classified as non-smoking flame. it means that the particulate produced is oxidized down to detection limit. This phenomenon is possible due to the configuration of the streamlines of this flame which force the particles to pass through the flame front on the top of the flame. It would be interesting to note the effect of fragmentation in the total soot oxidation rate.

According with consideration of the relation between soot and temperature, the analysis of flame structure moves from figure 9.24, in which maps of concentration for temperature OH radical fuel and oxygen are reported. Looking at the maximum temperature and even more of OH radical, it is possible to distinguish the flame front location. It appears clear that modeling results predict the

closure of the flame on the top. Moreover velocity vector, reported in temperature map, evidenced the peculiar shape of normal coflow diffusion flames. It is worth to note that as the flame closes on the top and the OH radical start to decrease the oxygen concentration become relevant in the order of 2-4%, whereas the temperature is still in the order of 1500K. These condition strongly favor the oxidation by O2 and thus also the oxidation-induced fragmentation.

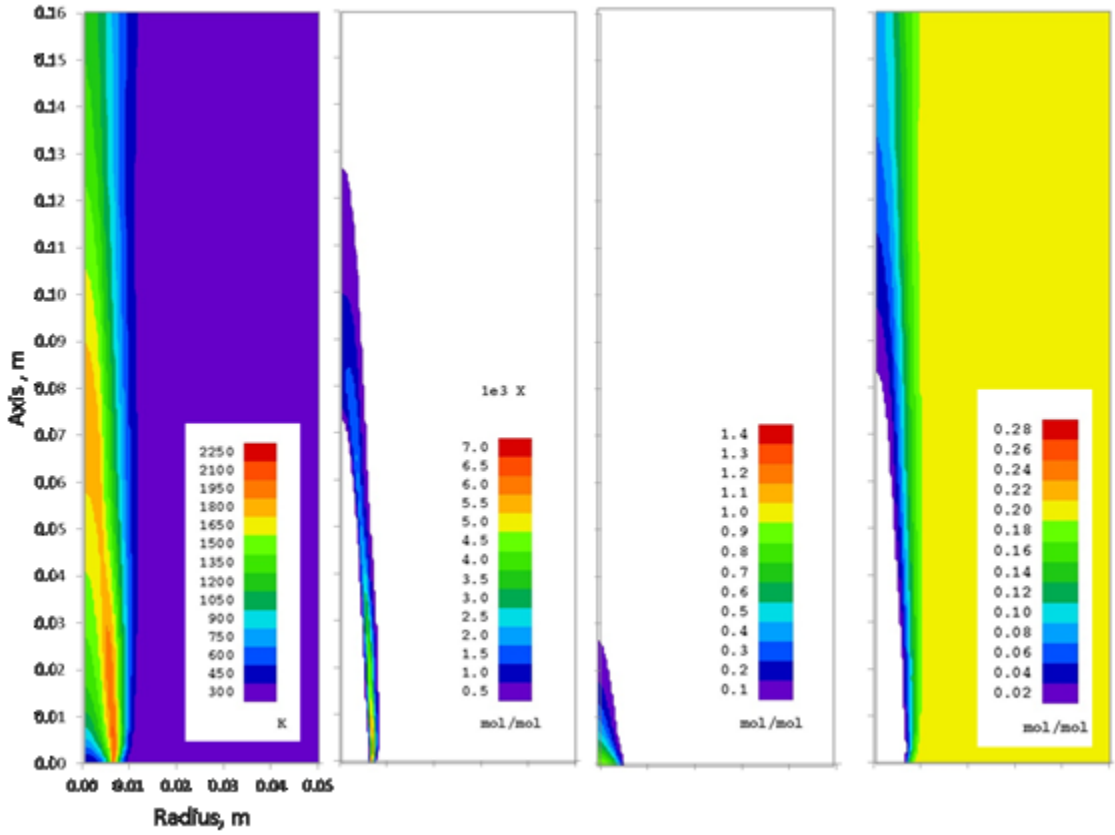

Figure 9.24 From left to the right: temperature and molar fraction of OH; C2H4; O2.

In the Figure 9.25, in similar way, principal gas phase species, i.e. acetylene, benzene, naphthalene and pyrene, responsible for particle formation and growth are reported. Looking at the values found in literature for this flame the maps show a fair agreement for these species. This means

that the main oxidation and pyrolysis processes are matched and the analysis of the particle evolution can be done without making large errors.

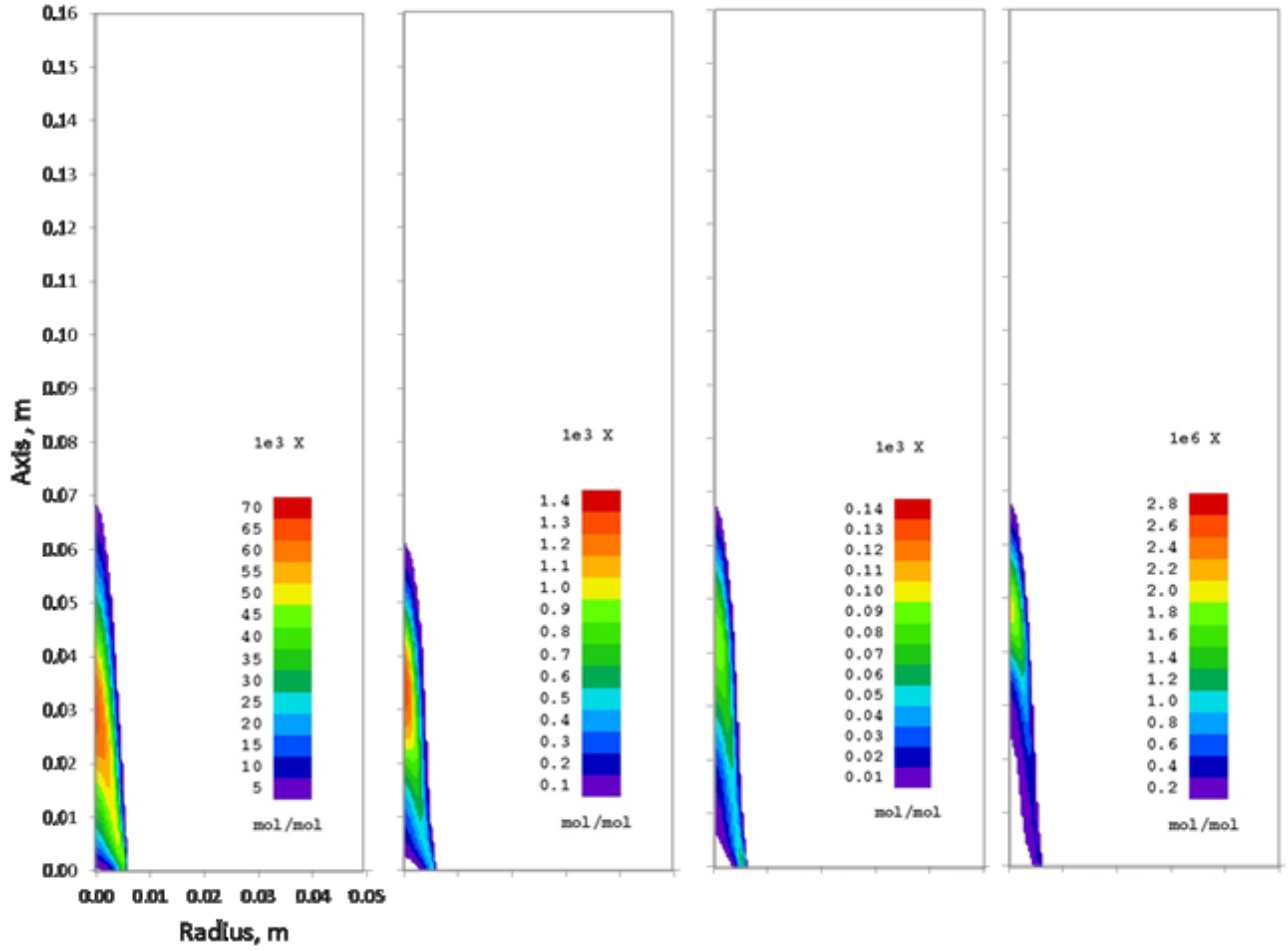

Figure 9.25 From left to the right: molar fraction of acetylene, benzene, naphthalene, and pyrene.

The shape of acetylene concentration suggests that strong formation occurs just after total consumption of ethylene. Moreover the concentration seems two follow a two zone view of the flame. Main production of acetylene occurs along the main streamline, however the maximum concentration is found in the inner part of the flame, i.e. along the central axis, in the pyrolytic zone. In this latter zone, temperature starts to be considerably high (X=0.03m, R=0; T=1500K) and pyrolysis become more effective. The influence of the diffusion is still to be considered, having generally the effect of smoothing the contours. Benzene shows the same trend of acetylene, remarking the strict link between these two compounds. The concentration map of benzene suggests that the formation of this compound immediately follows the acetylene one. Looking at first PAHs, which strongly

depend on acetylene and benzene concentration, they appear again shifted toward higher heights in the flame which means also higher residence time according with the analysis of velocity field.

Finally the analysis of particle produced in this flame is reported in figure 9.26. Maps of concentration of volume fraction of total particulate are reported together with the volume fraction of the different morphologies accounted in the model: Molecules, Clusters and Aggregates. It appears evident that the large part of total particulate is constituted by aggregates. Molecules volume fraction exhibits a shape similar to this of gas phase PAHs increasing along the streamline and reaching the maximum on the center axis. Conversely Clusters volume fraction shows a peculiar shape: after a very fast increase in the first part of the flame their concentration decrease along the streamline; finally in the top of the flame another raise in concentration is present in correspondence of the maximum of PAHs and Molecules concentration. Aggregates start increase when cluster concentration decrease suggesting a rapid conversion between these two morphologies due the coalescence/aggregation ratio change. Their concentration is strictly confined by the flame front defined by OH, Temperature and O2 concentration. This means that Oxidation is quite active on the border line of the flame. Moreover, for these compounds only a small raise in concentration is possible to be seen on the top of the flames. The most interesting pint is probably due to the raise in particle concentration in the inner part of the flame. In fact this can be due to a different inception mechanism enhanced by the local conditions of temperature.

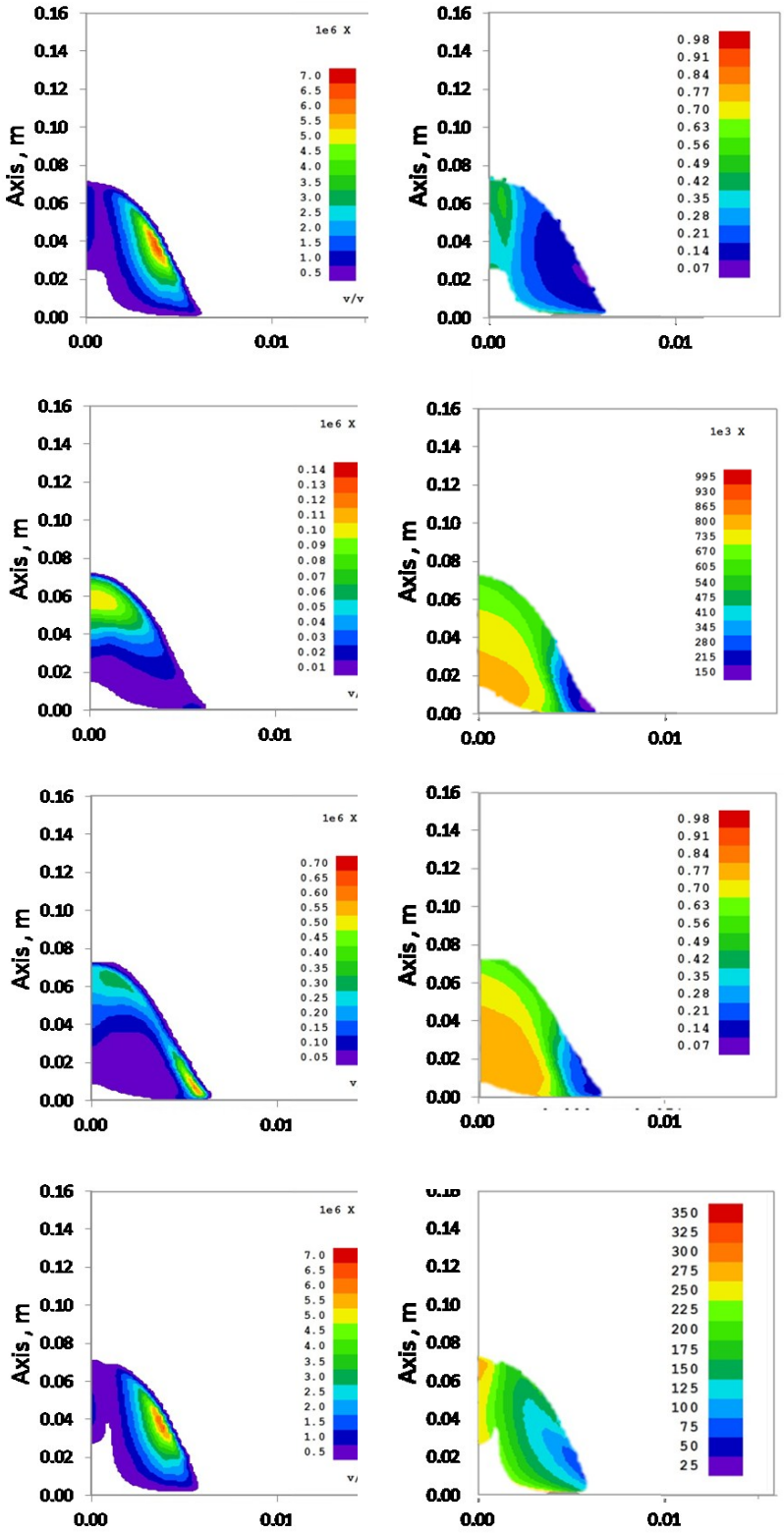

Figure 9.26 Volume fractions (left column) and respective H/C ratios (right) of total particulate (1st raw) Molecules (2nd raw), Clusters (3rd raw) and Aggregates (4th raw).

This picture of particle formation in coflow flame can be confirmed looking at the H/C ratio of total particulate and three classes considered. Total particulate exhibit a very low H/C ratio in the zone of maximum production whereas in the top of the flame the H/C approach value quite higher, up to 0.5. Looking at single classes these different processes are even more defined. In fact Molecules and cluster exhibit very low values only in the very first part of the flame, where radical concentration and temperature are higher. In the top of the flame this dehydrogenation process has to be less effective and the Both Molecule and Clusters reaches very high value of H/C ratio. Aggregates follow the same trend probably better evidencing the phenomenon. This behavior is quite similar to that found for opposed flow diffusion flame. In this conditions where the residence time is considerable higher the growth process leads to large compounds than in opposed flow flame.

This result is important in order to understand which the characteristic of emitted compound are. In this case oxidation is very effective and particles are totally burnt out. However in some condition total oxidation can be not reached. Partial oxidation can be selective with respect to particle feature and thus the emitted particle can have peculiar feature due this process more than to inception and growth. However also in this case some information about how the oxidation is affective on the particles can be gained. To test the effect of fragmentation, a test case has been also conducted without this reaction. The results are reported in figure 9.27. On the left column the case with fragmentation is reported: map of volume fraction of total particulate is showed together with the particle size distribution function calculated at different axial and radial positions. These positions are representative of the maximum volume fraction in the inner of the flame and of the flame front, i.e. the outer of the flame where oxidation occurs. It is worth to note that in the base case the PSD remains bimodal both in the phase of production and when particles are oxidized. However, when oxidation occurs, particle size distribution becomes orders of magnitude lower in numerical concentration, moving toward smaller diameters. When fragmentation is neglected particles are not totally oxidized. Moreover, the size of particles remains quite larger and the bimodal shape is totally missed. This demonstrates one again that fragmentation is fundamental in order to get not only the correct volume fraction of particles but also their effective shape and morphology.

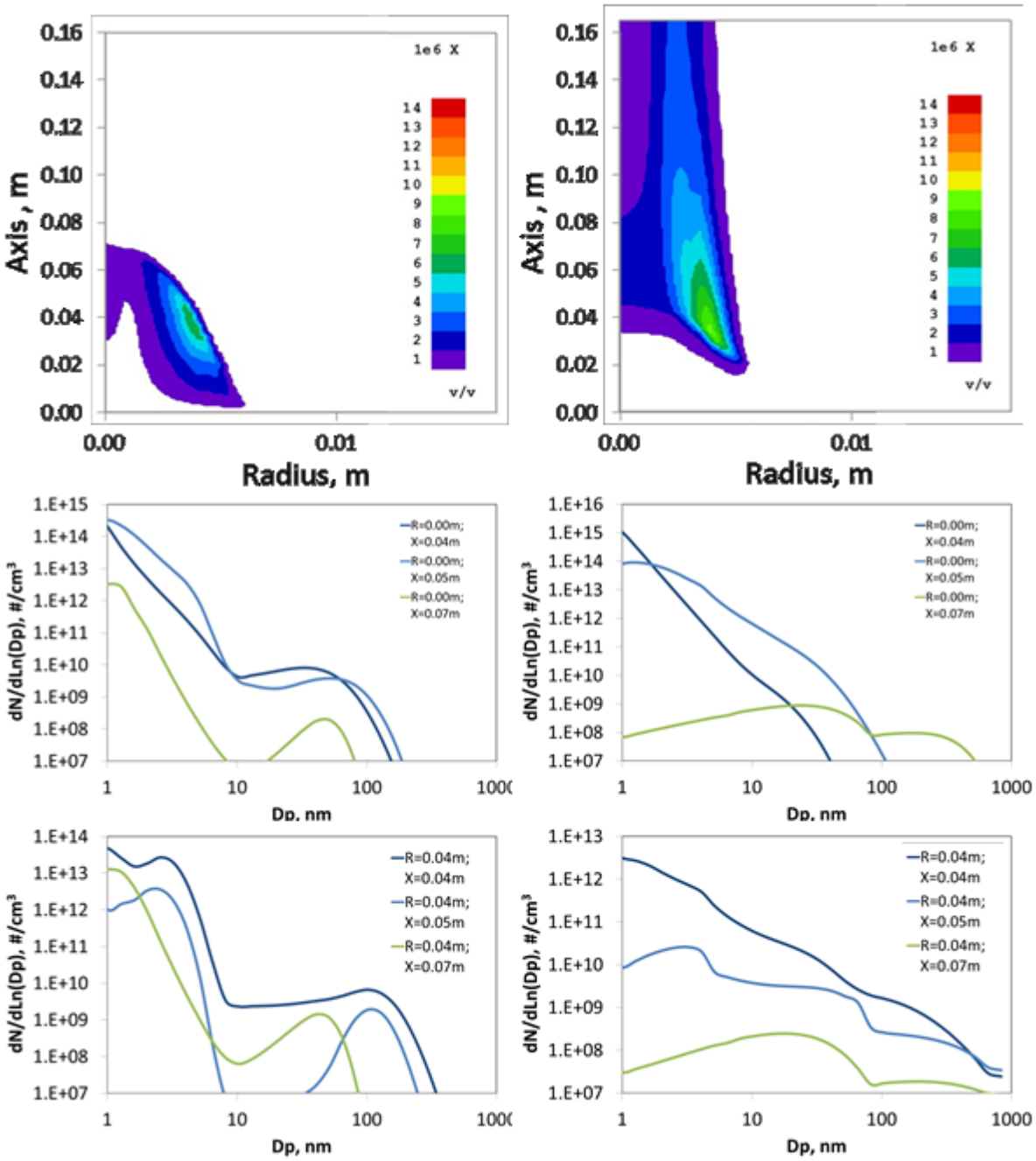

Figure 9.27 Top: Total particulate volume fraction; middle and bottom: PSD modeled in coflow flame modeled considering oxidation-induced fragmentation (left) and neglecting it (right).

9.2. Innovative reactor with tunable parameters

In this paragraph few words will be spent on preliminary result of non-conventional reactor for studying the evolution of particles in controlled conditions of temperature and species concentration.

In particular this new reactor will be explained in detail and preliminary result obtained on the evolution due to coagulation process.

9.2.1. Plug flow reactor for particle evolution – preliminary results

A plug flow reactor has been set up for the study of the evolution of particle in controlled temperature conditions. This reactor mainly constituted by a pipe of special steel (AISI 310) suitable for high temperature. This tube is positioned inside an oven in which ceramic resistances maintain a constant temperature. Moreover, the temperature is measured inside the tube at the entrance and at the exit of the oven. The tube is 13m long which allows to have very long residence time, in the order of seconds for the flow conditions normally used. The tube is fed with a nitrogen gas that is previously warm up to the set point temperature. This allows to have minimum perturbation and thus to consider the system at constant temperature. Particles are fed to the reactor by sampling material from a premixed flame. This allows to have a sample containing particle with a specific concentration and know particle size distribution. Moreover changing the flame conditions is possible to obtain different feed to the reactors and thus study the properties of different particles. Sampling probe is horizontal disposed in flame and it is mainly constituted by section of the reactor on which a small pinhole is made. By tuning with an opportune valve the under pressure at the pinhole it is possible to vary the amount of sampled material. Sampled material is then immediately diluted with the nitrogen gas sent in the reactor tube. The dilution with the inert hot gas allows to have both an immediately freezing of the chemical reactions and a stable temperature in the reactor.

The diluted sample after passed in the 13m-long reactor is sent to a differential mobility analyzer. However, to avoid damages to the instrument a successive dilution is made with cold Argon stream in order to cool down the flow. Finally particle size distribution of particles is evaluated after undergoing coagulation process within the reactor at constant temperature. A sketch of the experimental apparatus is showed in fig. 9.28.

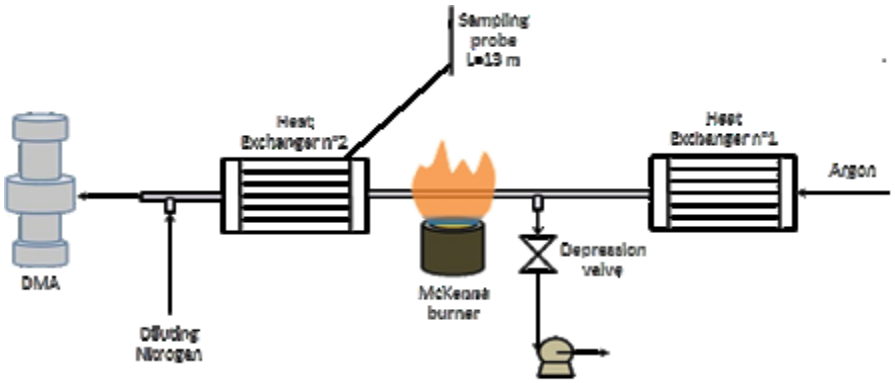

Figure 9.28 Sketch of the experimental set up used for the study of the temperature on nanoparticle coagulation efficiency

Preliminary study on this reactor has been conducted, investigating the evolution of nanoparticle and the effect of temperature on their coagulation efficiency. Temperature was changed from 300K, room temperature, up to 700K. In order to isolate the effect of temperature from other parameters, such as concentration of particles within reactor tube or residence time, the flow rate of hot nitrogen has been opportunely set up to take into account the expansion by volume due to raised temperature. This allows to have the same residence time in all investigated conditions. The under pressure at the pinhole has been kept constant to in order to have the same concentration of particles in all investigated conditions. Details on calculation used to set the parameters are reported in formulas below:

$$Mass_{N_2}^{T} = Mass_{N_2}^{300}\ \frac{300}{T} \tag{9.2}$$

$$y_P = \frac{S}{Mass_{N_2}^{300}}\ \frac{T}{300} \tag{9.3}$$

$$R_{COAG} = K_{COAG}(T)\ {y_P}^2 \frac{P^2}{(RT)^2} = K_{COAG}(T) \left(\frac{S}{Mass_{N_2}^{300}}\ \frac{T}{300}\right)^2 \frac{P^2}{(RT)^2}$$

$$= K_{COAG}(T) \left(\frac{S}{Mass_{N_2}^{300}}\ \frac{P}{300\ R}\right)^2 \tag{9.4}$$

where $Mass_{N_2}$ is the mass flow rate of nitrogen at reference (300K and set temperature), S is the mass flow rate of sampling trough the pinhole - assumed constant, $y_P$is the molar fraction of particles, $K_{COAG}(T)$ is the kinetic constant of coagulation which is variable with temperature. It is possible to note that particles coagulation rate shows temperature dependence only within the kinetic constant, which is the focus of this study.

As source of particulate matter, a premixed flame of ethylene/air with C/O ratio of 0.67, i.e. equivalence ratio of 2.01, has been stabilized on a porous bronze water cooled McKenna burner. This flame has been already characterized by in situ optical measurements and DMA analysis. To get a particle size distribution with no large aggregates, the probe was positioned at 10mm above the burner.

Results are reported in fig 9.29. Particle size distributions measured when the long probe is used exhibit a peak remarkably shifted toward large diameter evidencing that particle coagulation is quite effective. Particles coagulated at room temperature, 300K, red dots in the figure, are peaked around 10nm and particle as small as 2nm are almost absent. In the same figure, particle size distributions evaluated for higher temperature are also reported. For a temperature within the probe line of 500K, orange dots in the figure, a significant less coagulation rate can be evaluated and particle size distribution is peaked at size around 7nm. However, a change with respect to the unperturbed size distribution is still evident. Looking at PSD evolved in higher temperature environment the situation is somewhat different. In fact the evolution of PSD and the change with respect to the unperturbed situation is less evident. For a temperature in the probe of 600Kand 700K, green and light blue dots respectively in the figure, particle size distribution are peaked around 4nm and particle with smaller diameter are present although in lower numerical concentration. However, giving a general evaluation of particle size distribution it seems that coagulation became less effective, i.e. particles are not able to form larger primary particle or aggregates with sizes larger than 10nm. However, the relative decrease of the particle as small as 2nm can have different explanations. The first one relies in a wrong correction to the measured particle size distribution for taking into account diffusion losses. This correction is size dependent; for this long residence time the losses of 2nm particles can be as high as 90% of the sampled ones. This high correction factor can easily induce an underestimation of the small nanoparticle concentration. Another possible explanation is related to the secondary dilution. Since this dilution is necessary to reduce the number of large particles it also reduces the signal of 2nm particles close to the bottom detection limit of the instrument, enlarging the uncertainty of the measure. Finally a change in particle arrangement that leads to different coagulation efficiency should not be neglected. Such change can affect the final concentration of very small particles.(Echavarria et al., 2011)

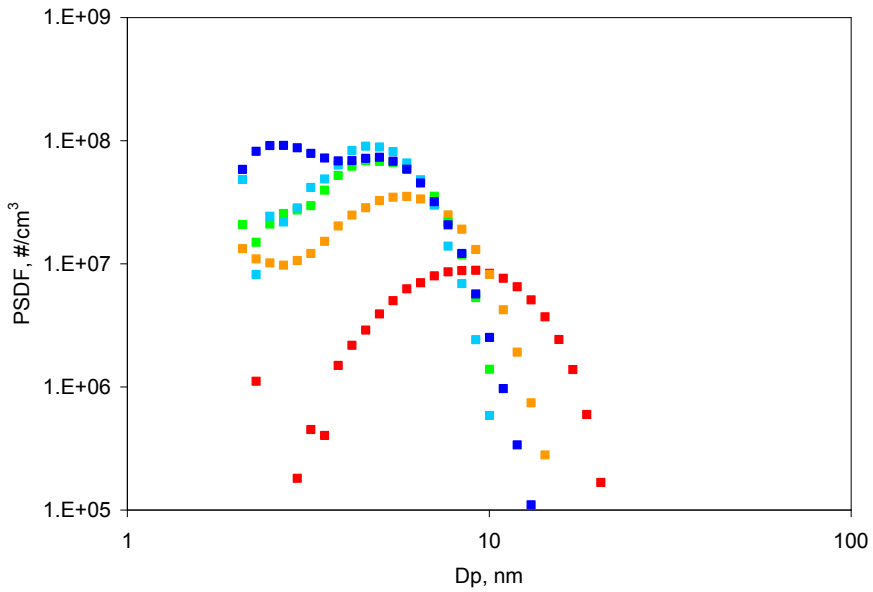

Figure 9.29 Evolution of particle size distribution at different temperatures (red dots – 300K; orange dots – 500K; green dots – 600K; light blue dots- 700K) for a residence time of 1.5s. Unperturbed PSD is also reported (blue dots)

10. Conclusions

In this work, experimental techniques and numerical model have been developed in order to characterize and control both particle production and characterization. Different reactor configurations have been investigated: premixed and diffusion flames have been characterized by using both experimental and numerical techniques. These reactors differ in terms of flame history and mixing condition, evidencing all possible particle formation pathways. Moreover the influence of several parameters on particle production has been evaluated. Equivalence ratio, fuel structure, flame temperature history have been considered. Finally the effect of some important step in particle evolution, such as oxidation-induced fragmentation, has been evidenced.

Most part of experimental investigation has been conducted coupling these techniques with numerical results. This allows to draw conclusion with higher reliability. An advanced Multi Sectional Method has been developed to gain information not only on total amount to of particles and size distribution but also on their composition and morphology. The method is based on discrete approach; now discretizations are made on the mass, H/C ratio and different possible morphology (Molecules, Cluster-Particles and Aggregates of Particles).

All the information gained from these investigations is fundamental in order to achieve the control of the particle formation process. The equivalence ratio effect has been investigated by using spectral analysis of laser induced emission. The correlation between wavelengths and aromatic nature of compounds has evidenced the process of aromatization of particles. In particular this process seems to precede the formation of very large aggregates responsible for incandescence signal. This means that tuning the equivalence ratio it might be possible to evidence and isolate this process producing more aromatized nanoparticles. Methane, ethylene and benzene premix flame have been investigated in order to evidence the role of the fuel nature on particle formation. Particles exhibit a different evolution when aromatic fuel is used In this case, the inception process is faster and the very first particles result more aromatized with respect to the aliphatic flame. Moreover the inception process seems to stop in the post combustion zone whereas aliphatic flame shows a more continuous growth process. This information can be quite useful in order to have a process in which the particles have to be produced only close to the flame front or needs to have a more marked aromatic character. Diffusion flames have been chosen in order to evidence the possibility to form particles through different inception channel. In the opposed flow flame a new optical technique has been used in order to gain information on particle morphology. This technique is based on the measure of decay time of fluorescence. A correlation between this decay time and particles morphology has been found: the more the structure is packed, the longer are the decay times of the collected signal. The results, also confirmed by numerical simulations, evidence the role of physical

inception more than chemical path in the pyrolytic zone of the opposed flow flame. This different inception turns into a more packed structure with less aromatic content due to the relative low temperature of that zone. The enhancement of this pathway can be determinant to control the final feature of small nanoparticles. The coflow flame has substantially confirmed this sketch of particle formation, also evidencing the role of a particular step in particle evolution: oxidation-induced fragmentation. An evaluation of these relatively new reactions has been conducted. Numerical tests conducted with and without considering this process suggest a key role for this reaction in final particle characterization. In fact, beside of changing the mean size and the particle concentration fragmentation is also able to determine the effective total oxidation rate and the final form of the particles. Very small particles can be formed by oxidation process instead of inception process. The final feature can be strongly more similar to soot aggregate when this process occurs.

Finally an analysis of particle evolution in a medium low temperature regime has been conducted by using an ad hoc plug flow reactor and a DMA. The plug flow allows to have a long residence time and a temperature up to 700K. In these conditions the particle size distribution fed to the system can evolve and undergo coagulation phenomenon. This allows to control the final form of the particles by tuning reactor parameters.

This set of experimental and numerical tool give the general keys to control particles formation process in high temperature environment.

11. References

ABID, A. D., CAMACHO, J., SHEEN, D. A. & WANG, H. 2009. Quantitative measurement of soot particle size distribution in premixed flames - The burner-stabilized stagnation flame approach. *Combustion and Flame,* 156**,** 1862-1870.

ABID, A. D., HEINZ, N., TOLMACHOFF, E. D., PHARES, D. J., CAMPBELL, C. S. & WANG, H. 2008. On evolution of particle size distribution functions of incipient soot in premixed ethylene-oxygen-argon flames. *Combustion and Flame,* 154**,** 775-788.

ADAMS, D. M., BRUS, L., CHIDSEY, C. E. D., CREAGER, S., CREUTZ, C., KAGAN, C. R., KAMAT, P. V., LIEBERMAN, M., LINDSAY, S., MARCUS, R. A., METZGER, R. M., MICHEL-BEYERLE, M. E., MILLER, J. R., NEWTON, M. D., ROLISON, D. R., SANKEY, O., SCHANZE, K. S., YARDLEY, J. & ZHU, X. 2003. Charge transfer on the nanoscale: Current status. *Journal of Physical Chemistry B,* 107**,** 6668-6697.

AFFOUNE, A. M., PRASAD, B. L. V., SATO, H., ENOKI, T., KABURAGI, Y. & HISHIYAMA, Y. 2001. Experimental evidence of a single nano-graphene. *Chemical Physics Letters,* 348**,** 17-20.

ALFÈ, M., APICELLA, B., BARBELLA, R., ROUZAUD, J. N., TREGROSSI, A. & CIAJOLO, A. Year. Structure-property relationship in nanostructures of young and mature soot in premixed flames. *In:* Proceeding of the Combustion Institute, 2009. 697-704.

ALFÈ, M., APICELLA, B., BARBELLA, R., TREGROSSI, A. & CIAJOLO, A. Year. Similarities and dissimilarities in n-hexane and benzene sooting premixed flames. *In:* Proceeding of the Combustion Institute, 2007. 585-591.

ALFÈ, M., APICELLA, B., ROUZAUD, J. N., TREGROSSI, A. & CIAJOLO, A. 2010. The effect of temperature on soot properties in premixed methane flames. *Combustion and Flame,* 157**,** 1959-1965.

ALONSO, M., KOUSAKA, Y., HASHIMOTO, T. & HASHIMOTO, N. 1997a. Penetration of nanometer-sized aerosol particles through wire screen and laminar flow tube. *Aerosol Science and Technology,* 27**,** 471-480.

ALONSO, M., KOUSAKA, Y., NOMURA, T., HASHIMOTO, N. & HASHIMOTO, T. 1997b. Bipolar charging and neutralization of nanometer-sized aerosol particles. *Journal of Aerosol Science,* 28**,** 1479-1490.

AMANS, D., CHENUS, A. C., LEDOUX, G., DUJARDIN, C., REYNAUD, C., SUBLEMONTIER, O., MASENELLI-VARLOT, K. & GUILLOIS, O. 2009. Nanodiamond synthesis by pulsed laser ablation in liquids. *Diamond and Related Materials,* 18**,** 177-180.

ANILKUMAR, P., LU, F., CAO, L., LUO, P. G., LIU, J. H., SAHU, S., TACKETT, K. N., WANG, Y. & SUN, Y. P. 2011. Fullerenes for applications in biology and medicine. *Current Medicinal Chemistry,* 18**,** 2045-2059.

APICELLA, B., CARPENTIERI, A., ALFÈ, M., BARBELLA, R., TREGROSSI, A., PUCCI, P. & CIAJOLO, A. Year. Mass spectrometric analysis of large PAH in a fuel-rich ethylene flame. *In:* Proceeding of the Combustion Institute, 2007 2007. 547-553.

ARISTOV, V. Y., URBANIK, G., KUMMER, K., VYALIKH, D. V., MOLODTSOVA, O. V., PREOBRAJENSKI, A. B., ZAKHAROV, A. A., HESS, C., HÄNKE, T., BÜCHNER, B., VOBORNIK, I., FUJII, J., PANACCIONE, G., OSSIPYAN, Y. A. & KNUPFER, M. 2010. Graphene synthesis on cubic SiC/Si wafers.

Perspectives for mass production of graphene-based electronic devices. *Nano Letters,* 10**,** 992-995.

ATTARIAN SHANDIZ, M. & SAFAEI, A. 2008. Melting entropy and enthalpy of metallic nanoparticles. *Materials Letters,* 62**,** 3954-3956.

ATTARIAN SHANDIZ, M., SAFAEI, A., SANJABI, S. & BARBER, Z. H. 2007. Modeling size dependence of melting temperature of metallic nanoparticles. *Journal of Physics and Chemistry of Solids,* 68**,** 1396-1399.

AVOURIS, P. 2010. Graphene: Electronic and photonic properties and devices. *Nano Letters,* 10**,** 4285-4294.

BALTHASAR, M. & FRENKLACH, M. 2005a. Detailed kinetic modeling of soot aggregate formation in laminar premixed flames. *Combustion and Flame,* 140**,** 130-145.

BALTHASAR, M. & FRENKLACH, M. Year. Monte-Carlo simulation of soot particle coagulation and aggregation: The effect of a realistic size distribution. *In:* Proceeding of Combustion Institute, 2005b. 1467-1475.

BALTHASAR, M. & KRAFT, M. 2003. A stochastic approach to calculate the particle size distribution function of soot particles in laminar premixed flames. *Combustion and Flame,* 133**,** 289-298.

BALTHASAR, M., SINGH, J., KRAFT, M. & WAGNER, W. Year. Stochastic modelling of the size distribution of soot particles in laminar premixed flames. *In:* Proocedding of the Combustion Institute, 2002. 47.

BARONE, A. C., D'ALESSIO, A. & D'ANNA, A. 2003. Morphological characterization of the early process of soot formation by atomic force microscopy. *Combustion and Flame,* 132**,** 181-187.

BITTNER, J. D. & HOWARD, J. B. 1981. Composition profiles and reaction mechanisms in a near-sooting premixed benzene/oxygen/argon flame. *Symposium (International) on Combustion,* 18**,** 1105-1116.

BLANQUART, G. & PITSCH, H. 2009. Analyzing the effects of temperature on soot formation with a joint volume-surface-hydrogen model. *Combustion and Flame,* 156**,** 1614-1626.

BOCKHORN, H. 1994. *Soot formation in combustion -Mechanismo and models,* Alemania, Springer-Verlag.

BOCKHORN, H., D'ANNA, A, SAROFIM, A.F., WANG, H. 2007. *Combustion Generated Fine Carbonaceous Particles - Proceedings of an International Workshop held in Villa Orlandi, Anacapri, Italy, May 13-16, 2007*.

BOISSEAU, P. & LOUBATON, B. 2011. Nanomedicine, nanotechnology in medicine. *Comptes Rendus Physique,* 12**,** 620-636.

BONACCORSO, F., SUN, Z., HASAN, T. & FERRARI, A. C. 2010. Graphene photonics and optoelectronics. *Nature Photonics,* 4**,** 611-622.

BRABEC, C. J., GOWRISANKER, S., HALLS, J. J. M., LAIRD, D., JIA, S. & WILLIAMS, S. P. 2010. Polymer-fullerene bulk-heterojunction solar cells. *Advanced Materials,* 22**,** 3839-3856.

BRUNO, A., DE LISIO, C. & MINUTOLO, P. 2005. Time resolved fluorescence polarization anisotropy of carbonaceous particles produced in combustion systems. *Optics Express,* 13**,** 5393-5408.

BRUNO, A., DE LISIO, C., MINUTOLO, P. & D'ALESSIO, A. 2007. Evidence of fluorescent carbon nanoparticles produced in premixed flames by time-resolved fluorescence polarization anisotropy. *Combustion and Flame,* 151**,** 472-481.

BRUNO, A., OSSLER, F., DE LISIO, C., MINUTOLO, P., SPINELLI, N. & D'ALESSIO, A. 2008. Detection of fluorescent nanoparticles in flame with femtosecond laser-induced fluorescence anisotropy. *Optics Express,* 16**,** 5623-5632.

CAIN, J. P., CAMACHO, J., PHARES, D. J., WANG, H. & LASKIN, A. 2011. Evidence of aliphatics in nascent soot particles in premixed ethylene flames. *Proceeding of The combustion Institute.* 1 ed.

CAIN, J. P., GASSMAN, P. L., WANG, H. & LASKIN, A. 2010. Micro-FTIR study of soot chemical composition - Evidence of aliphatic hydrocarbons on nascent soot surfaces. *Physical Chemistry Chemical Physics,* 12**,** 5206-5218.

CALCOTE, H. F. 1981. Mechanisms of soot nucleation in flames--A critical review. *Combustion and Flame,* 42**,** 215-242.

CALCOTE, H. F. & MANOS, D. M. 1983. Effect of molecular structure on incipient soot formation. *Combustion and Flame,* 49**,** 289-304.

CAMENZIND, A., CASERI, W. R. & PRATSINIS, S. E. 2010. Flame-made nanoparticles for nanocomposites. *Nano Today,* 5**,** 48-65.

CAMPOS-DELGADO, J., ROMO-HERRERA, J. M., JIA, X., CULLEN, D. A., MURAMATSU, H., KIM, Y. A., HAYASHI, T., REN, Z., SMITH, D. J., OKUNO, Y., OHBA, T., KANOH, H., KANEKO, K., ENDO, M., TERRONES, H., DRESSELHAUS, M. S. & TERRONES, M. 2008. Bulk production of a new form of sp2 carbon: Crystalline graphene nanoribbons. *Nano Letters,* 8**,** 2773-2778.

CASSELL, A. M., RAYMAKERS, J. A., KONG, J. & DAI, H. 1999. Large Scale CVD Synthesis of Single-Walled Carbon Nanotubes. *Journal of Physical Chemistry B,* 103**,** 6484-6492.

CASTALDI, M. J., MARINOV, N. M., MELIUS, C. F., HUANG, J., SENKAN, S. M., PIT, W. J. & WESTBROOK, C. K. 1996. Experimental and modeling investigation of aromatic and polycyclic aromatic hydrocarbon formation in a premixed ethylene flame. *Symposium (International) on Combustion,* 26**,** 693-702.

CHARALAMPOPOULOS, T. T. 1992. Morphology and dynamics of agglomerated particulates in combustion systems using light scattering techniques. *Progress in Energy and Combustion Science,* 18**,** 13-45.

CHARALAMPOPOULOS, T. T. & CHANG, H. 1991. Agglomerate parameters and fractal dimension of soot using light scattering - effects on surface growth. *Combustion and Flame,* 87**,** 89-99.

CHAVY, C., JOACHIM, C. & ALTIBELLI, A. 1993. Interpretation of STM images: C60 on the gold (110) surface. *Chemical Physics Letters,* 214**,** 569-575.

CHEN, B., CHENG, Y., DING, S. & HU, R. R. 2007. Particle growth in the flame synthesis of titanium dioxide nanoparticles. *Guocheng Gongcheng Xuebao/The Chinese Journal of Process Engineering,* 7**,** 944-951.

CHEN, X. & SCHLUESENER, H. J. 2008. Nanosilver: A nanoproduct in medical application. *Toxicology Letters,* 176**,** 1-12.

CHOI, B. C. & FOSTER, D. E. 2006. Overview of the effect of catalyst formulation and exhaust gas compositions on soot oxidation in DPF. *Journal of Mechanical Science and Technology,* 20**,** 1-12.

CHUNG, S. H. & VIOLI, A. 2010. Nucleation of fullerenes as a model for examining the formation of soot. *Journal of Chemical Physics,* 132.

CHUNG, S. H. & VIOLI, A. Year. Peri-condensed aromatics with aliphatic chains as key intermediates for the nucleation of aromatic hydrocarbons. *In:* Proceeding of the Combustion Institute, 2011. 693-700.

CIAJOLO, A., APICELLA, B., BARBELLA, R., TREGROSSI, A., BERETTA, F. & ALLOUIS, C. 2001a. Depletion of fuel aromatic components and formation of aromatic species in ia spray flame as characterized by fluorescence spectroscopy. *Energy and Fuels,* 15**,** 987-995.

CIAJOLO, A., BARBELLA, R., TREGROSSI, A. & BONFANTI, L. 1998. Spectroscopic and compositional signatures of PAH-loaded mixtures in the soot inception region of a premixed ethylene flame. *Symposium (International) on Combustion,* 1**,** 1481-1487.

CIAJOLO, A., D'ANNA, A., BARBELLA, R. & TREGROSSI, A. 1994. The formation of aromatic carbon in sooting ethylene flames. *Symposium (International) on Combustion,* 25**,** 679-685.

CIAJOLO, A., D'ANNA, A., BARBELLA, R., TREGROSSI, A. & VIOLI, A. 1996. The effect of temperature on soot inception in premixed ethylene flames. *Symposium (International) on Combustion,* 26**,** 2327-2333.

CIAJOLO, A., RAGUCCI, R., APICELLA, B., BARBELLA, R., DE JOANNON, M. & TREGROSSI, A. 2001b. Fluorescence spectroscopy of aromatic species produced in rich premixed ethylene flames. *Chemosphere,* 42**,** 835-841.

CIAJOLO, A., TREGROSSI, A., BARBELLA, R., RAGUCCI, R., APICELLA, B. & DE JOANNON, M. 2001c. The relation between ultraviolet-excited fluorescence spectroscopy and aromatic species formed in rich laminar ethylene flames. *Combustion and Flame,* 125**,** 1225-1229.

COLKET, M. B. & SEERY, D. J. 1994. Reaction mechanisms for toluene pyrolysis. *Symposium (International) on Combustion,* 25**,** 883-891.

CUI, H., YANG, X., BAYLOR, L. R. & LOWNDES, D. H. 2005. Growth of multiwalled-carbon nanotubes using vertically aligned carbon nanofibers as templates/scaffolds and improved field-emission properties. *Applied Physics Letters,* 86**,** 1-3.

D'ALESSIO, A., BARONE, A. C., CAU, R., D'ANNA, A. & MINUTOLO, P. Year. Surface deposition and coagulation efficiency of combustion generated nanoparticles in the size range from 1 to 10 nm. *In:* Proceeding of the Combustion Institute, 2005. 2595-2603.

D'ALESSIO, A., D'ANNA, A., D'ORSI, A., MINUTOLO, P., BARBELLA, R. & CIAJOLO, A. 1992. Precursor formation and soot inception in premixed ethylene flames. *Symposium (International) on Combustion,* 24**,** 973-980.

D'ANNA, A. Available: http://wpage.unina.it/anddanna/ [Accessed].

D'ANNA, A. 2009. Combustion-formed nanoparticles. *Proceedings of the Combustion Institute,* 32**,** 593-613.

D'ANNA, A., COMMODO, M., SIRIGNANO, M., MINUTOLO, P. & PAGLIARA, R. 2009. Particle formation in opposed-flow diffusion flames of ethylene: An experimental and numerical study. *Proceedings of the Combustion Institute,* 32**,** 793-801.

D'ANNA, A., D'ALESSIO, A. & KENT, J. 2001a. A computational study of hydrocarbon growth and the formation of aromatics in coflowing laminar diffusion flames of ethylene. *Combustion and Flame,* 125**,** 1196-1206.

D'ANNA, A., D'ALESSIO, A. & MINUTOLO, P. 1994. *Spectroscopic and chemical characterization of soot inception processes in premixed laminar flames at atmospheric pressure*.

D'ANNA, A., SIRIGNANO, M. & KENT, J. 2010. A model of particle nucleation in premixed ethylene flames. *Combustion and Flame,* 157**,** 2106-2115.

D'ANNA, A., VIOLI, A. & D'ALESSIO, A. 2000. Modeling the rich combustion of aliphatic hydrocarbons. *Combustion and Flame,* 121**,** 418-429.

D'ANNA, A., VIOLI, A., D'ALESSIO, A. & SAROFIM, A. F. 2001b. A reaction pathway for nanoparticle formation in rich premixed flames. *Combustion and Flame,* 127**,** 1995-2003.

DE FILIPPO, A., SGRO, L. A., LANZUOLO, G. & D'ALESSIO, A. 2009. Probe measurements and numerical model predictions of evolving size distributions in premixed flames. *Combustion and Flame,* 156**,** 1744-1754.

DOBBINS, R. A., GOVATZIDAKIS, G. J., LU, W., SCHWARTZMAN, A. F. & FLETCHER, R. A. 1996. Carbonization rate of soot precursor particles. *Combustion science and technology,* 121**,** 103-121.

DOBBINS, R. A. & MEGARIDIS, C. M. 1987. Morphology of flame-generated soot as determined by thermophoretic sampling. *Langmuir,* 3**,** 254-259.

DOLMATOV, V. Y. & KOSTROVA, L. N. 2000. Detonation synthesis of nanodiamonds and the feasibility of developing a new generation of drugs. *Sverkhtverdye Materialy***,** 82-85.

DONCHEV, A. G. 2006. Ab initio quantum force field for simulations of nanostructures. *Physical Review B - Condensed Matter and Materials Physics,* 74.

DONNET, J. B., LE MOIGNE, C., WANG, T. K., SAMIRANT, M. & ECKHARDT, A. 1998. "Onion-like" and equilibrium structure of carbon. *Structures « type oignon » et structure d'équilibre du carbone,* 1**,** 431-434.

DU, M., GUO, B. & JIA, D. 2010. Newly emerging applications of halloysite nanotubes: A review. *Polymer International,* 59**,** 574-582.

DUPLOCK, E. J., SCHEFFLER, M. & LINDAN, P. J. D. 2004. Hallmark of perfect graphene. *Physical Review Letters,* 92**,** 225502-1.

DUPUIS, A. C. 2005. The catalyst in the CCVD of carbon nanotubes-a review. *Progress in Materials Science,* 50**,** 929-961.

ECHAVARRIA, C. A., JARAMILLO, I. C., SAROFIM, A. F. & LIGHTY, J. S. 2011. Studies of soot oxidation and fragmentation in a two-stage burner under fuel-lean and fuel-rich conditions. *Proceedings of the Combustion Institute,* 33**,** 659-666.

EHRMAN, S. H., FRIEDLANDER, S. K. & ZACHARIAH, M. R. 1999. Phase segregation in binary SiO2/TiO2 and SiO2/Fe2O3 nanoparticle aerosols formed in a premixed flame. *Journal of Materials Research,* 14**,** 4551-4561.

ENDO, M. & KROTO, H. W. 1992. Formation of carbon nanofibers. *Journal of Physical Chemistry,* 96**,** 6941-6944.

FANG, X., BANDO, Y., GAUTAM, U. K., YE, C. & GOLBERG, D. 2008. Inorganic semiconductor nanostructures and their field-emission applications. *Journal of Materials Chemistry,* 18**,** 509-522.

FARIAS, T. L., CARVALHO, M. G., KOEYLU, U. O. & FAETH, G. M. 1995. Computational evaluation of approximate Rayleigh-Debye-Gans/fractal-aggregate theory for the absorption and scattering properties of soot. *Journal of Heat Transfer,* 117**,** 152-159.

FAROKHZAD, O. C. & LANGER, R. 2009. Impact of nanotechnology on drug delivery. *ACS Nano,* 3**,** 16-20.

FLAGAN, R. C. 1998. History of electrical aerosol measurements. *Aerosol Science and Technology,* 28**,** 301-380.

FRENKLACH, M. 1985. Dynamics of discrete distribution for Smoluchowski coagulation model. *Journal of Colloid and Interface Science,* 108**,** 237-242.
FRENKLACH, M. 1996. On surface growth mechanism of soot particles. *Symposium (International) on Combustion,* 26**,** 2285-2293.
FRENKLACH, M. 2002a. Method of moments with interpolative closure. *Chemical Engineering Science,* 57**,** 2229-2239.
FRENKLACH, M. 2002b. Reaction mechanism of soot formation in flames. *Physical Chemistry Chemical Physics,* 4**,** 2028-2037.
FRENKLACH, M., BOWMAN, T., SMITH, G. & GARDINER JR, W. C. 2011. Available: http://www.me.berkeley.edu/gri-mech/ [Accessed].
FRENKLACH, M., CLARY, D. W., GARDINER JR, W. C. & STEIN, S. E. 1985. Detailed kinetic modeling of soot formation in shock-tube pyrolysis of acetylene. *Symposium (International) on Combustion,* 20**,** 887-901.
FRENKLACH, M., MORIARTY, N. W. & BROWN, N. J. 1998. Hydrogen migration in polyaromatic growth. *Symposium (International) on Combustion,* 27**,** 1655-1661.
FRENKLACH, M. & WANG, H. 1991. Detailed modeling of soot particle nucleation and growth. *Symposium (International) on Combustion,* 23**,** 1559-1566.
FRENKLACH, M. & WANG, H. 1994. *Detailed mechanism and modeling of soot particle formation*.
FRENKLACH, M., YUAN, T. & RAMACHANDRA, M. K. 1988. Soot formation in binary hydrocarbon mixtures. *Energy and Fuels,* 2**,** 462-480.
FRIEDLANDER, S. K. & WANG, C. S. 1966. The self-preserving particle size distribution for coagulation by brownian motion. *Journal of Colloid and Interface Science,* 22**,** 126-132.
FULLER, B. R. 1954. *Geodesic Dome*. U.S. patent application 261168.
GAMALY, E. G. & EBBESEN, T. W. 1995. Mechanism of carbon nanotube formation in the arc discharge. *Physical Review B,* 52**,** 2083-2089.
GARO, A., PRADO, G. & LAHAYE, J. 1990. Chemical aspects of soot particles oxidation in a laminar methane-air diffusion flame. *Combustion and Flame,* 79**,** 226-233.
GEORGE, R., KASHYAP, K. T., RAHUL, R. & YAMDAGNI, S. 2005. Strengthening in carbon nanotube/aluminium (CNT/Al) composites. *Scripta Materialia,* 53**,** 1159-1163.
GLASSMAN, I. & YACCARINO, P. 1981. The temperature effect in sooting diffusion flames. *Symposium (International) on Combustion,* 18**,** 1175-1183.
GOEL, A., HEBGEN, P., VANDER SANDE, J. B. & HOWARD, J. B. 2002. Combustion synthesis of fullerenes and fullerenic nanostructures. *Carbon,* 40**,** 177-182.
GOLDBERGER, J., HE, R., ZHANG, Y., LEE, S., YAN, H., CHOI, H. J. & YANG, P. 2003. Single-crystal gallium nitride nanotubes. *Nature,* 422**,** 599-602.
GONZÁLEZ, J., GUINEA, F. & VOZMEDIANO, M. A. H. 2001. Electron-electron interactions in graphene sheets. *Physical Review B - Condensed Matter and Materials Physics,* 63**,** 1344211-1344218.
GRAULE, T. J., BARNA, E., BOMMER, B., KÜRSTEINER, J., VITAL, A., TRZEBIATOWSKI, O., SCHMID, B., VAN LEEUWEN, J. & KOCH, W. 2005. Synthesis of spherical, non-aggregated silica nanoparticles for nanocomposite coatings. *KGK Kautschuk Gummi Kunststoffe,* 58**,** 252-255.
GROTHEER, H. H., POKORNY, H., BARTH, K. L., THIERLEY, M. & AIGNER, M. 2004. Mass spectrometry up to 1 million mass units for the simultaneous detection of primary soot and of soot precursors (nanoparticles) in flames. *Chemosphere,* 57**,** 1335-1342.

GROTHEER, H. H., WOLF, K. & HOFFMANN, K. 2011. Photoionization mass spectrometry for the investigation of combustion generated nascent nanoparticles and their relation to laser induced incandescence. *Applied Physics B: Lasers and Optics,* 104**,** 367-383.

GUO, Y., BAO, C., SONG, L., YUAN, B. & HU, Y. 2011. In situ polymerization of graphene, graphite oxide, and functionalized graphite oxide into epoxy resin and comparison study of on-the-flame behavior. *Industrial and Engineering Chemistry Research,* 50**,** 7772-7783.

HAFNER, J. H., CHEUNG, C. L., WOOLLEY, A. T. & LIEBER, C. M. 2001. Structural and functional imaging with carbon nanotube AFM probes. *Progress in Biophysics and Molecular Biology,* 77**,** 73-110.

HARRIS, S. J. & MARICQ, M. M. 2002. The role of fragmentation in defining the signature size distribution of diesel soot. *Journal of Aerosol Science,* 33**,** 935-942.

HAYNES, B. S. & WAGNER GG, H. 1981. Soot formation. *Progress in Energy and Combustion Science,* 7**,** 229-273.

HEBARD, A. F. 1993. Buckminsterfullerene. *Annual Review of Materials Science,* 23**,** 159-191.

HEIGHT, M. J., HOWARD, J. B. & TESTER, J. W. 2003. Flame Synthesis of Carbon Nanotubes. *Materials Research Society Symposium - Proceedings,* 772**,** 55-61.

HEIGHT, M. J., HOWARD, J. B. & TESTER, J. W. 2005. Flame synthesis of single-walled carbon nanotubes. *Proceedings of the Combustion Institute,* 30**,** 2537-2543.

HERDMAN, J. D. & MILLER, J. H. 2008. Intermolecular potential calculations for polynuclear aromatic hydrocarbon clusters. *Journal of Physical Chemistry A,* 112**,** 6249-6256.

HERNANDEZ, Y., NICOLOSI, V., LOTYA, M., BLIGHE, F. M., SUN, Z., DE, S., MCGOVERN, I. T., HOLLAND, B., BYRNE, M., GUN'KO, Y. K., BOLAND, J. J., NIRAJ, P., DUESBERG, G., KRISHNAMURTHY, S., GOODHUE, R., HUTCHISON, J., SCARDACI, V., FERRARI, A. C. & COLEMAN, J. N. 2008. High-yield production of graphene by liquid-phase exfoliation of graphite. *Nature Nanotechnology,* 3**,** 563-568.

HOMANN, K. H. 1998. Fullerenes and soot formation - New pathways to large particles in flames. *Angewandte Chemie - International Edition,* 37**,** 2434-2451.

HORIUCHI, S., GOTOU, T., FUJIWARA, M., ASAKA, T., YOKOSAWA, T. & MATSUI, Y. 2004. Single graphene sheet detected in a carbon nanofilm. *Applied Physics Letters,* 84**,** 2403-2405.

HOU, S. S., CHUNG, D. H. & LIN, T. H. 2009. High-yield synthesis of carbon nano-onions in counterflow diffusion flames. *Carbon,* 47**,** 938-947.

HOWARD, J. B., MCKINNON, J. T., MAKAROVSKY, Y., LAFLEUR, A. L. & JOHNSON, M. E. 1991. Fullerenes C60 and C70 in flames. *Nature,* 352**,** 139-141.

HWANG, K. C. 1995. Efficient cleavage of carbon graphene layers by oxidants. *Journal of the Chemical Society, Chemical Communications***,** 173-174.

IIJIMA, S. 1991. Helical microtubules of graphitic carbon. *Nature,* 354**,** 56-58.

IIJIMA, S. & ICHIHASHI, T. 1993. Single-shell carbon nanotubes of 1-nm diameter. *Nature,* 363**,** 603-605.

IRLE, S., ZHENG, G., WANG, Z. & MOROKUMA, K. 2006. The C60 formation puzzle "solved": QM/MD simulations reveal the shrinking hot giant road of the dynamic fullerene self-assembly mechanism. *Journal of Physical Chemistry B,* 110**,** 14531-14545.

JIMÉNEZ, V., NIETO-MÁRQUEZ, A., DÍAZ, J. A., ROMERO, R., SÁNCHEZ, P., VALVERDE, J. L. & ROMERO, A. 2009. Pilot plant scale study of the influence of the operating conditions in the production of carbon nanofibers. *Industrial and Engineering Chemistry Research,* 48**,** 8407-8417.

KAPTEIJN, F., MEIJER, R., MOULIJN, J. A. & CAZORLA-AMÓROS, D. 1994. On why do different carbons show different gasification rates: A transient isotopic CO2 gasification study. *Carbon,* 32**,** 1223-1231.

KASPER, M., SIEGMANN, K. & SATTLER, K. 1997. Evaluation of an in situ sampling probe for its accuracy in determining particle size distributions from flames. *Journal of Aerosol Science,* 28**,** 1569-1578.

KATAURA, H., MANIWA, Y., KODAMA, T., KIKUCHI, K., HIRAHARA, K., SUENAGA, K., IIJIMA, S., SUZUKI, S., ACHIBA, Y. & KRÄTSCHMER, W. 2001. High-yield fullerene encapsulation in single-wall carbon nanotubes. *Synthetic Metals,* 121**,** 1195-1196.

KAZAKOV, A., WANG, H. & FRENKLACH, M. 1995. Detailed modeling of soot formation in laminar premixed ethylene flames at a pressure of 10 bar,. *Combustion and Flame,* 100**,** 111-120.

KENNEDY, I. M. 1997. Models of soot formation and oxidation. *Progress in Energy and Combustion Science,* 23**,** 95-132.

KENT, J. H. & WAGNER, H. G. 1985. Temperature and fuel effects in sooting diffusion flames. *Symposium (International) on Combustion,* 20**,** 1007-1015.

KLOEPFER, H. 1942. *Verfahren zum Reinigen von hochdispersen Oxyden von Metallen bzw*.

KOYLU, U. O. & FAETH, G. M. 1992. Structure of overfire soot in buoyant turbulent diffusion flames at long residence times. *Combustion and Flame,* 89**,** 140-156.

KÖYLÜ, Ü. Ö., FAETH, G. M., FARIAS, T. L. & CARVALHO, M. G. 1995. Fractal and projected structure properties of soot aggregates. *Combustion and Flame,* 100**,** 621-633.

KROTO, H. W. 1992. Carbon onions introduce new flavour to fullerene studies. *Nature,* 359**,** 670-671.

KROTO, H. W., HEATH, J. R., O'BRIEN, S. C., CURL, R. F. & SMALLEY, R. E. 1985. C60: Buckminsterfullerene. *Nature,* 318**,** 162-163.

KUBICKI, J. D. 2005. Computational chemistry applied to studies of organic contaminants in the environment: Examples based on benzo[a]pyrene. *American Journal of Science,* 305**,** 621-644.

KUBICKI, J. D. 2006. Molecular simulations of benzene and PAH interactions with soot. *Environmental Science and Technology,* 40**,** 2298-2303.

LAI, F. S., FRIEDLANDER, S. K., PICH, J. & HIDY, G. M. 1972. The self-preserving particle size distribution for Brownian coagulation in the free-molecule regime. *Journal of Colloid and Interface Science,* 39**,** 395-405.

LAM, R. & HO, D. 2009. Nanodiamonds as vehicles for systemic and localized drug delivery. *Expert Opinion on Drug Delivery,* 6**,** 883-895.

LEMME, M. C., BELL, D. C., WILLIAMS, J. R., STERN, L. A., BAUGHER, B. W. H., JARILLO-HERRERO, P. & MARCUS, C. M. 2009. Etching of graphene devices with a helium ion beam. *ACS Nano,* 3**,** 2674-2676.

LI, J., KAZAKOV, A. & DRYER, F. L. 2004. Experimental and numerical studies of ethanol decomposition reactions. *Journal of Physical Chemistry A,* 108**,** 7671-7680.

LI, J., ZHU, Y., LI, W., ZHANG, X., PENG, Y. & HUANG, Q. 2010. Nanodiamonds as intracellular transporters of chemotherapeutic drug. *Biomaterials,* 31**,** 8410-8418.

LI, Y. Y., WEI, L. X., TIAN, Z., YANG, B., WANG, J., ZHANG, T. C. & QI, F. 2008. A comprehensive experimental study of low-pressure premixed C3-oxygenated hydrocarbon flames with tunable synchrotron photoionization. *Combustion and Flame,* 152**,** 336-359.

LI, Z., ZHU, H., XIE, D., WANG, K., CAO, A., WEI, J., LI, X., FAN, L. & WU, D. 2011. Flame synthesis of few-layered graphene/graphite films. *Chemical Communications,* 47**,** 3520-3522.

LIVERMORE, L. Available: https://www-pls.llnl.gov/?url=science_and_technology-chemistry-combustion-mechanisms [Accessed].

LOU, L., NORDLANDER, P. & SMALLEY, R. E. 1995. Fullerene nanotubes in electric fields. *Physical Review B,* 52**,** 1429-1432.

MARICQ, M. M., HARRIS, S. J. & SZENTE, J. J. 2003. Soot size distributions in rich premixed ethylene flames. *Combustion and Flame,* 132**,** 328-342.

MARINOV, N. M., PITZ, W. J., WESTBROOK, C. K., CASTALDI, M. J. & SENKAN, S. M. 1996. Modeling of aromatic and polycyclic aromatic hydrocarbon formation in premixed methane and ethane flames. *Combustion science and technology,* 116-117**,** 211-287.

MARINOV, N. M., PITZ, W. J., WESTBROOK, C. K., LUTZ, A. E., VINCITORE, A. M. & SENKAN, S. M. 1998a. Chemical kinetic modeling of a methane opposed-flow diffusion flame and comparison to experiments. *Symposium (International) on Combustion,* 1**,** 605-613.

MARINOV, N. M., PITZ, W. J., WESTBROOK, C. K., VINCITORE, A. M., CASTALDI, M. J., SENKAN, S. M. & MELIUS, C. F. 1998b. Aromatic and polycyclic aromatic hydrocarbon formation in a laminar premixed n-butane flame. *Combustion and Flame,* 114**,** 192-213.

MASER, W. K., MUÑOZ, E., BENITO, A. M., MARTÍNEZ, M. T., DE LA FUENTE, G. F., MANIETTE, Y., ANGLARET, E. & SAUVAJOL, J. L. 1998. Production of high-density single-walled nanotube material by a simple laser-ablation method. *Chemical Physics Letters,* 292**,** 587-593.

MATTAUSCH, A. & PANKRATOV, O. 2007. Ab initio study of graphene on SiC. *Physical Review Letters,* 99.

MAUSS, F., SCHÄFER, T. & BOCKHORN, H. 1994. Inception and growth of soot particles in dependence on the surrounding gas phase. *Combustion and Flame,* 99**,** 697-705.

MAZUMDER, S., GHOSH, S. & PURI, I. K. 2011. Non-premixed flame synthesis of hydrophobic carbon nanostructured surfaces. *Proceedings of the Combustion Institute,* 33**,** 3351-3357.

MCMURRY, P. H. 2000. A review of atmospheric aerosol measurements. *Atmospheric Environment,* 34**,** 1959-1999.

MEGARIDIS, C. M., GRIFFIN, D. W. & KONSUR, B. 1996. Soot-field structure in laminar soot-emitting microgravity nonpremixed flames. *Symposium (International) on Combustion,* 26**,** 1291-1299.

MELIUS, C. F., COLVIN, M. E., MARINOV, N. M., PIT, W. J. & SENKAN, S. M. 1996. Reaction mechanisms in aromatic hydrocarbon formation involving the C5H5 cyclopentadienyl moiety. *Symposium (International) on Combustion,* 26**,** 685-692.

MEMON, N. K., TSE, S. D., AL-SHARAB, J. F., YAMAGUCHI, H., GONCALVES, A.-M. B., KEAR, B. H., JALURIA, Y., ANDREI, E. Y. & CHHOWALLA, M. 2011a. Flame synthesis of graphene films in open environments. *Carbon,* 49**,** 5064-5070.

MEMON, N. K., TSE, S. D., AL-SHARAB, J. F., YAMAGUCHI, H., GONCALVES, A. M. B., KEAR, B. H., JALURIA, Y., ANDREI, E. Y. & CHHOWALLA, M. 2011b. Flame synthesis of graphene films in open environments. *Carbon*.

MERCHAN-MERCHAN, W., SAVELIEV, A. V., KENNEDY, L. & JIMENEZ, W. C. 2010. Combustion synthesis of carbon nanotubes and related nanostructures. *Progress in Energy and Combustion Science,* 36**,** 696-727.

MERCHAN-MERCHAN, W., SAVELIEV, A. V. & KENNEDY, L. A. 2003. Carbon nanostructures in opposed-flow methane oxy-flames *Combustion Science and Technology,* 175 2217-2236

MERCHAN-MERCHAN, W., SAVELIEV, A. V. & KENNEDY, L. A. 2004. High-rate flame synthesis of vertically aligned carbon nanotubes using electric field control. *Carbon,* 42**,** 599-608.

MESSERER, A., NIESSNER, R. & POSCHL, U. 2006. Comprehensive kinetic characterization of the oxidation and gasification of model and real diesel soot by nitrogen oxides and oxygen under engine exhaust conditions: Measurement, Langmuir-Hinshelwood, and Arrhenius parameters. *Carbon,* 44**,** 307-324.

MEYYAPPAN, M. 2009. A review of plasma enhanced chemical vapour deposition of carbon nanotubes. *Journal of Physics D: Applied Physics,* 42.

MILLER, J. A. & MELIUS, C. F. 1992a. Kinetic and thermodynamic issues in the formation of aromatic compounds in flames of aliphatic fuels. *Combustion and Flame,* 91**,** 21-39.

MILLER, J. A. & MELIUS, C. F. 1992b. The reactions of imidogen with nitric oxide and molecular oxygen. *Symposium (International) on Combustion,* 24**,** 719-726.

MILLER, J. H. 1991. The kinetics of polynuclear aromatic hydrocarbon agglomeration in flames. *Symposium (International) on Combustion,* 23**,** 91-98.

MIN, H., SAHU, B., BANERJEE, S. K. & MACDONALD, A. H. 2007. Ab initio theory of gate induced gaps in graphene bilayers. *Physical Review B - Condensed Matter and Materials Physics,* 75.

MINUTOLO, P., D'ANNA, A., COMMODO, M., PAGLIARA, R., TONIATO, G. & ACCORDINI, C. 2008. Emission of ultrafine particles from natural gas domestic burners. *Environmental Engineering Science,* 25**,** 1357-1363.

MINUTOLO, P., GAMBI, G. & D'ALESSIO, A. 1996. The optical band gap model in the interpretation of the UV-visible absorption spectra of rich premixed flames. *Symposium (International) on Combustion,* 26**,** 951-957.

MINUTOLO, P., GAMBI, G. & D'ALESSIO, A. 1998. Properties of carbonaceous nanoparticles in flat premixed C2H4/air flames with C/O ranging from 0.4 to soot appearance limit. *Symposium (International) on Combustion,* 1**,** 1461-1469.

MITCHELL, P. & FRENKLACH, M. 1998. Monte carlo simulation of soot aggregation with simultaneous surface growth-why primary particles appear spherical. *Symposium (International) on Combustion,* 27**,** 1507-1514.

MOREAU, F., LANGLET, R., LAMBIN, P., KUZHIR, P. P., BYCHANOK, D. S. & MAKSIMENKO, S. A. 2009. Onion-like-carbon-based composite films: Theoretical modeling of electromagnetic response *Solid State Sciences,* 11**,** 1752-1756.

MORIARTY, N. W., BROWN, N. J. & FRENKLACH, M. 1999. Hydrogen migration in the phenylethen-2-yl radical. *Journal of Physical Chemistry A,* 103**,** 7127-7135.

MUKHOPADHYAY, S. M., JOSHI, P. & PULIKOLLU, R. V. 2005. Thin films for coating nanomaterials. *Tsinghua Science and Technology,* 10**,** 709-717.

NEOH, K. G., HOWARD, J. B. & SAROFIM, A. F. 1985. Effect of oxidation on the physical structure of soot. *Symposium (International) on Combustion,* 20**,** 951-957.

NIEMANN, M. U., SRINIVASAN, S. S., PHANI, A. R., KUMAR, A., GOSWAMI, D. Y. & STEFANAKOS, E. K. 2008. Nanomaterials for hydrogen storage applications: A review. *Journal of Nanomaterials*.

NOMURA, K. & MACDONALD, A. H. 2006. Quantum hall ferromagnetism in graphene. *Physical Review Letters,* 96.

NOVOSELOV, K. S., GEIM, A. K., MOROZOV, S. V., JIANG, D., KATSNELSON, M. I., GRIGORIEVA, I. V., DUBONOS, S. V. & FIRSOV, A. A. 2005a. Two-dimensional gas of massless Dirac fermions in graphene. *Nature,* 438**,** 197-200.

NOVOSELOV, K. S., JIANG, D., SCHEDIN, F., BOOTH, T. J., KHOTKEVICH, V. V., MOROZOV, S. V. & GEIM, A. K. 2005b. Two-dimensional atomic crystals. *Proceedings of the National Academy of Sciences of the United States of America,* 102**,** 10451-10453.

OSSLER, F., METZ, T. & ALDÉN, M. 2001a. Picosecond laser-induced fluorescence from gas-phase polycyclic aromatic hydrocarbons at elevated temperatures. I. Cell measurements. *Applied Physics B: Lasers and Optics,* 72**,** 465-478.

OSSLER, F., METZ, T. & ALDÉN, M. 2001b. Picosecond laser-induced fluorescence from gas-phase polycyclic aromatic hydrocarbons at elevated temperatures. II. Flame-seeding measurements. *Applied Physics B: Lasers and Optics,* 72**,** 479-489.

OSSLER, F., WAGNER, J. B., CANTON, S. E. & WALLENBERG, L. R. 2010. Sheet-like carbon particles with graphene structures obtained from a Bunsen flame. *Carbon,* 48**,** 4203-4206.

OVERBYE, D. 2010 Physics Nobel Honors Work on Ultra-Thin Carbon. *New York Times*.

PARK, S. & RUOFF, R. S. 2009. Chemical methods for the production of graphenes. *Nature Nanotechnology,* 4**,** 217-224.

PARK, S., SRIVASTAVA, D. & CHO, K. 2003. Generalized chemical reactivity of curved surfaces: Carbon nanotubes. *Nano Letters,* 3**,** 1273-1277.

PATTERSON, R. I. A. & KRAFT, M. 2007. Models for the aggregate structure of soot particles. *Combustion and Flame,* 151**,** 160-172.

PHILIPPE, R., MORANÇAIS, A., CORRIAS, M., CAUSSAT, B., KIHN, Y., KALCK, P., PLEE, D., GAILLARD, P., BERNARD, D. & SERP, P. 2007. Catalytic production of carbon nanotubes by fluidized-bed CVD. *Chemical Vapor Deposition,* 13**,** 447-457.

PICH, J., FRIEDLANDER, S. K. & LAI, F. S. 1970. The self-preserving particle size distribution for coagulation by Brownian motion-III. Smoluchowski coagulation and simultaneous Maxwellian condensation. *Journal of Aerosol Science,* 1**,** 115-126.

PINILLA, J. L., LÁZARO, M. J., SUELVES, I., MOLINER, R. & PALACIOS, J. M. 2010. Characterization of nanofibrous carbon produced at pilot-scale in a fluidized bed reactor by methane decomposition. *Chemical Engineering Journal,* 156**,** 170-176.

POPE, C. J. & HOWARD, J. B. 1997. Simultaneous particle and molecule modeling (SPAMM): An approach for combining sectional aerosol equations and elementary gas-phase reactions. *Aerosol Science and Technology,* 27**,** 73-94.

POPE, C. J., MARR, J. A. & HOWARD, J. B. 1993. Chemistry of fullerenes C60 and C70 formation in flames. *Journal of Physical Chemistry,* 97**,** 11001-11013.

PRADO, G., JAGODA, J., NEOH, K. & LAHAYE, J. 1981. A study of soot formation in premixed propane/oxygen flames by in-situ optical techniques and sampling probes. *Symposium (International) on Combustion,* 18**,** 1127-1136.

PRATSINIS, S. E. 1998. Flame aerosol synthesis of ceramic powders. *Progress in Energy and Combustion Science,* 24**,** 197-219.

PURI, R., RICHARDSON, T. F., SANTORO, R. J. & DOBBINS, R. A. 1993. Aerosol dynamic processes of soot aggregates in a laminar ethene diffusion flame. *Combustion and Flame,* 92**,** 320-333.

QI, X., DENG, Y., ZHONG, W., YANG, Y., QIN, C., AU, C. & DU, Y. 2010. Controllable and large-scale synthesis of carbon nanofibers, bamboo-like nanotubes, and chains of nanospheres over Fe/SnO2 and their microwave-absorption properties. *Journal of Physical Chemistry C,* 114**,** 808-814.

QIU, Y., YU, J., RAFIQUE, J., YIN, J., BAI, X. & WANG, E. 2009. Large-scale production of aligned long boron nitride nanofibers by multijet/multicollector electrospinning. *Journal of Physical Chemistry C,* 113**,** 11228-11234.

RADOVIC, L. R. & BOCKRATH, B. 2005. On the chemical nature of graphene edges: Origin of stability and potential for magnetism in carbon materials. *Journal of the American Chemical Society,* 127**,** 5917-5927.

RANZI, E., DENTE, M., GOLDANIGA, A., BOZZANO, G. & FARAVELLI, T. 2001. Lumping procedures in detailed kinetic modeling of gasification, pyrolysis, partial oxidation and combustion of hydrocarbon mixtures. *Progress in Energy and Combustion Science,* 27**,** 99-139.

RANZI, E., FARAVELLI, T. & FRASSOLDATI, A. Available: http://creckmodeling.chem.polimi.it/kinetic.html [Accessed].

RETAILLEAU, L., VONARB, R., PERRICHON, V., JEAN, E. & BIANCHI, D. 2004. Catalytic oxidation of a diesel soot formed in the presence of a cerium additive. I. Characterization of the cerium fraction using magnetic susceptibility and temperature-programmed desorption. *Energy & Fuels,* 18**,** 872-882.

RICHTER, H. & HOWARD, J. B. 2000a. Formation of polycyclic aromatic hydrocarbons and their growth to soot--a review of chemical reaction pathways. *Progress in Energy and Combustion Science,* 26**,** 565-608.

RICHTER, H. & HOWARD, J. B. 2000b. Formation of polycyclic aromatic hydrocarbons and their growth to soot-a review of chemical reaction pathways. *Progress in Energy and Combustion Science,* 26**,** 565-608.

ROBERTSON, D. H., BRENNER, D. W. & MINTMIRE, J. W. 1992. Energetics of nanoscale graphitic tubules. *Physical Review B,* 45**,** 12592-12595.

ROSNER, D. E. 2005. Flame synthesis of valuable nanoparticles: Recent progress/current needs in areas of rate laws, population dynamics, and characterization. *Industrial and Engineering Chemistry Research,* 44**,** 6045-6055.

ROSTRUP-NIELSEN, J. R. 1984. Sulfur-passivated nickel catalysts for carbon-free steam reforming of methane. *Journal of Catalysis,* 85**,** 31-43.

ROTELLO, V. M., HOWARD, J. B., YADAV, T., CONN, M. M., VIANI, E., GIOVANE, L. M. & LAFLEUR, A. L. 1993. Isolation of fullerene products from flames: Structure and synthesis of the C60-cyclopentadiene adduct. *Tetrahedron Letters,* 34**,** 1561-1562.

ROTH, P. 2007. Particle synthesis in flames. *Proceedings of the Combustion Institute,* 31**,** 1773-1788.

SABBAH, H., BIENNIER, L., KLIPPENSTEIN, S. J., SIMS, I. R. & ROWE, B. R. 2010. Exploring the role of PAHs in the formation of soot: Pyrene dimerization. *Journal of Physical Chemistry Letters,* 1**,** 2962-2967.

SANCHEZ, F. & SOBOLEV, K. 2010. Nanotechnology in concrete – A review. *Construction and Building Materials,* 24**,** 2060-2071.

SARDAR, R., FUNSTON, A. M., MULVANEY, P. & MURRAY, R. W. 2009. Gold nanoparticles: Past, present, and future. *Langmuir,* 25**,** 13840-13851.

SATTLER, K. 1995. Scanning tunneling microscopy of carbon nanotubes and nanocones. *Carbon,* 33**,** 915-920.

SCHEU, M., VEEFKIND, V., VERBANDT, Y., GALAN, E. M., ABSALOM, R. & FÖRSTER, W. 2006. Mapping nanotechnology patents: The EPO approach. *World Patent Information,* 28**,** 204-211.

SCHRAML, S., DANKERS, S., BADER, K., WILL, S. & LEIPERTZ, A. 2000. Soot temperature measurements and implications for time-resolved laser-induced incandescence (TIRE-LII). *Combustion and Flame,* 120**,** 439-450.

SCHUETZ, C. A. & FRENKLACH, M. 2002. Nucleation of soot: Molecular dynamics simulations of pyrene dimerization. *Proceedings of the Combustion Institute,* 29**,** 2307-2314.

SCHULZ, C., KOCK, B. F., HOFMANN, M., MICHELSEN, H., WILL, S., BOUGIE, B., SUNTZ, R. & SMALLWOOD, G. 2006. Laser-induced incandescence: Recent trends and current questions. *Applied Physics B: Lasers and Optics,* 83**,** 333-354.

SEIPENBUSCH, M., ERVEN, J. V., SCHALOW, T., WEBER, A. P., LANGEVELD, A. D. V., MARIJNISSEN, J. C. M. & FRIEDLANDER, S. K. 2005. Catalytic soot oxidation in microscale experiments. *Applied Catalysis B: Environmental,* 55**,** 31-37.

SEIPENBUSCH, M. & FRIEDLANDER, S. K. 2004. Catalytic soot oxidation in microscale experiments: Simulation of interactions between co-deposited graphitic nanoparticle agglomerates and platinum nanoparticles. *Journal of Nanoparticle Research,* 6**,** 605-611.

SERVICE, R. F. 2004. Nanotechnology grows up. *Science,* 304**,** 1732-1734.

SERVICE, R. F. 2009. Carbon sheets an atom thick give rise to graphene dreams. *Science,* 324**,** 875-876+877.

SGRO, L. A., BARONE, A. C., COMMODO, M., D'ALESSIO, A., DE FILIPPO, A., LANZUOLO, G. & MINUTOLO, P. Year. Measurement of nanoparticles of organic carbon in non-sooting flame conditions. *In:* Proceeding of the Combustion Institute, 2009. 689-696.

SGRO, L. A., BASILE, G., BARONE, A. C., D'ANNA, A., MINUTOLO, P., BORGHESE, A. & D'ALESSIO, A. 2003. Detection of combustion formed nanoparticles. *Chemosphere,* 51**,** 1079-1090.

SGRO, L. A., DE FILIPPO, A., LANZUOLO, G. & D'ALESSIO, A. Year. Characterization of nanoparticles of organic carbon (NOC) produced in rich premixed flames by differential mobility analysis. *In:* Proceeding of the Combustion Institute, 2007. 631-638.

SHADDIX, C. R., HARRINGTON, J. E. & SMYTH, K. C. 1994. Quantitative measurements of enhanced soot production in a flickering methane/air diffusion flame. *Combustion and Flame,* 99**,** 723-732.

SHADDIX, C. R. & SMYTH, K. C. 1996. Laser-induced incandescence measurements of soot production in steady and flickering methane, propane, and ethylene diffusion flames. *Combustion and Flame,* 107**,** 418-452.

SHEEHAN, P. E. & WHITMAN, L. J. 2005. Detection limits for nanoscale biosensors. *Nano Letters,* 5**,** 803-807.

SHEEN, D. A., YOU, X., WANG, H. & LØVÅS, T. Year. Spectral uncertainty quantification, propagation and optimization of a detailed kinetic model for ethylene combustion. *In:* Proceedings of the Combustion Institute, 2009. 535-542.

SHI, Z., LIAN, Y., ZHOU, X., GU, Z., ZHANG, Y., IIJIMA, S., ZHOU, L., YUE, K. T. & ZHANG, S. 1999. Mass-production of single-wall carbon nanotubes by arc discharge method. *Carbon,* 37**,** 1449-1453.

SHIOYAMA, H. 2001. Cleavage of graphite to graphene. *Journal of Materials Science Letters,* 20**,** 499-500.

SIMMIE, J. M. 2003. Detailed chemical kinetic models for the combustion of hydrocarbon fuels. *Progress in Energy and Combustion Science,* 29**,** 599-634.

SINGER, J. M. & GRUMER, J. 1958. Carbon formation in very rich hydrocarbon-air flames-I. Studies of chemical content, temperature, ionization and particulate matter. *Symposium (International) on Combustion,* 7**,** 559-569.

SIRIGNANO, M., ALFE, M., TREGROSSI, A., CIAJOLO, A. & D'ANNA, A. 2011. Experimental and modeling study on the molecular weight distribution and properties of carbon particles in premixed sooting flames. *Proceedings of the Combustion Institute,* 33**,** 633-640.

SIRIGNANO, M., KENT, J. & D'ANNA, A. 2010. Detailed modeling of size distribution functions and hydrogen content in combustion-formed particles. *Combustion and Flame,* 157**,** 1211-1219.

SMOLUCHOWSKI, M. V. 1916. Drei Vortrage uber Diffusion, Brownsche Bewegung und Koagulation von Kolloidteilchen. *Physik. Zeit,* 17**,** 557-585.

SOLDANO, C., MAHMOOD, A. & DUJARDIN, E. 2010. Production, properties and potential of graphene. *Carbon,* 48**,** 2127-2150.

SORENSEN, C. M. 2001. Light scattering by fractal aggregates: A review. *Aerosol Science and Technology,* 35**,** 648-687.

STANMORE, B. R., BRILHAC, J. F. & GILOT, P. 2001. The oxidation of soot: a review of experiments, mechanisms and models. *Carbon,* 39**,** 2247-2268.

STAUBER, T., GUINEA, F. & VOZMEDIANO, M. A. H. 2005. Disorder and interaction effects in two-dimensional graphene sheets. *Physical Review B - Condensed Matter and Materials Physics,* 71**,** 1-4.

STEIN, S. E. & FAHR, A. 1985. High temperature stabilities of hydrocarbons. *Journal of Physical Chemistry,* 82**,** 3714-3725.

STROBEL, R., BAIKER, A. & PRATSINIS, S. E. 2006. Aerosol flame synthesis of catalysts. *Advanced Powder Technology,* 17**,** 457-480.

STROBEL, R. & PRATSINIS, S. E. 2007. Flame aerosol synthesis of smart nanostructured materials. *Journal of Materials Chemistry,* 17**,** 4743-4756.

SUBRAMONEY, S. 1998. Novel nanocarbons - Structure, properties, and potential applications. *Advanced Materials,* 10**,** 1157-1171.

TAATJES, C. A., HANSEN, N., OSBORN, D. L., KOHSE-HÖINGHAUS, K., COOL, T. A. & WESTMORELAND, P. R. 2008. "Imaging" combustion chemistry via multiplexed synchrotron-photoionization mass spectrometry. *Physical Chemistry Chemical Physics,* 10**,** 20-34.

TAKEHARA, H., FUJIWARA, M., ARIKAWA, M., DIENER, M. D. & ALFORD, J. M. 2005. Experimental study of industrial scale fullerene production by combustion synthesis. *Carbon,* 43**,** 311-319.

TENNE, R. 2006. Inorganic nanotubes and fullerene-like nanoparticles. *Nature nanotechnology,* 1**,** 103-111.

TERRY, R., BAKER, K. & RODRIGUEZ, N. M. 1994. Catalytic growth of carbon nanofibers and nanotubes. *Materials Research Society Symposium - Proceedings,* 349**,** 251-256.

THOMPSON, B. C. & FRÉCHET, J. M. J. 2008. Polymer-fullerene composite solar cells. *Angewandte Chemie - International Edition,* 47**,** 58-77.

TIMOTHY V, D. 2011. Applications of nanotechnology in food packaging and food safety: Barrier materials, antimicrobials and sensors. *Journal of Colloid and Interface Science,* 363**,** 1-24.

TREGROSSI, A., CIAJOLO, A. & BARBELLA, R. 1999. The combustion of benzene in rich premixed flames at atmospheric pressure. *Combustion and Flame,* 117**,** 553-561.

UDDIN, F. 2008. Advancement in nanotechnology of polymers and fibres. *International Dyer,* 193**,** 33-35.

VANDER WAL, R. L. 1996a. Laser-induced incandescence: Detection issues. *Applied Optics,* 35**,** 6548-6559.

VANDER WAL, R. L. 1996b. Soot precursor material: Visualization via simultaneous lIF-LII and characterization via tem. *Symposium (International) on Combustion,* 26**,** 2269-2275.

VANDER WAL, R. L. 2000. Flame synthesis of substrate-supported metal-catalyzed carbon nanotubes. *Chemical Physics Letters,* 324**,** 217-223.

VANDER WAL, R. L. 2002. Flame synthesis of Ni-catalyzed nanofibers. *Carbon,* 40**,** 2101-2107.

VANDER WAL, R. L., HALL, L. J. & BERGER, G. M. 2001. Single-walled carbon nanotube synthesis within a flame environment. *Chemical and Physical Processes in Combustion, Fall Technical Meeting, The Eastern States Section.*

VANDER WAL, R. L. & TOMASEK, A. J. 2003. Soot oxidation: Dependence upon initial nanostructure. *Combustion and Flame,* 134**,** 1-9.

VARADAN, V. K. & XIE, J. 2002. Synthesis of carbon nanocoils by microwave CVD. *Smart Materials and Structures,* 11**,** 728-734.

VILLASENOR, R. & KENNEDY, I. M. 1992. Soot formation and oxidation in laminar diffusion flames. *Symposium (International) on Combustion,* 24**,** 1023-1030.

VIOLI, A., SAROFIM, A. F. & VOTH, G. A. 2004. Kinetic monte carlo-molecular dynamics approach to model soot inception. *Combustion science and technology,* 176**,** 991-1005.

WANG, H. Year. Formation of nascent soot and other condensed-phase materials in flames. *In*, 2011. 41-67.

WANG, H. & FRENKLACH, M. 1997. A detailed kinetic modeling study of aromatics formation in laminar premixed acetylene and ethylene flames. *Combustion and Flame,* 110**,** 173-221.

WANG, Y., WEI, F., LUO, G., YU, H. & GU, A. 2002. The large-scale production of carbon nanotubes in a nano-agglomerate fluidized-bed reactor. *Chemical Physics Letters,* 364**,** 568-572.

WEGNER, K. & PRATSINIS, S. E. 2004. Flame synthesis of nanoparticles. *Chimica Oggi,* 22**,** 27-29.

WESTERVELT, R. M. 2008. Applied physics: Graphene nanoelectronics. *Science,* 320**,** 324-325.

WHITESIDES, R., DOMIN, D., SALOMÓN-FERRER, R., LESTER JR., W. A. & FRENKLACH, M. 2009. Embedded-ring migration on graphene zigzag edge. *Proceedings of the Combustion Institute,* 32**,** 577-583.

WHITESIDES, R., KOLLIAS, A. C., DOMIN, D., LESTER, J., WILLIAM A. & FRENKLACH, M. 2007. Graphene layer growth: Collision of migrating five-member rings. *Proceedings of the Combustion Institute,* 31**,** 539-546.

WINKLMAYR, W., REISCHL, G. P., LINDNER, A. O. & BERNER, A. 1991. New electromobility spectrometer for the measurement of aerosol size distributions in the size range from 1 to 1000 nm. *Journal of Aerosol Science,* 22**,** 2889-2296.

WOODS, I. T. & HAYNES, B. S. 1994. *Active sites in soot growth*.

XING, Y., KOLE, T. P. & KATZ, J. L. 2003. Shape-controlled synthesis of iron oxide nanoparticles. *Journal of Materials Science Letters,* 22**,** 787-790.

XU, F., EL-LEATHY, A. M., KIM, C. H. & FAETH, G. M. 2003. Soot surface oxidation in hydrocarbon/air diffusion flames at atmospheric pressure. *Combustion and Flame,* 132**,** 43-57.

YANG, B., LI, Y., WEI, L., HUANG, C., WANG, J., TIAN, Z., YANG, R., SHENG, L., ZHANG, Y. & QI, F. Year. An experimental study of the premixed benzene/oxygen/argon flame with tunable synchrotron photoionization. *In*, 2007. 555-563.

YANG, Y., ARIAS, F., ECHEGOYEN, L., CHIBANTE, L. P. F., FLANAGAN, S., ROBERTSON, A. & WILSON, L. J. 1995. Reversible fullerene electrochemistry: Correlation with the HOMO-LUMO energy difference for C60, C70, C76, C78, and C84. *Journal of the American Chemical Society,* 117**,** 7801-7804.

YAZYEV, O. V. & LOUIE, S. G. 2010. Electronic transport in polycrystalline graphene. *Nature Materials,* 9**,** 806-809.

YIN, M., WU, C. K., LOU, Y., BURDA, C., KOBERSTEIN, J. T., ZHU, Y. & O'BRIEN, S. 2005. Copper oxide nanocrystals. *Journal of the American Chemical Society,* 127**,** 9506-9511.

YOU, X., WHITESIDES, R., ZUBAREV, D., LESTER JR, W. A. & FRENKLACH, M. 2011. Bay-capping reactions: Kinetics and influence on graphene-edge growth. *Proceedings of the Combustion Institute,* 33**,** 685-692.

YUAN, L., LI, T. & SAITO, K. 2002. Synthesis of multi-walled carbon nanotubes using methane-air diffusion flames. *29th International Symposium on Combustion.*

ZÁDOR, J., TAATJES, C. A. & FERNANDES, R. X. 2011. Kinetics of elementary reactions in low-temperature autoignition chemistry. *Progress in Energy and Combustion Science,* 37**,** 371-421.

ZHANG, L., CHENG, B. & SAMULSKI, E. T. 2004. In situ fabrication of dispersed, crystalline platinum nanoparticles embedded in carbon nanofibers. *Chemical Physics Letters,* 398**,** 505-510.

ZHANG, X., GU, H. & FUJII, M. 2006. Effective thermal conductivity and thermal diffusivity of nanofluids containing spherical and cylindrical nanoparticles. *Journal of Applied Physics,* 100.

ZHAO, B., YANG, Z., JOHNSTON, M. V., WANG, H., WEXLER, A. S., BALTHASAR, M. & KRAFT, M. 2003. Measurement and numerical simulation of soot particle size distribution functions in a laminar premixed ethylene-oxygen-argon flame. *Combustion and Flame,* 133**,** 173-188.